

ELECTRON PARAMAGNETIC RESONANCE STUDIES OF POLYMER CHAIN
DYNAMICS IN SOLUTION

Sooyeon Sim

A dissertation submitted to the faculty of the University of North Carolina at Chapel Hill in
partial fulfillment of the requirements for the degree of Doctor of Philosophy in the Department
of Material Science.

Chapel Hill
2014

Approved by:
Malcolm D. E. Forbes
Andrew M. Moran
Edward T. Samulski
Sergei S. Sheiko
Yue Wu

© 2014
Sooyeon Sim
ALL RIGHTS RESERVED

ABSTRACT

SOOYEON SIM: Electron Paramagnetic Resonance Studies of Polymer Chain Dynamics
in Solution
(Under the direction of Malcolm D. E. Fobes)

The temperature and side-chain structure dependencies of the time-resolved electron paramagnetic resonance (TREPR) spectra of acrylic polyhedral oligosilsesquioxane (POSS)-based copolymers and acrylic block copolymers are presented. The carbon-centered radicals within the main chain of an acrylic polyhedral oligosilsesquioxane (POSS)-based copolymers and acrylic block copolymers are produced in dilute solution at temperatures ranging from 25 °C to over 120 °C by direct excitation (248 nm) of the ester group in the polymers leading to Norrish I α -cleavage of the side chain ester moiety and provides a means to investigate the conformational energy landscape using a highly localized, minimally perturbative spin probe.

The observed photochemical degradation mechanism of those copolymers is quite similar to that previously observed in photolysis of homo poly (methacrylate)s. As expected, chromophores with POSS group side chains do not participate in the photodegradation process, which suggests that POSS utilize a beneficial effect against UV light photodegradation in these copolymers. The resulting experimental spectra suggest since all of the investigated methacrylate-POSS copolymers show the same photodegradation phenomena, that POSS could play an important roles in preventing UV degradation and improving photoresistance in such materials. The recent development of several controlled and free radical polymerization mechanisms have allowed the synthesis of many types of block copolymers, especially acrylics. Thus, the

photophysical and photochemical behavior of acrylic blocks in dilute solution, especially the site selective photochemistry was studied here by TREPR.

It is interesting to note that alternating line broadening effects due to the modulated hyperfine constant caused by a bulky ester side chain are observed in high temperature TREPR spectra of both *t*-butyl methacrylate-POSS block copolymer and poly *t*-butyl methacrylate rich block copolymers. The excellent fit of the simulations allow for identification of the signal carriers. The spectra show a strong signal from the *tert*-butyl radical after decarboxylation of the oxo-acyl radical. This process is rarely observed in high temperature fast limit TREPR spectra.

The temperature dependence of TREPR spectra of all block copolymers presented here shows similar conformational dynamics to those reported in our previous papers.

Radical-triplet pair interactions are used to investigate the dynamics of acrylic polymers in dilute solution. Methyl methacrylate was randomly copolymerized with a small amount of an amine-containing monomer to create the polymers. The amine subunits were then oxidized to nitroxide moieties (stable free radicals). Using TREPR spectroscopy on the sub-microsecond time scale, competition is observed between two deactivation processes of the ester side chain triplet state: 1) Norrish I α -cleavage, leading to a main chain free radical studied previously in our laboratory, and 2) spin polarization transfer or quenching by a nearby stable nitroxide radical. The two processes have TREPR spectral signatures that are easily distinguished by their widths, number of transitions, and chemically induced electron spin polarization (CIDEP) mechanisms. The main chain polymeric radical signal dominates the TREPR spectrum if the probability of radical-triplet pair encounters is low. These competing reactions show a strong dependence on nitroxide incorporation (mol %), temperature, solvent, and acrylic polymer ester side chain structure. A comparison of steady-state EPR and TREPR signals from inter- vs. intramolecular

processes clearly demonstrates the influence of polymer chain dynamics on the observed phenomena.

To my family and my advisor, I couldn't have done this without you.
Thank you for all your support along the way.

ACKNOWLEDGMENTS

I take this opportunity to express my profound gratitude and deep regards to my guide Professor Malcolm D. E. Forbes for his exemplary guidance, monitoring and constant encouragement throughout the course of this thesis. The blessing, help and guidance given by him time to time shall carry me a long way in the journey of life on which I am about to embark. My great mentor, Prof. Chongseung Yoon in Hanyang University, encouraged me to study in US. He introduced me joy of studying science and has been a continued source of friendship and wisdom.

I also take this opportunity to express a deep sense of gratitude to all our group members, for their kindly support, valuable information and encouragement, which helped me in completing this task through various stages and particularly to Lauren Jarocho, for being able to explain or fix anything; Renat , for making me happy and encouraging me all the time. Prof. Sang Wook Wu who was a research associate in Pederson group, we had nice discussion about quantum mechanics, and Spin Hamiltonian. It was the best discussion ever in my life.

For their support of my graduate school experience, I must acknowledge the members of my family, mom, dad, my brother and my Korean fiends in NC and in Korea, especially, Alley Choo, Sukyung Kim and Yeejee Han.

TABLE OF CONTENTS

LIST OF TABLES	xi
LIST OF FIGURES	xii
LIST OF ABBREVIATIONS AND SYMBOLS	xvii
CHAPTER	
1. Introduction.....	1
1.1 Study of Polymer Chain Dynamics in Solution.....	1
1.2 Characterization of Main-Chain Radicals from the Photodegradation of Acrylic Polymers	6
1.3 Experimental overview of TREPR	15
1.3.1 Steady-state EPR (SSEPR) vs. TREPR	15
1.3.2 Experimental considerations for TREPR.....	21
1.4 Chemically Induced Electron Spin Polarization (CIDEP) Mechanisms	25
1.4.1 The Triplet Mechanism (TM)	28
1.4.2 The Radical-Triplet Pair Mechanism (RTPM)	30
2. Photochemistry of acrylate-POSS block copolymers and dynamic effects in copolymer radicals	37
2.1 Introduction.....	37
2.1.1 POSS and POSS based Polymers	38
2.1.2 Degradation studies of POSS-based Polymer.....	41
2.2 Results and discussion	43

2.3 Summary and Implications	
2.4 Experimental	58
3. Photodegradation of Acrylic Block Copolymers	60
3.1 Introduction.....	60
3.1.1 Structure of Block Copolymers	61
3.1.2 Photochemistry of Acrylic Polymers	64
3.2 Result and Discussion	69
3.2.1 TREPR spectra of Block Copolymers	77
3.2.1.1 Poly (methyl methacrylate)–b–Poly (tert-butyl methacrylate) Copolymers	77
3.2.1.2 Poly (methyl methacrylate)–b–Poly (n-butyl methacrylate) Copolymers	84
3.2.1.3 Poly (methyl methacrylate)–b–Poly (ethyl acrylate) Copolymers....	87
3.3 Summary and Outlook	92
3.4 Experimental	93
3.4.1 Materials	93
3.4.2 Synthesis	93
3.4.2.1 Anionic Polymerization	93
3.4.2.2 Free radical Polymerization	94
3.4.3 Analysis of polymer samples	94
3.4.3.1 Gel Permeation Chromatography (GPC)	94
3.4.3.2 High temperature TREPR set-up	95
4. Radical-Triplet Pair Interactions as Probes of Long-Range Polymer Motion in Solution	97
4.1 Introduction.....	97

4.2 The Microscopic Order–Macroscopic Disorder Model (MOMD)	99
4.3 Studies of Segmental Rotational Dynamics of Spin-labeled PMMA in Dilute Solution.....	103
4.4 TREPR Studies of Chain Dynamics of Spin-labeled Polymers in Dilute Solutions	111
4.5 Conclusions.....	127
4.6 Experimental.....	128
4.6.1 Analysis of polymer samples	129
5. REFERENCES	131

LIST OF TABLES

Table 1.1	Parameters used to simulate TREPR spectra (Fig. 1.3) of Polymer Main-Chain radicals and Acyl Radicals.....	11
Table 3.1	The structure and molecular weight of block copolymers.....	70
Table 4.1	Parameters used in the simulation temperature dependence of the SSEPR spectra of 1 mol % nitroxide copolymer sample in PC.....	107
Scheme 1.1	Graphical representation of Local vs. non-Local probes.....	1

LIST OF FIGURES

Figure 1.1	Photochemistry and free radicals resulting from 248 nm excimer laser excitation of acrylic polymers in solution	7
Figure 1.2	Structures of polymers characterized by TREPR	8
Figure 1.3	(A–E) Experimental TREPR spectra (left) and simulated spectra (right) for main-chain acrylic radicals observed at 0.8 μ s after 248 nm laser flash photolysis for the polymers indicated (see Fig. 1.2 for polymer structures and Table 1.1 for radical structures). (A) PEA, (B) PEMA, (C) PECA, (D) PMMA, (E) PMMA-d ₃ , all obtained in propylene carbonate. (F) TREPR spectrum (left, experimental; right, simulated) of the oxo-acyl radical from PFOMA, obtained in the high boiling fluorinated solvent mixture FC-70. For PMMA, the material is isotactic (91% by NMR), but all other polymer samples are atactic material. Simulation parameters (ref. [10]) are listed in Table 1.1.	10
Figure 1.4	Symmetry relationships between the nuclear hyperfine coupling constants in acrylic polymers as a function of polymer tacticity	13
Figure 1.5	Energy level diagram depicting a single spin system in a external magnetic field. When the resonance condition is met, a single observable transition can occur between the two spin states, as shown by the double arrow in the figure	17
Figure 1.6	Energy level diagram demonstrating the hyperfine interaction and observable transitions of a radical coupled to a neighboring nucleus with I=1	18
Figure 1.7	Steady-state EPR detection using 100 kHz field modulation and the resulting first derivative line shape	20
Figure 1.8	Block diagram of the TREPR experiment using a boxcar signal averager	22
Figure 1.9	Timing sequence for the TREPR experiment using a boxcar signal averager	24
Figure 1.10	(A) Energy level diagram of a single electron in the magnetic field with population distribution in these two level (B) Spin polarization: Enhanced absorption and emission observe because excess population is created in a higher energy level by putting energy into the system from an external source such as photolysis	26
Figure 1.11	The TM of CIDEP	29
Figure 1.12	Energy levels of a radical–triplet pair as a function of their separation. Schematic explanation of net emission CIDEP created by excited triplet quenching by stable free radical	32

Figure 1.13	Energy levels of a radical–triplet pair as a function of their separation. Schematic explanation of net absorption CIDEF created by excited singlet quenching by stable free radical.	33
Figure 2.1	Chemical structures of silsesquioxanes. non-caged (left) vs. caged (right).....	40
Figure 2.2	Schematic drawing of chemical structures of POSS-based polymeric nanocomposites: (left) norbornyl-POSS copolymers; (middle) methacrylate-POSS copolymers and (right) styryl-POSS copolymers.	42
Figure 2.3	Structures of polymers characterized by TREPR: (1) [(propylmethacryl-heptaisobutyl-POSS)- <i>co</i> -(<i>t</i> -butyl methacrylate)]; (2) [(propylmethacryl-heptaisobutyl-POSS)- <i>co</i> -(<i>n</i> -butyl methacrylate)]; (3)[(propylmethacryl-heptaisobutyl-POSS)- <i>co</i> -(methyl methacrylate)]; (4) Poly (<i>t</i> -butyl methacrylate); (5) Poly (methyl methacrylate) and (6) Poly (<i>n</i> -butyl methacrylate)].....	44
Figure 2.4	Two solvents for TREPR experiments at high Temperature.....	46
Figure 2.5	Experimental High-temperature TREPR spectra for the main-chain radical from 248 nm irradiation of the following polymers: (A) PSS 25 wt % of Poly [(propylmethacryl-heptaisobutyl-POSS)- <i>co</i> -(<i>t</i> -butyl methacrylate)], (B) PSS 45 wt % of Poly [(propylmethacryl-heptaisobutyl-POSS)- <i>co</i> -(<i>t</i> -butyl methacrylate)], (C) P(<i>t</i> -butyl methacrylate) in diethyl glycol dimethyl ether at 125 °C, shown for comparison.....	47
Figure 2.6	The 10-line <i>t</i> -butyl radical spectrum from decarboxylation of poly (<i>t</i> -butyl methacrylate) oxo–acyl radical in diethylene glycol dimethyl ether at 125 °C with following total sweep width: (top) 300 G, 100 G, 50 G, and (bottom) 30 G and delay time: 500 ns.....	49
Figure 2.7	Photochemistry and free radicals resulting from 248nm excimer laser excitation of Poly (<i>t</i> -butyl methacrylate) in solution	50
Figure 2.8	(Top) The photochemistry of PFOMA. (Bottom left) experimental and (Bottom right) simulated high temperature TREPR spectra of the oxo-acyl radical from PFOMA in perfluorinated solvent FC-70 at 110 °C and delay time 0.5 s.	52
Figure 2.9	Two proposed simulated high temperature TREPR spectra of poly (<i>t</i> -butyl methacrylate) after photolysis at 120°C and delay time of 500 ns	53
Figure 2.10	The temperature dependence of TREPR spectra for the main-chain radical from 248 nm irradiation of Poly [(propylmethacryl-heptaisobutyl-POSS)- <i>co</i> -(<i>n</i> -butyl methacrylate)] in propylene carbonate.....	56

Figure 2.11	The temperature dependence of TREPR spectra for the main-chain radical from 248 nm irradiation of Poly [(propylmethacryl-heptaisobutyl-POSS)-co-(<i>n</i> ethyl methacrylate)] in diglyme	57
Figure 3.1	Phase diagram for polymer solution.....	62
Figure 3.2	(Top) The photochemistry of PFOMA. (Bottom left) experimental and (Bottom right) simulated high temperature TREPR spectra of the oxo-acyl radical from PFOMA in perfluorinated solvent FC-70 at 110 °C and delay time 0.5 μ s	68
Figure 3.3	Two solvents for TREPR experiments at high Temperature.....	73
Figure 3.4	Experimental high temperature TREPR spectra for radicals observed after 248 nm laser flash photolysis of the following polymers and their structures.....	74
Figure 3.5	Simulated high temperature TREPR spectra for radicals observed after 248 nm laser flash photolysis of the following polymers and their structures	75
Figure 3.6	Block chain length ratio dependence of Poly (methyl methacrylate)-b-poly (t-butyl methacrylate) copolymer TREPR spectra in diglyme at 500 ns at 125 °C	78
Figure 3.7	The 10-line t-butyl radical spectrum from decarboxylation of poly (t-butyl methacrylate) oxo-acyl radical in diethylene glycol dimethyl ether at 125 °C with following total sweep width: (top) 300 G, 100 G, 50 G, and (bottom) 30 G and delay time: 500 ns.....	80
Figure 3.8	Structure of propagating radical of poly (t-butyl methacrylate) and simulated EPR spectra of the propagating radical of poly (t-butyl methacrylate) (left) direct detection and (right) 1'st derivative at 150 °C	82
Figure 3.9	The temperature dependence of TREPR spectra for the main-chain radical from 248 nm irradiation of all three Poly (methyl methacrylate)-b-poly (t-butyl methacrylate) copolymer in either diglyme or propylene carbonate.....	83
Figure 3.10	Block chain length ratio dependence of Poly (methyl methacrylate)-b-poly (n-butyl methacrylate) copolymer TREPR spectra in diglyme at 500 ns at 115 °C	85
Figure 3.11	The temperature dependence of TREPR spectra for the main-chain radical from 248 nm irradiation of all two Poly (methyl methacrylate)-b-poly (t-butyl methacrylate) copolymer in either diglyme or propylene carbonate.....	88
Figure 3.12	(Left) Experimental high temperature TREPR spectra and (Right) simulated spectra for main-chain radicals observed at 500 ns after 248 nm laser flash photolysis of the following polymers: Poly (methyl methacrylate)-b-poly ethyl acrylate) copolymer (Top) n:m = 9:1 , 1:1 , poly methacrylate , and (bottom) poly ethyl acrylate for comparison in propylene carbonate (1g polymer in 25 ml solvent)	90

Figure 3.13	The temperature dependence of TREPR spectra for the main-chain radical from 248 nm irradiation of all two Poly (methyl methacrylate)-b-poly (ethyl acrylate) copolymer in propylene carbonate (1g of polymer in 25 ml of solvent) at delay time of 500 ns	91
Figure 4.1	Norrish I α -cleavage reaction of poly(methyl methacrylate) (PMMA) and graphical representation of the fast rotation of the side chain along one axis and the much slower conformational motion along the polymer chain.	98
Figure 4.2	(a) Different coordinate systems (laboratory: L, director: D, and magnetic: m) used to define motion parameters for a nitroxide spin label. (b) Diffusion rotation angles used to define the magnetic axes relative to the diffusion axes. Note that the reference system for these angles is the is diffusion frame. (c) Structure of spin-labeled PMMA with 2,2,6,6,-tetra-methyl-4-hydroxypiperidiny-1-oxy and the assumed conformation of spin label bounded at the end of the side chain (ref. 104, 105).....	101
Figure 4.3	The structure of nitroxide containing random PMMA copolymer studied in this chapter.....	104
Figure 4.4	Top: X-band SSEPR (dark) spectra of the nitroxide-doped copolymer from Figure 4.3, acquired at room temperature in the solvents indicated. Bottom: Computer simulations using the Freed model REF with rotational correlation times of (left to right) 0.18 ns, 0.45 ns, and 0.72ns respectively.....	105
Figure 4.5	(Left)X-band SSEPR spectra of the nitroxide-doped copolymer and (Right) the same mol % nitroxide (TEMPO) and PMMA in PC at the given temperature	107
Figure 4.6	Arrhenius plot for rotational correlation time data from nitroxide-doped polymer (Figure 4.5). Squares are the simulated data, and the solid line is the linear fit with $E_a = 23$ KJ/mol	110
Figure 4.7	Graphical representation of spin polarization created by TM, RTPM and ESPT ..	113
Figure 4.8	TREPR spectra of the nitroxide-containing copolymer shown in figure 4.3, acquired in propylene carbonate solution at 120°C, as a function of nitroxide incorporation (in mol %) the indicated to the left. Asterisks in the 1.0 mole % spectrum indicate transitions from the main chain polymeric radical of PMMA that is dominant in the 0.5 and 0.1 mol % spectra	117
Figure 4.9	TREPR spectra of the nitroxide-containing polymer shown in Figure 4.3 (1 mol % nitroxide) in propylene carbonate solution at the temperatures indicated. Asterisks in the 120°C spectrum indicate transitions from the main chain polymeric radical of PMMA, which is very broad but still observable in the 25 °C spectrum (top). The delay time is 500 ns and the sweep width is 150 G in each spectrum	121

- Figure 4.10 Inter- vs. intramolecular competition between TM and RTPM. (Top) TREPR spectra of unattached TEMPO (1.5mM) and PMMA (5 wt %) in propylene carbonate after 248 nm laser excitation at 120°C. (Bottom) TREPR spectrum of the nitroxide containing PMMA copolymer (loading level is 1 mol %) under the same conditions. Asterisks in the bottom spectrum indicate transitions due to the main chain polymeric radical of PMMA. The delay time is 500 ns and the sweep width is 150 G in both spectra. 123
- Figure 4.11 TREPR spectra of the 1 mol% of nitroxide-containing PMMA polymer as a function of concentration. The spectra were acquired in propylene carbonate solution at 120 °C. Asterisks in the bottom spectrum indicate transitions due to the main chain polymeric radical of PMMA. The delay time is 500 ns and the sweep width is 150 G in both spectra 124
- Figure 4.12 TREPR spectra of nitroxide-containing poly(n-butyl methacrylate) at 70°C (top) and poly(tert-butyl methacrylate) at 130°C (bottom) in diglyme. The sweep width is 200 G and the delay time is 500 ns in both spectra. The degree of nitroxide incorporation is 1 mol % for both polymers. Both signals are attributed to the respective main chain polymeric radicals, i.e., RTPM/quenching involving the nitroxide is not taking place 126

LIST OF ABBREVIATIONS AND SYMBOLS

A. ABBREVIATIONS

AIBN	2,2'-azobisisobutyronitrile
a-PMMA	atactic poly(methyl methacrylate)
CH ₃	methyl group
CH ₂	methylene group
CO	carbon monoxide
CO ₂	carbon dioxide
CW	continuous wave
CIDEP	chemically induced electron polarization
DPE	1,1-diphenylethylene
DLS	dynamic light scattering
d ₃ -PMMA	poly(methyl d ₃ -methacrylate)
diglyme	diethylene glycol dimethyl ether
EA	ethyl acrylate
EPR	electron paramagnetic resonance
ESPT	electron spin polarization transfer
GPC	gel permeation chromatography
ISC	intersystem crossing
i-PMMA	isotactic poly (methyl methacrylate)
LW	linewidth
MeOH	methanol

MMA	methyl methacrylate
NMR	nuclear magnetic resonance
n-BMA	n-butyl methacrylate
n-BuLi	n-Butyllithium
PC	propylene carbonate
PDI	poly disperse index
PEA	poly(ethyl acrylate)
PEMA	poly(ethyl methacrylate)
PFOMA	poly(fluorooctyl methacrylate)
P(isoBMA)	poly(iso-butyl methacrylate)
POSS	polyhedral oligomeric silsesquioxane
PMMA	poly(methyl methacrylate)
P(n-BMA)	poly(n-butyl methacrylate)
PS	poly(styrene)
P(t-BMA)	poly(t-butyl methacrylate)
RPM	radical pair mechanism
RTPM	radical triplet pair mechanism
S/N	signal to noise ratio
s-PMMA	syndiotactic poly(methyl methacrylate)
SSEPR	steady state electron paramagnetic resonance
SCRP	spin correlated radical pair polarization
THF	tetrahydrofuran
TM	triplet mechanism

TREPR	time resolved electron paramagnetic resonance
UV	ultraviolet
UV/VIS	ultraviolet/visible absorption spectroscopy

B. ROMAN SYMBOLS

A	Absorption
a	polymer segment length
aH	hyperfine coupling constant
B	applied magnetic field
C	Carbon
C	Concentration
^{13}C	carbon-13
C*	critical concentration
d	doublet
E	emission
E	energy
G	gauss
g	grams
g	g-factor
mg	milligrams
GHz	gigahertz
H	hydrogen
^1H	proton

h	Plank constant
h	hour
Hz	Hertz
I	nuclear spin quantum number
I	Intensity
J	exchange interaction
K	Kelvin
k	Boltzmann constant
k	rate constant
KJ	kilojoules
KrF	krypton-fluoride
M	molarity
Mn	number average molecular weight
Ms	quantum number
Mw	weight average molecular weight
mL	milliliters
μL	microliters
mM	millimolar
mm	millimeter
nm	nanometer
N	degree of polymerization
N	nitrogen
N _A	Avogadro's number

R_F	end-to-end distance of the chain
R_g	radius of gyration
μs	microseconds
ns	nanoseconds
S	excited singlet state
S_0	ground state
S_1	first excited singlet state
s	singlet
T	temperature
T	excited triplet energy level
T_g	glass transition temperature
T_m	melting temperature
T_1	first excited triplet state
T_1	spin-lattice relaxation
t	triplet
t	time
v	volumn

C. GREEK SYMBOLS

α	upper energy level of electron
β	lower energy level of electron
β_e	Bohr magneton
γ_e	gyromagnetic ratio of the electron

δ	chemical shift
ε	extinction coefficient
Φ	quantum yield
η	viscosity
λ	wavelength
ν	excluded volume index
ν	frequency
ν	Flory exponent
θ	dihedral angle
ρ	density
τ	rotational correlation time
χ	Flory-Huggins segmental interaction parameter
ω	frequency
ϕ	concentration
ϕ^*	overlap concentration

Chapter 1. Introduction

1.1 Study of Polymer Chain Dynamics in Solution

Polymer chain dynamics in melts and highly concentrated solutions is a well-studied area of science [1, 2]. In such systems, the chain dynamics are not affected by the solvent and instead reflect bulk properties, where entanglement plays a major role, e.g., in the rheology of melts.

It can be difficult to understand their macroscopic behavior of polymer solutions due to the complexities of entanglement. In this regard, physical measurements of polymer conformational dynamics in dilute solution can be very informative as they can provide more information about the intrinsic polymer properties.

The conformational dynamics of macromolecules is a topic of great interest and has been well-studied in polymer physics [3, 4], however most theoretical models in the field are based on so-called “coarse-grain” methods, i.e., balls and springs with standard potentials such as Lennard-Jones or modifications thereof. There are very few models in the literature that use information at the molecular level [5a,b]; indeed there is only one published report of a molecular dynamics simulation of a polymer chain with solvent molecules included explicitly [5c]. Unlike a protein simulation, most polymer solution simulations cannot use water as their solvent, and therefore need to add one more term related to the interaction energies between polymer and solvent.

In the work discussed here, molecular level parameters such as conformational energy

potentials (well depths and activation barriers), are sought in order to assess the *intrinsic* properties of polymer chains in the absence of entanglements. By careful analysis of intrinsic polymer properties the role of entanglement in melt properties might be better understood (by eliminating them).

In order to understand polymer behaviors at the molecular level, a polymer dilute solution can be used without entanglement, and with no overlapping chains. The polymer chain in solution can be isolated at special conditions where it is below critical concentration, and at theta (θ) temperature where the effective monomer and monomer interaction are weak thus polymer coil can consider as ideal chain.

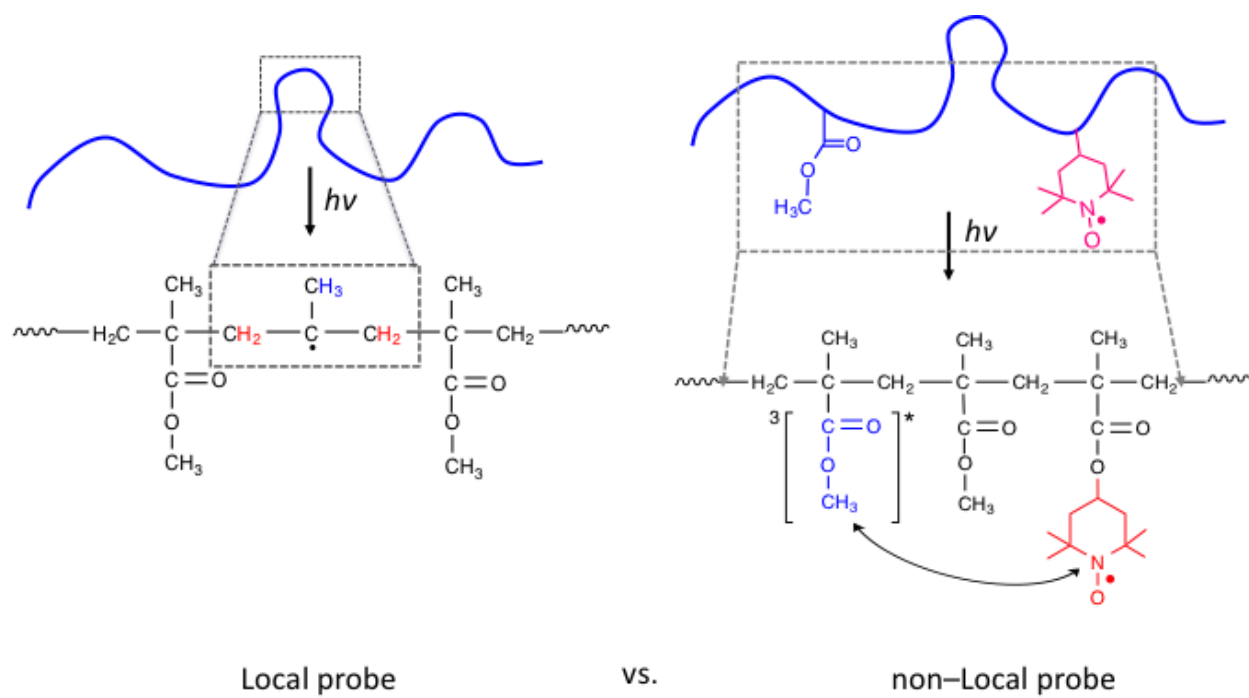
Nuclear magnetic resonance (NMR) has been the most widely used to study of polymer motions and conformation so far. ^{13}C can be used in a NMR spin probe of polymer chain dynamic because of the sensitivity of ^{13}C resonance frequencies or chemical shifts, $\delta^{13}\text{C}$, to polymer configuration and conformation [6]. Also, the measurement of segment diffusion and NMR spin-lattice relaxation is a suitable method for studying polymer chain dynamics [7].

Like NMR, Electron paramagnetic resonance (EPR) spectroscopy has been used to obtain information about polymer motions and local chain behavior by using a spin probes, commonly stable nitroxide radicals. Depending on their rotational and translational motion, with correlation times (τ_c) along the polymer chain, the appearance of the EPR spectrum can be quite different [8]. Thus, studying their line shapes and widths as a function of the correlation times (τ_c) provides useful information about the segmental dynamics of a polymer. However, using a nitroxide spin probe is more suitable for investigation the bulk properties of polymer chain, not for extracting the molecular level parameters such as conformational energies.

In this thesis, we investigate both short- and long-range conformational motion in

polymer chains in dilute solutions as a function of polymer main chain and side chain structure, temperature, solvent and concentration using a EPR study of localized vs. non-localized spin probes.

The basic strategy for these studies is summarized in scheme 1. On the left side of the scheme 1 is the creation of carbon-centered radicals within the main chain of an acrylic polymer by photolysis (248nm) creates a highly localized, minimally perturbative spin probe, thus an EPR study of this localized spin probe is suitable to investigate the conformational energy landscape of polymer chains [9,10]. The main chain radical can only be observed in solution using the time-resolved EPR (TREPR) technique: under steady-state conditions its rearrangement to the propagating radical via beta-scission is facile at room temperature and above. Because the electron-nuclear hyperfine interactions in the main chain radical depend on the dihedral angle between the p orbital containing the unpaired electron and the neighboring C-H sigma bond, the TREPR spectra of these main chain radicals show a strong temperature dependence for both line widths and line positions [11]. Changes in line width are related to the “jump time” between conformations, while changes in line position (at constant width) reflect changes in the populations of certain rotational conformers (“rotamers”). For this reason, the observed TREPR spectra are rich in information regarding the conformational landscape of the polymers, and this data can be obtained with only a minimal perturbation of the polymer chain structure. Thus, the degradation of acrylic polymers has been a subject of intense study in the Forbes laboratory for the past decade, and this thesis seeks to extend this work to create a workable “atom-specific” model for macromolecular chain dynamics that has so far proven elusive for these complex structures. In the process of creating the model, we will be using TREPR to study acrylic polymers that have not been investigated before but which appear to



Scheme 1.1 Graphical representation of Local vs. non-Local probes studied this thesis

show novel degradation pathways and different chain dynamics.

The right side of Scheme 1 shows a longer-range conformational change that can also be probed using TREPR. In this case, the polymer is synthesized with a small percentage of stable nitroxide free radicals as side chains. When a photoexcited triplet state is created, it can be quenched by the nitroxide, or it can engage in Heisenberg spin exchange with the stable radical. In both cases the nitroxide radical receives additional population of its electron spin states that are non-Boltzmann. The magnitude of this polarization is directly proportional to the number of encounters made between the stable radical and the excited triplet state, and is therefore an indirect measure of the rate of intra-chain contact between the two sites.

The photodegradation mechanism of several acrylate polymers and copolymers (block, random and hybrid) and TREPR characterization of their free radical reactive intermediates created after UV laser flash photolysis in dilute solution are described in Chapters 2 and 3. In these chapters, the dynamic effects and conformational s of several blockcopolymers will be presented and discussed. Their dynamics behavior depends on polymer chain stiffness, temperature, block chain length and chain configuration will be discussed. Fast motion TREPR spectra obtained at high temperature will be used to allow for accurate simulations of their main-chain polymer radicals. Chapter 4 describes radical-triplet pair interactions, which are used to detect long-range chain motion in acrylic polymers in dilute solution by incorporating a nitroxide into the polymer chain by means of covalent bonds, we can generate RTPM polarization via *intramolecular* encounters that depend on several structural and physical features of the polymer/solvent system. Additionally, Chapter 4 will present the dependence of the RTPM polarization in the covalently linked system as a function of nitroxide incorporation (mol%), temperature, solvent, and acrylic polymer ester side chain structure.

This chapter provides background information about the previous work in the Forbes laboratory on acrylic polymer degradation, the TREPR experiment itself and the relevant CIDEP mechanisms to the new work presented in this thesis.

1.2 Characterization of Main-Chain Radicals from the Photodegradation of Acrylic Polymers

The photodegradation mechanisms of polymers have been a subject of intense interest in for many years [12], and many of these reactions involve free-radical intermediates [13]. In our laboratory, we have used TREPR spectroscopy to investigate the degradation of acrylic polymers as a function of polymer structure, solvent, pH, and temperature [9, 10, 14, 15]. The generic main-chain acrylic polymer radical (Figure 1.A, top center), obtained after 248 nm laser flash photolysis of the ester side chain, rapidly rearranges to the so-called propagating radical (Figure 1.B, bottom left) and an alkene via β -scission. For this reason, the main-chain radical is not generally observable with high spectral resolution in SSEPR experiments involving acrylic polymers [16]. However, the TREPR experiment is fast enough to observe both main-chain acrylic radicals and, in some cases, the corresponding oxo-acyl counter radicals (Figure 1.C, top right) on the microsecond timescale. Here is the brief review of our recent findings regarding the structure and dynamics of acrylic main-chain radicals created by 248 nm laser flash photolysis of the polymers shown in Figure 1.2.

Poly(ethyl acrylate) (PEA) was the starting point for our investigation as it has the simplest structure. The following two polymers in this series, poly(ethyl methacrylate) (PEMA) and poly(ethyl cyanoacrylate) (PECA), have the same ester side chains (b-substituent $-\text{CH}_2\text{CH}_3$), as PEA. However, the α -substituent of the polymer backbone is different in all three of the ethyl acrylates. The side-chain structural differences in these polymers can have a strong influence on

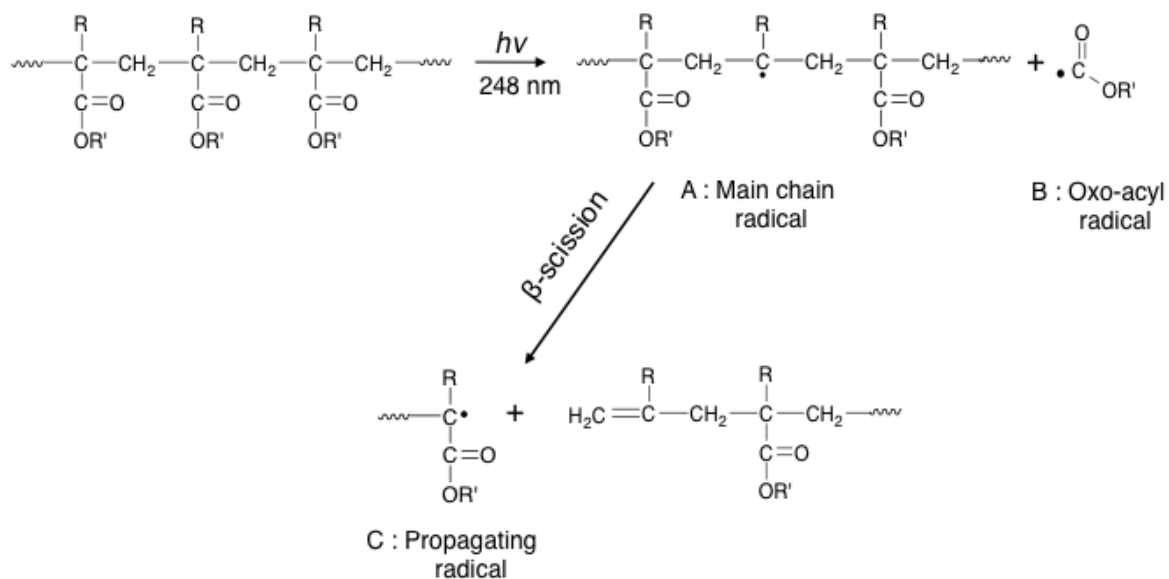
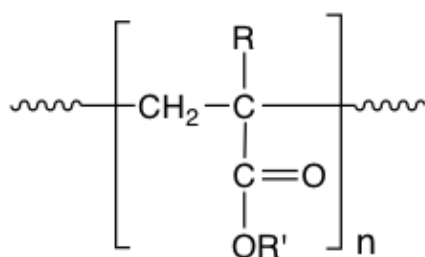


Figure 1.1 Photochemistry and free radicals resulting from 248 nm excimer laser excitation of acrylic polymers in solution



	<u>Polymer</u>	<u>Acronym</u>	<u>R</u>	<u>R'</u>
1	Poly(ethyl acrylate)	PEA	H	CH ₂ CH ₃
2	Poly(ethyl methacrylate)	PEMA	CH ₃	CH ₂ CH ₃
3	Poly(ethyl cyanoacrylate)	PECA	CN	CH ₂ CH ₃
4	Poly(methyl methacrylate)	PMMA	CH ₃	CH ₃
5	Poly(methyl <i>d</i> ₃ -methacrylate)	<i>d</i> ₃ -PMMA	CD ₃	CH ₃
6	Poly(fluorooctyl methacrylate)	PFOMA	CH ₃	CH ₂ (CF ₂) _x CF ₃

Figure 1. 2 Structures of polymers characterized by TREPR

the appearance of TREPR spectra, especially the line widths. The next polymer, poly (methyl methacrylate) (PMMA), has been extensively studied in our previous papers because of the interesting nuclear spin symmetry properties of their main-chain radicals as a function of polymer tacticity. In addition, PMMA-d₃ was also investigated to confirm the spectral assignments by isotopic labeling with TREPR. The last polymer structure listed in Figure 1.2 is Poly(fluorooctyl methacrylate) (PFOMA), where, the β -substituent is the $-\text{CH}_2(\text{CF}_2)_6\text{CF}_3$ bulky ester side chain, which has very different physical properties from other acrylate polymers [17]. The stiffness of the main chain due to the bulky side chain produces a huge change in the TREPR spectral appearance of the resulting radicals.

The TREPR spectra obtained 0.8 μs after 248 nm laser flash photolysis of six acrylic polymers are shown in Figure 1.2, along with simulations for some of the spectra computed using magnetic parameters listed in Table 1.1. All TREPR spectra shown in Figure 1.3 were recorded at high temperature (above 100 °C) where the “fast-motion” regime of the polymer dominated. The TREPR spectra of the main-chain polymeric radicals mentioned in our previous work exhibit alternating line widths at room temperature, a phenomenon that is highly indicative of conformationally modulated hyperfine interactions (slow motion). However, upon heating, most acrylic polymer main-chain radicals show motional narrowing with sharp line widths, allowing us to simulate the spectra using an average set of hyperfine coupling constants.

Figure 1.3A shows the experimental high-temperature TREPR spectrum obtained after photolysis of PEA in propylene carbonate solution. This radical shows six major transitions with the doublets of the innermost lines attributed to two β -methylene hyperfine couplings of 23.0 and 24.7 G and one α -hyperfine coupling of 21.5 G, which were comparable to the reported literature values for radicals of similar chemical structure. The oxo-acyl radical from PEA was not

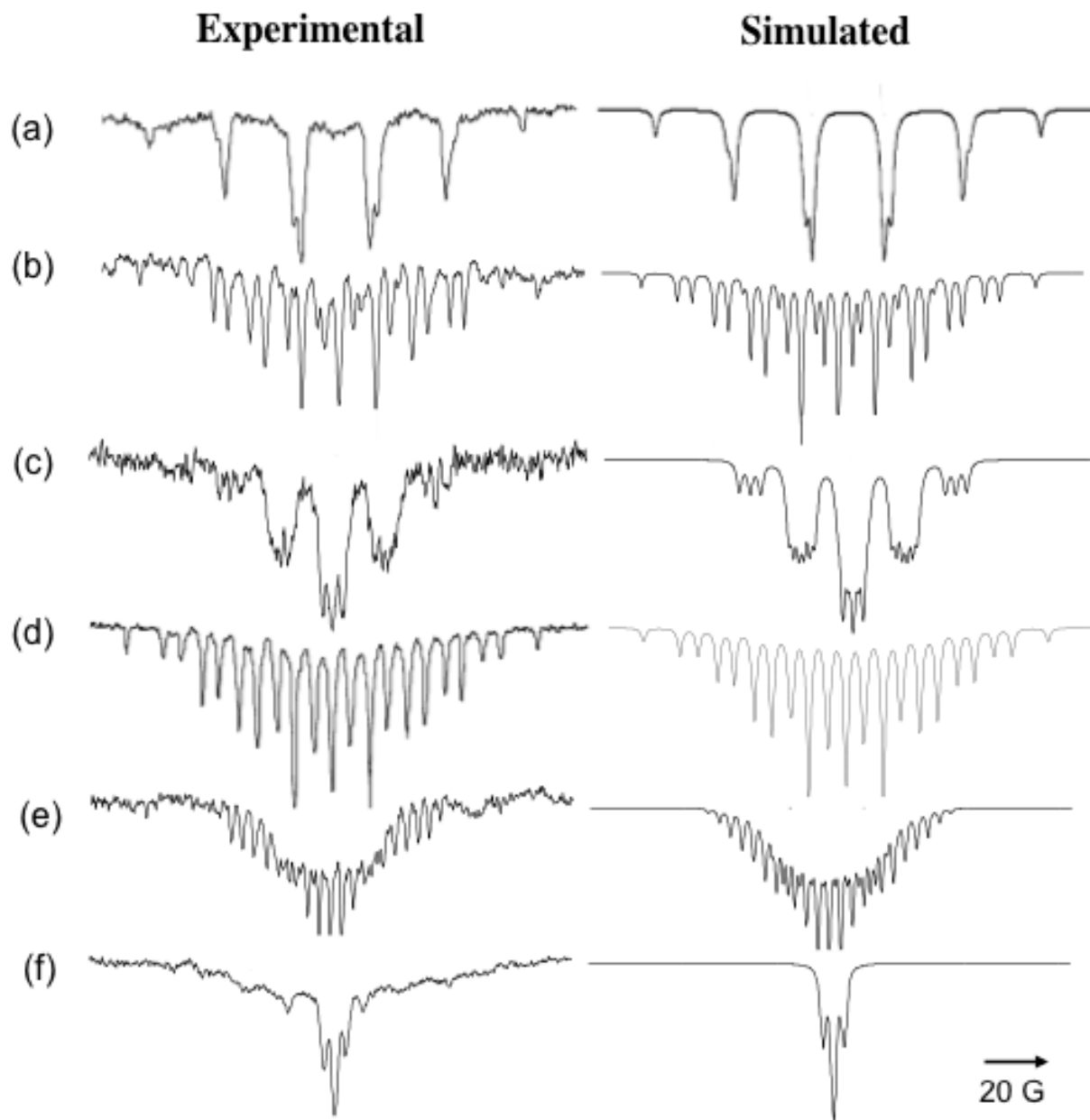
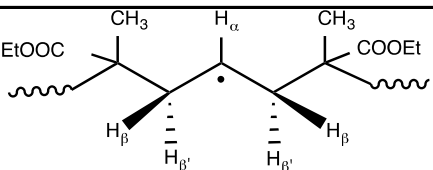
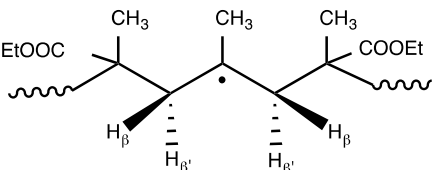
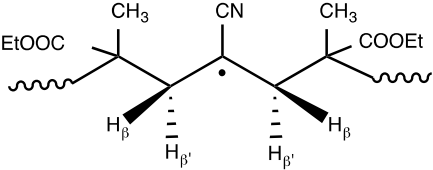
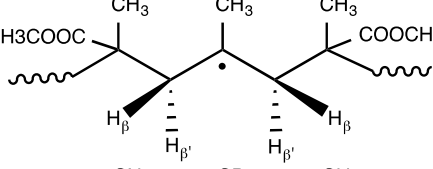
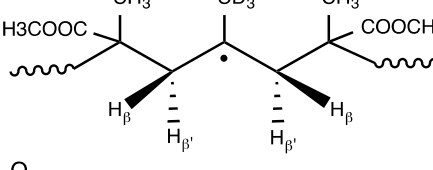
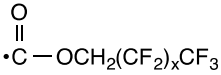


Figure 1.3 (A–E) Experimental TREPR spectra (left) and simulated spectra (right) for main-chain acrylic radicals observed at 0.8 μ s after 248 nm laser flash photolysis for the polymers indicated (see Fig. 1.2 for polymer structures and Table 1.1 for radical structures). (A) PEA, (B) PEMA, (C) PECA, (D) PMMA, (E) PMMA- d_3 , all obtained in propylene carbonate. (F) TREPR spectrum (left, experimental; right, simulated) of the oxo-acyl radical from PFOMA, obtained in the high boiling fluorinated solvent mixture FC-70. For PMMA, the material is isotactic (91% by NMR), but all other polymer samples are atactic material. Simulation parameters (ref. [10]) are listed in Table 1.1.

Table 1.1 Parameters Used to Simulate TREPR Spectra (Fig. 1.3) of Polymer Main-Chain radicals and Oxo-Acyl Radicals, Created Using the Photochemistry Outlined in Fig. 1.1

Acronym	Structure	Hyperfine Constant
PEA radical (1a)		$H_{\alpha} = 21.7 \text{ G}$ $H_{\beta} = 23.5 \text{ G}$ $H_{\beta'} = 23.8 \text{ G}$
PEMA radical (2a)		$\text{CH}_3 = 22.9 \text{ G}$ $H_{\beta} = 15.8 \text{ G}$ $H_{\beta'} = 11.2 \text{ G}$
PECA radical (3a)		$\text{N} = 3.3 \text{ G}$ $H_{\beta} = 16.3 \text{ G}$ $H_{\beta'} = 14.8 \text{ G}$
PMMA radical (4a)		$\text{CH}_3 = 22.9 \text{ G}$ $H_{\beta} = 16.7 \text{ G}$ $H_{\beta'} = 11.2 \text{ G}$
d_3 -PMMA radical (5a)		$\text{CD}_3 = 3.5 \text{ G}$ $H_{\beta} = 16.7 \text{ G}$ $H_{\beta'} = 11.2 \text{ G}$
PFOMA (6b) oxo- acyl radical		$\text{CH}_2 = 3.2 \text{ G}$ $\text{CF}_2 = 0.8 \text{ G}$

observed at high temperature because the signal from this radical decays rapidly due to fast spin relaxation [18]. Compared to PEA, the α -substituent methyl group in PEMA has a large effect on the appearance of the TREPR spectrum. For example, the spectrum resulting from photolysis of PEMA (Figure 1.3B) consists of a 27 line spectrum associated with three separate isotropic hyperfine coupling constants. There is coupling to the methyl group to form a quartet (22.9 G), which is split further into a triplet from one set of diastereotopic β -methylene protons (15.8 G) and another triplet from the other set (11.2 G). Technically, the maximum expected number of observable transitions is 36 (a quartet of triplets of triplets) for the PEMA radical spectrum, but there are accidental degeneracies, leading to a smaller number of observed transitions.

Similar to the α -substituent dependence described earlier, the spectrum from the PECA radical is quite different from the TREPR spectrum of the PEA radical. At a glance, there are five transitions (Figure 1.3C) from coupling to the β -methylene protons, but each peak is further split into three additional lines from the γ -nitrogen ($I=1$) in the nitrile group. From the simulation parameters in Table 1.1, a hyperfine coupling of 3.3 G is assigned to the γ -nitrogen and couplings of 16.3 and 14.8 G are assigned to the β -methylene protons. Figure 1.3D shows the TREPR spectrum of the main-chain polymeric radical from photolysis of i-PMMA along with computer-simulated TREPR spectrum.

We have previously studied the temperature dependence of all three tacticities (isotactic, syndiotactic, or atactic) of main-chain radicals from PMMA and noticed that β -methylene hyperfine coupling constants in the PMMA main-chain radical enjoy a symmetrical relationship because there are stereogenic centers on every carbon atom in the polymer. This relationship is expressed graphically on the right hand side of Figure 1.4 along with the possible main-chain radicals created by UV photolysis. After loss of the ester side chain, the polymeric main-chain

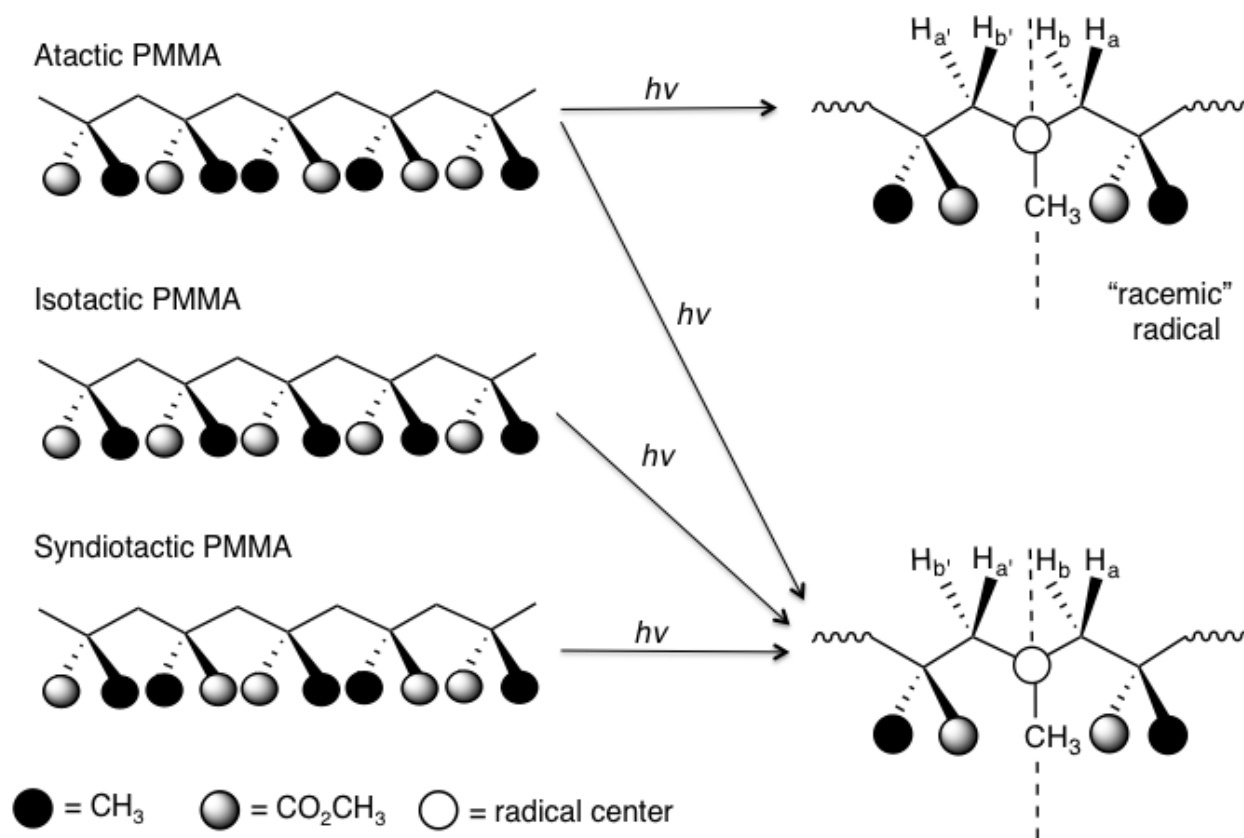


Figure 1.4 Symmetry relationships between the nuclear hyperfine coupling constants in acrylic polymers as a function of polymer tacticity

radicals can exist as either meso radicals or racemic radicals. The fast-motion spectrum of the PMMA radical from i-PMMA, which has a more flexible chain due to its slightly lower T_g than the other two PMMA tacticities, consists of 21 lines attributed to three separate isotropic hyperfine coupling constants. As noted in Fig. 1.3D, the splitting pattern for PMMA is expected to show 36 lines, but a smaller number of transitions are observed, while syndiotactic and atactic PMMA show 27-lines, due to a lifting of an accidental degeneracy. It is also possible that we have not completely reached true “fast motion” at these temperatures for these stiffer polymers. These accidental degeneracies arise because one of the β -methylene coupling constant (11.7 G) is almost exactly half of the value of the methyl proton coupling constant (22.9 G). Figure 1.3E shows the experimental and simulated TREPR spectra obtained during the photolysis of PMMA-d₃, which was used to confirm the assignment of the experimental spectrum from PMMA in Figure 1.3D.

All of the spectra from polymeric radicals shown here exhibit strong net emissive spin polarization from the TM, and none from the Radical pair Mechanism (RPM) or the Spin correlated radical pair (SCRIP) mechanism. As shown in Fig. 1, both main-chain radicals and oxo-acyl radicals are created after photolysis, and these radicals have drastically different diffusional properties in solution. The oxo-acyl radical is small and will diffuse faster than the main-chain radical. This will lead to weak RPM polarization and will completely quench the SCRIP mechanism. The radical-producing reaction here is predominantly from the triplet state and quite efficient, given the rather weak absorbance ($A \sim 0.1$ for our solutions) at 248 nm. In fact, these polymer solutions begin to absorb at about 250 nm, which is just on the edge of the $n-\pi^*$ excitation of the ester carbonyl group. The photochemistry does not create a large amount of radicals with each laser flash, but the triplet polarization they carry must be extremely intense.

It is also of interest to consider why the oxo-acyl radicals are not observed at high temperatures. All of the spectra from the polymeric radicals previously presented and discussed (Figure 1.3A–E) show very intense main-chain radical signals, whereas the oxo-acyl radical signal is weak or absent from the TREPR spectrum at high temperature due to fast spin relaxation. The opposite relative intensities are observed for PFOMA (Figure 1.3F): In this case, the polymeric main-chain radical did not show a fast-motion spectrum even at very high temperatures, and only the oxo-acyl radical from the side chain was observed. This is understandable because of the steric bulk and conformational rigidity of the perfluoroalkyl ester side chains. Also, the fluorinated oxo-acyl radical has a much longer rotational correlation time than its alkyl analog.

1.3 Experimental overview of TREPR

1.3.1 Steady-state EPR (SSEPR) vs. TREPR

Paramagnetic species such as radicals and molecules in the excited triplet state are important intermediate species in photochemical reactions [19]. EPR is one of the desirable tools that give us direct information about their structure and dynamics, and, typically, there are two different techniques which are used: SSEPR and TREPR.

EPR deals with the interaction between electromagnetic radiation and the magnetic moment of one or more electrons with an external magnetic field. In the absence of an external magnetic field, the two spin states of an unpaired electron, with symbols α and β (or with the numbers $M_s = \pm \frac{1}{2}$), are degenerate. In the presence of an applied field, the magnetic moment of the electron aligns itself either parallel ($-\frac{1}{2}$) or antiparallel ($+\frac{1}{2}$) to the field, with the parallel alignment being lower in energy. The separation in energy levels of the two states of the electron (ΔE) is dependent on the strength of the magnetic field and is given by:

$$\Delta E = g_e \beta_e B_0 = h\nu \quad (1.1)$$

where β_e is the Bohr magneton, B_0 is the applied magnetic field, and g is the chemical shift of the electron. These energies are called Zeeman energies, and Figure 1.5 shows the energy level diagram for one unpaired electron in a magnetic field. Transitions can occur between two energy levels (labeled α and β in figure 1.5) via absorption of electromagnetic radiation from a specific magnetic field when the frequency of the microwave (ν) matches the separation energy (ΔE).

The EPR spectrum of a radical is sensitive to the spin state of neighboring nuclei and other nearby electrons [19]. The interaction between an unpaired electron and a neighboring, nuclear-dipole moment causes splitting of the resonance (referred to as the hyperfine interaction) and the resulting splitting in the EPR spectrum is known as the hyperfine structure.

Figure 1.6 shows the energy level diagram of a radical hyperfine interaction with neighboring nuclei for $I=1$. All observable EPR transitions must follow quantum mechanical selection rules, $\Delta M_s = 1$ and $\Delta M_I = 0$, which results in possible transitions for three transitions when $I=1$. The EPR spectrum of a radical is sensitive to the spin state of neighboring nuclei and other nearby electrons [19]. The interaction between an unpaired electron and a neighboring, nuclear-dipole moment causes splitting of the resonance (referred to as the hyperfine interaction) and the resulting splitting in the EPR spectrum is known as the hyperfine structure.

TREPR is a direct detection technique, and the time response of TREPR (50 ns) is about 3 orders of magnitude faster than is that of the SSEPR (40 μ s). For all experiments described in this thesis, a fixed frequency of electromagnetic radiation at 9.5 GHz (X-band) was applied and

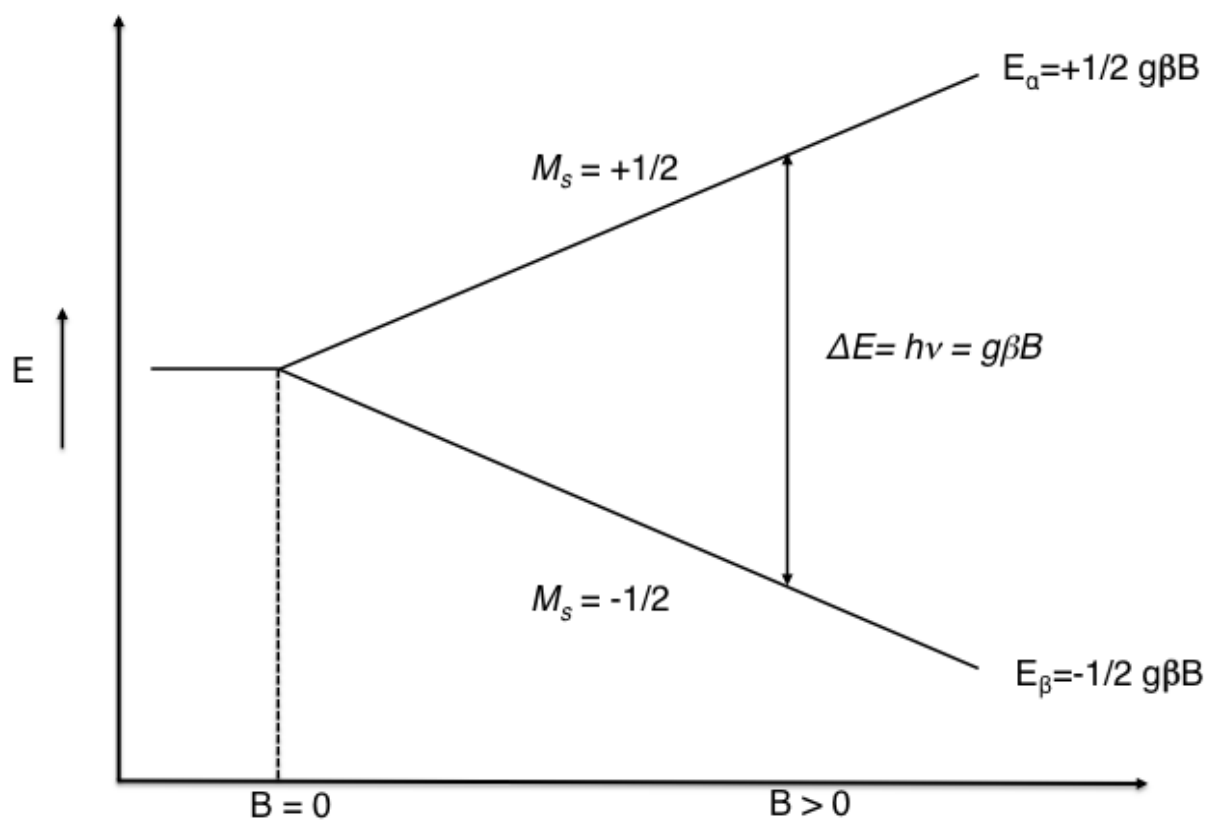


Figure 1.5 Energy level diagram depicting a single spin system in a external magnetic field. When the resonance condition is met, a single observable transition can occur between the two spin states, as shown by the double arrow in the figure

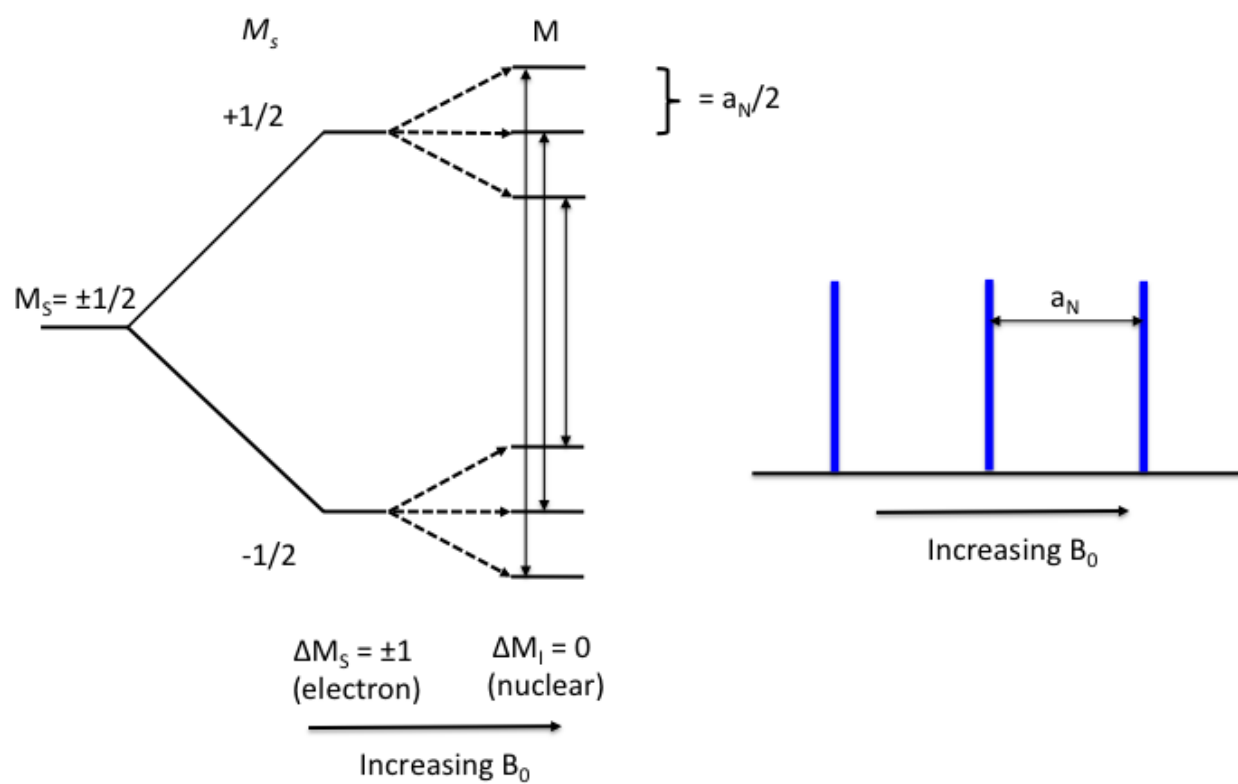


Figure 1.6 Energy level diagram demonstrating the hyperfine interaction and observable transitions of a radical coupled to a neighboring nucleus with $I=1$

the strength of the magnetic field was gradually increased. TREPR uses continuous wave excitation in the same way as a SSEPR spectrometer. A standard “out of the box” commercial instrument operating at X-band will typically use a cylindrical microwave resonator tuned to its resonant frequency with a capillary sample in the center. The EPR transitions are detected by sweeping an external magnetic field B_0 (provided by an electromagnet with a range of 0 to ~ 6 kG) through each resonance at a constant microwave frequency ω_0 [19].

A key feature that separates the SSEPR experiment from any others is that the external field is modulated as it is swept, usually at a frequency of 100 kHz, so that phase-sensitive detection can be used to increase the signal-to-noise (S/N) ratio. The resulting spectra have first-derivative line shapes, which often help to improve spectral resolution (Figure 1.7). Care is taken to keep the amplitude of the field modulation smaller than the line widths of the signals to avoid line shape distortions. A consequence of the use of 100-kHz field modulation is that the time response of the spectrometer becomes limited to, at best, the inverse of the modulation frequency. Practically, for good S/N, three or four cycles of modulation are necessary, which means that species with chemical lifetimes less than about 40 μ s become difficult to detect. Since most organic radicals have lifetimes in solution on the order of 10–100 μ s, their detection can be problematic when using SSEPR at room temperature.

The “direct detection EPR” or Time-resolved (CW) EPR is distinguished from SSEPR methods. The term “direct detection” arises from the fact that the 100-KHz field modulation employed in SSEPR is bypassed and instead the EPR signal coming directly from the spectrometer’s microwave bridge preamplifier circuit is sampled electronically on short timescale after its creation. The method finds a balance between sensitivity (about the same as SSEPR in terms of radical concentrations in liquids) and time response (about 50 ns at X-band

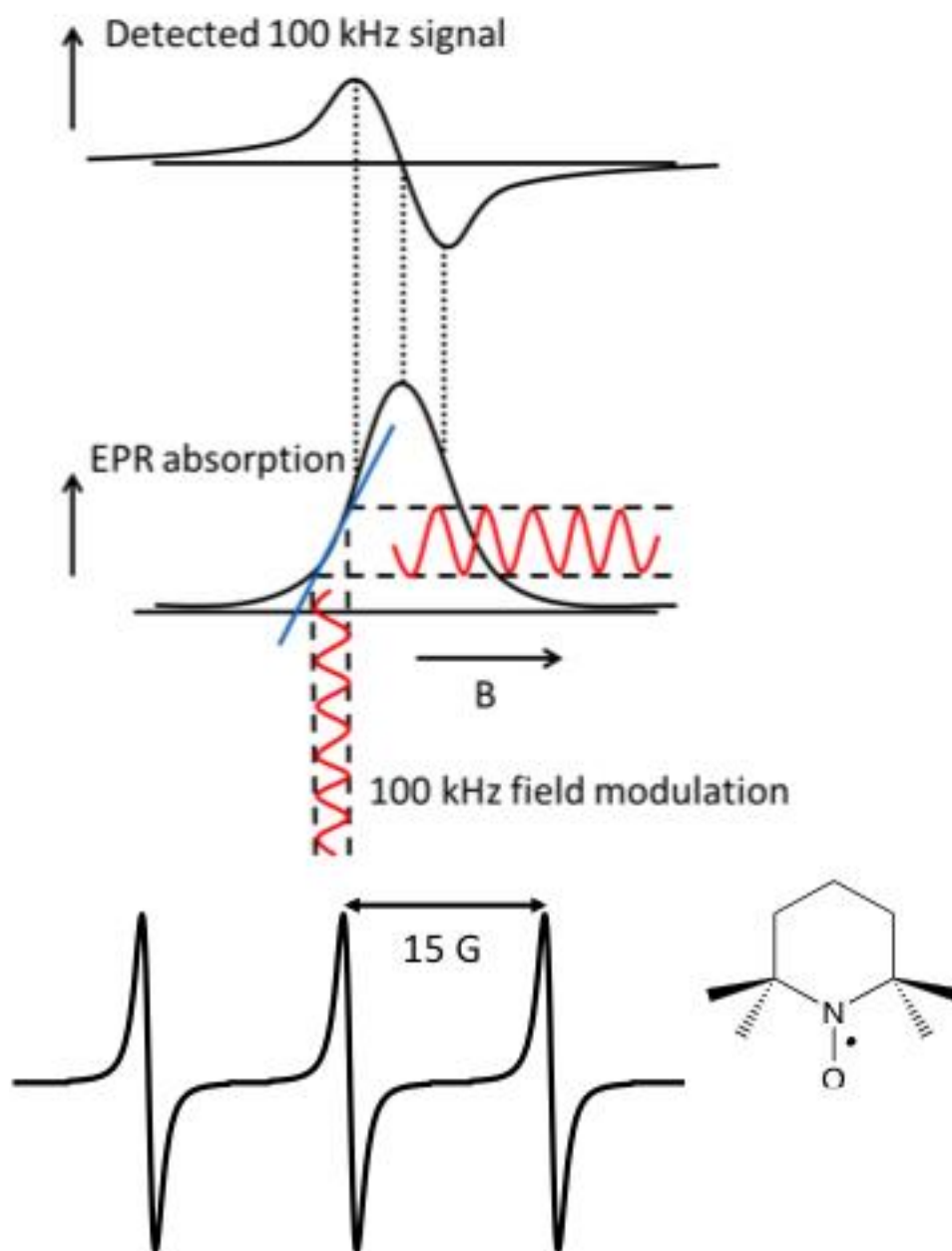


Figure 1.7 Steady-state EPR detection using 100 kHz field modulation and the resulting first derivative line shape

and 10 ns at Q-band, three orders of magnitude faster than SSEPR). The time response at X-band is generally limited by the resonator quality factor (more on this later). The TREPR method is most useful for obtaining high-resolution EPR spectra of organic free radicals in the sub-microsecond time domain without the restriction on spectral width associated with pulsed methods.

In addition, a major advantage of the direct detection TREPR technique is the observation, on the timescale of typical free-radical electron spin relaxation times (0.1–10 μ s), of several chemically induced spin polarization processes that give insight into the mechanism of the reaction that generated the radicals, their motional dynamics (both intra- and intermolecular), and other characteristics regarding the photochemical precursors such as their spin multiplicity.

1.3.2 Experimental considerations for TREPR

Figure 1.8 shows how the components for TREPR experiments are arranged and connected to the commercial instrument [20].

In addition to an operational EPR spectrometer (commercial or home-built), the TREPR experiment requires the following instrumentation: a pulsed laser to initiate radical reactions along with any required optics to guide the beam into the resonator, a boxcar signal averager or transient digitizer for trapping the EPR signal on the sub-microsecond timescale, a computer interface to the spectrometer to collect field-swept EPR data, a fast photodiode for observation of the laser pulse, an oscilloscope to monitor the timing of the experiment, and a pulse delay generator to control the timing of the laser pulses and fast signal detection. Other useful additions include a micro pump for flowing samples, a source of dry nitrogen gas for purging the samples as they are circulated, and a quartz flat cell to maximize the sample volume exposed to the laser

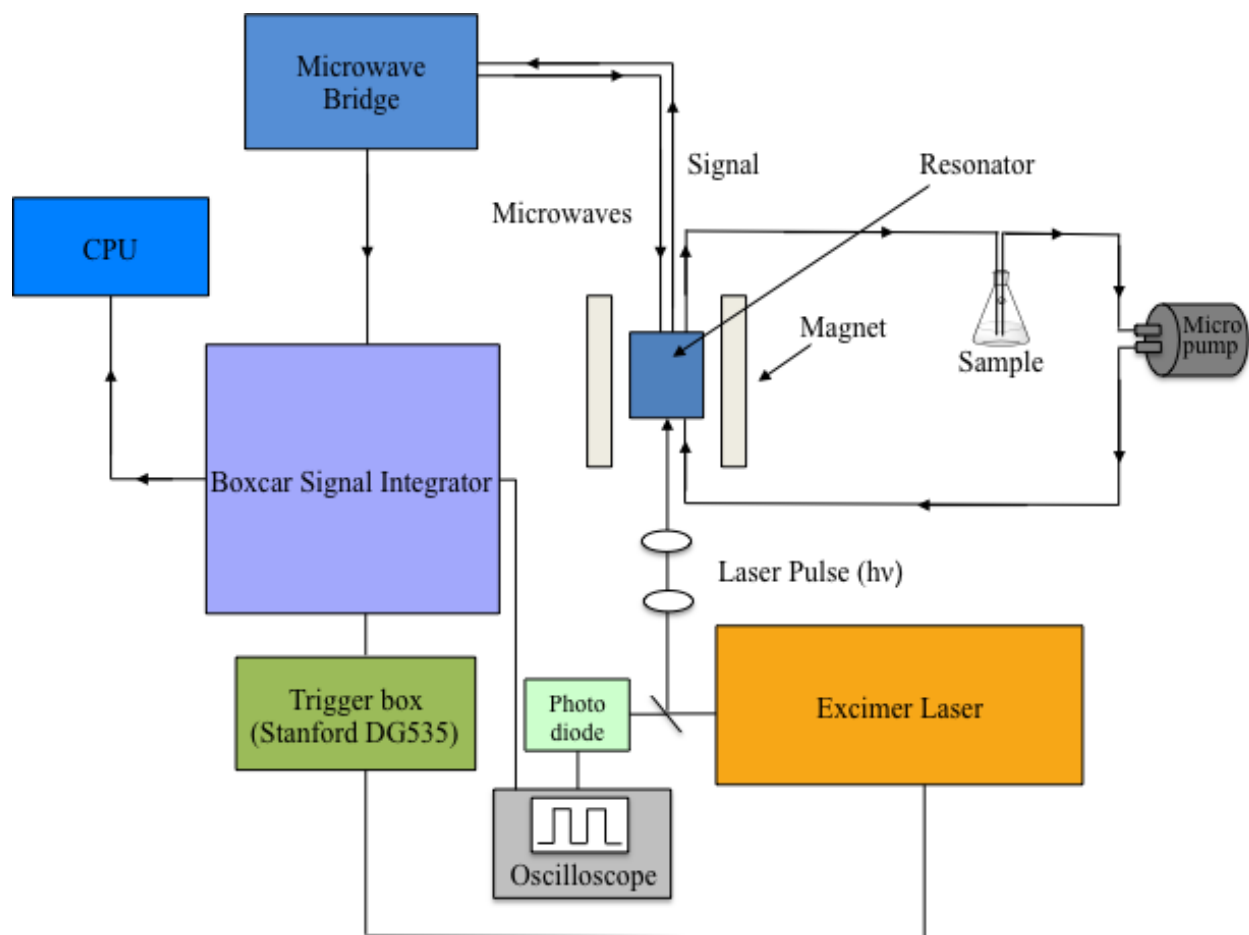


Figure 1.8 Block diagram of the TREPR experiment using a boxcar signal averager

beam (the flat cell also allows for the experiment to be conducted with high dielectric solvents such as water). A mechanism for heating or cooling the sample as it enters or exits the EPR resonator can be desirable.

It is instructive to outline the timing sequence for the various electronic components and discuss how they affect the overall performance of a TREPR experiment. Such a sequence is shown in Figure 1.9. For the TREPR experiment, the external magnetic field sweep, which is controlled either internally by clock pulses in the spectrometer or externally by a computer-generated ramp. In either case, the field sweep is divided up into a certain number of data points (in our instrument 1000 points) that can be saved, along with the TREPR signal intensity at that point, as an x - y array in the computer.

The timing sequence originates from a pulse generator (in our case, a Stanford DG535 digital delay generator providing TTL output pulses), from which the laser and boxcar (or digitizer) are triggered. The repetition rate of the experiment is 60–100 Hz for an excimer laser and 10–30 Hz for a Nd:YAG laser, with the actual rate depending on the laser model in each case. Typical sweep times are 2 or 4 min with the laser repetition rate set at 60 Hz. This means that in a 4-min scan, there are $60 \text{ s}^{-1} \sim 240 \text{ s}/1000 \sim 14$ laser flashes per magnetic field data point. The sampling gates are 100–300 ns wide, with one positioned in front of the laser flash to collect the dark EPR signal and one after the flash to collect the light+dark signal. Subtraction of the two gate voltages gives the light induced TREPR signal. The fast photodiode allows the laser flash to be observed on the oscilloscope so that the boxcar gates can be properly positioned.

It is important to note here two disadvantages of the TREPR technique. It is not generally possible to observe a Boltzmann (equilibrium) population of spin states using the boxcar method, because of the $1/f$ noise. Also, lifetime broadening effects are observed when the second boxcar

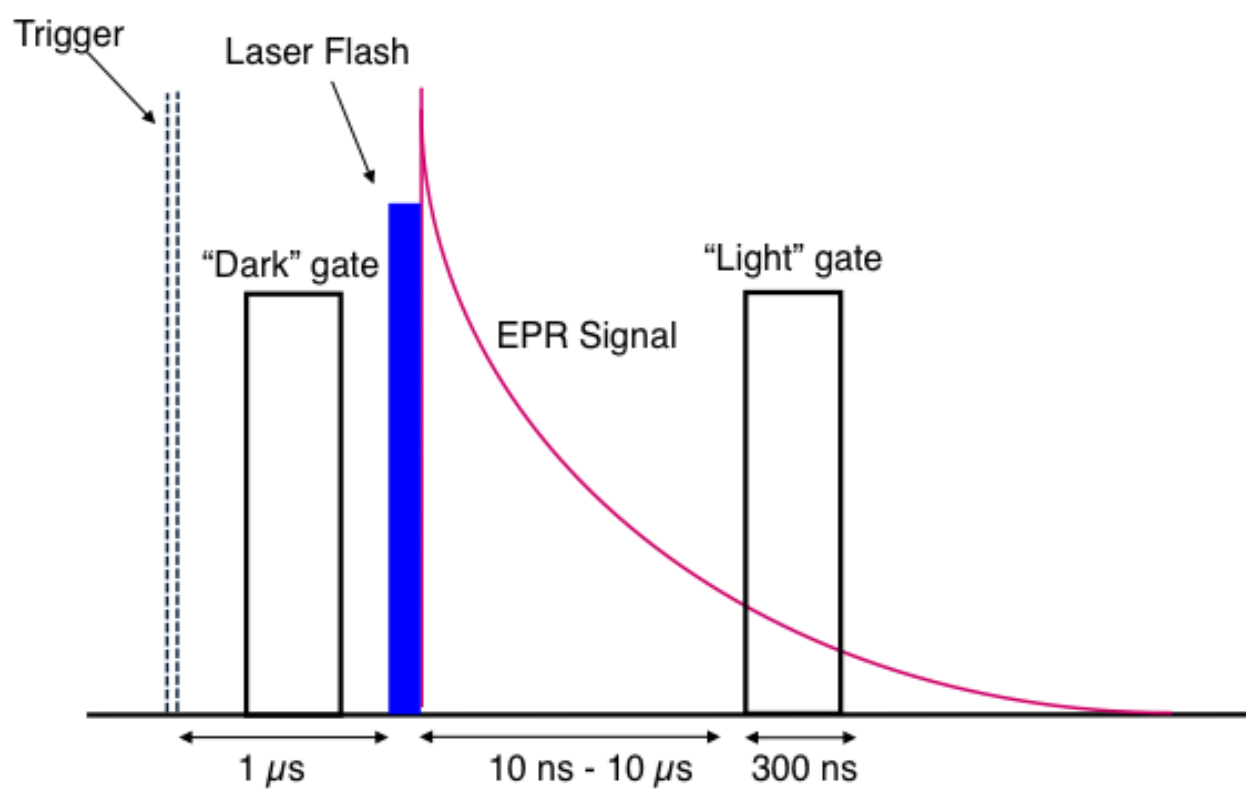


Figure 1.9 Timing sequence for the TREPR experiment using a boxcar signal averager

gate is placed close in time to the laser flash. This is a consequence of having the microwave excitation running continuously in TREPR. Near the laser flash, and during the photochemical events that produce radicals, the apparatus is attempting to excite spin states that are still in the process of forming. As stated earlier, small interactions such as hyperfine couplings take time to evolve and may not be visible in the TREPR spectrum for several hundreds of nanoseconds after the laser flash. When structural information about an unknown radical is desired, it is important to collect spectra at multiple delay times to make sure maximum spectral resolution has been achieved.

1.4 Chemically Induced Electron Spin Polarization (CIDEP) Mechanisms

In spectroscopy, it is common for transitions to be observed as absorptive lines because the Boltzmann distribution, at equilibrium, ensures a higher population of the lower state than the upper state (Figure 1.10 A). Examples where emission is observed, which are by definition non-equilibrium situations, are usually cases where an excess population is created in a higher energy level by adding energy to the system from an external source such as photolysis. CIDEP phenomena in EPR spectroscopy can show both enhanced absorption (greater absorptive signal intensity than predicted by the Boltzmann factors) and emission in the observed spectra. (Figure 1.10 B) What makes the non-Boltzmann populations observed in TREPR experiments so unusual is that, in some cases, electron- and/or nuclear spin dependent chemical reactions (homolytic bond breaking or forming) are responsible for the process. While it requires energy to break a chemical bond, once it is broken, the mixing of spin wave functions in the resulting radical pair (RP) is all that is necessary to make some NMR and EPR transitions appear with the so-called spin polarization.

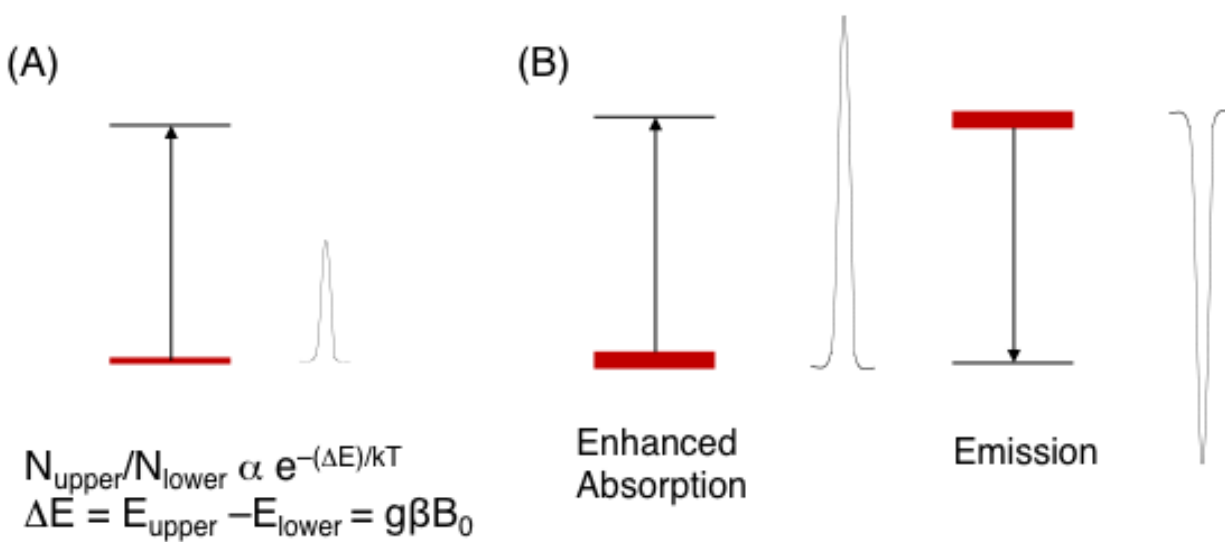


Figure 1.10 (A) Energy level diagram of a single electron in the magnetic field with population distribution in these two level (B) Spin polarization: Enhanced absorption and emission observe because excess population is created in a higher energy level by putting energy into the system from an external source such as photolysis

The idea that the nuclear spin state energy-level differences (which are much smaller than kT at room temperature) could be responsible for different chemical reaction rates was revolutionary and somewhat controversial, especially with the observation of the nuclear spin polarization phenomenon (CIDNP) in NMR spectroscopy. As more and more experiments were performed to investigate this phenomenon, the idea rapidly gained acceptance and in fact helped connect solution dynamics of small molecules to spin quantum mechanics in a very natural and informative way. Later on in the development of CIDEPR theories, the requirement for chemical reaction to take place was lifted - many of these cases will be presented in this work.

CIDEPR phenomena are observed in most TREPR-detected photochemical reactions that produce radicals, radical ions, or biradicals. Indeed, it is from CIDEPR that some of the sensitivity is regained that was lost in bypassing the phase-sensitive detection unit (100 kHz field modulation) is regained.

An additional improvement in TREPR sensitivity comes from the use of the boxcar to signal average. In all of the TREPR spectra shown in this dissertation, transitions below the baseline are in emission (E), while those above the baseline are in enhanced absorption (A). This is different from conventional SSEPR spectra, which, as noted in Figure 1.7, are displayed as first-derivative curves representing the change in detected intensity with the external field.

There are four well-known CIDEPR mechanisms: the Triplet Mechanism (TM), the Radical Triplet Pair Mechanism (RTPM), Radical Pair Mechanism (RPM), Spin Correlated Radical Pair Mechanism (SCRPM). The spectra presented in this dissertation exhibit polarization from the TM and RTPM, and the following two sections of this chapter will briefly outline the basic phenomenon of these two types of CIDEPR mechanisms and provide an example of each mechanism that highlights the specific spectral features.

1.4.1 The Triplet Mechanism (TM)

The TM is often considered to be the simplest CIDEP mechanism [21]. Qualitatively, the mechanism is outlined in Figure 1.11, which suggests that the intersystem crossing (ISC) process, usually by spin-orbit coupling, from excited singlet state (S_1) to excited triplet state (T) in the organic molecules will populate the triplet spin states T_X , T_Y , and T_Z differently even in the absence of a magnetic field.

The labels T_X , T_Y , and T_Z represent the triplet state energy levels in the molecular coordinate system (frame of reference); these are known as the zero-field basis functions. Because spin orbit coupling is anisotropic in this frame, the T_Z spin state is overpopulated in Figure 1.11 (thicker bars represent higher populations) during ISC process, and this excess population is then transferred to the spin state T_+ ($=|\alpha\alpha\rangle$) of the laboratory frame of reference (in which the Z-axis is directed along the applied magnetic field of the spectrometer). The net polarization of the electron spins in the triplet, created during the spin-orbit coupling (SOC) process from S_1 to T, is transferred to the radicals resulting from photochemical reactions of the triplet. Over time, the populations of the spin states of the triplet relax to their Boltzmann equilibrium values. Experimentally, it is observed that all of the resonance lines of both radicals in the TREPR spectrum of such systems are polarized equally and either are polarized positively (enhanced absorption, A) or polarized negatively (emission, E). Several examples of TM will be discussed in chapters 2 and 3. Most TREPR spectrum of polymer main chain radicals discussed in those two chapters show net emissive polarization.

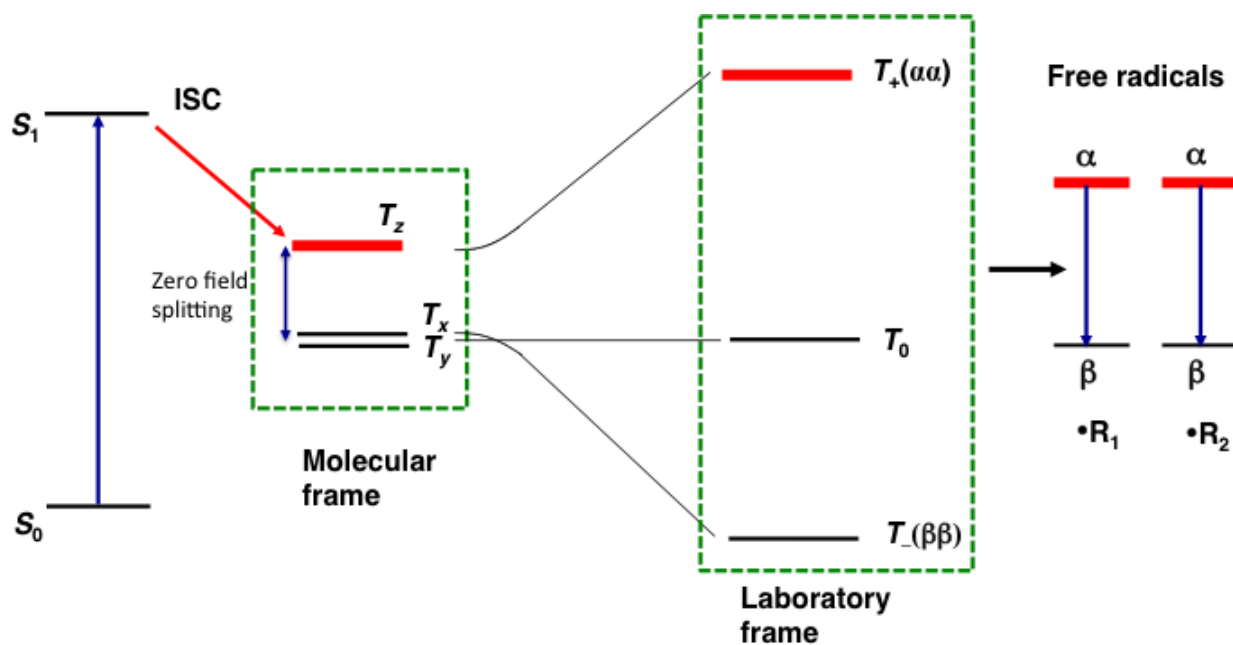


Figure 1.11 The TM of CIDEP. (A) Photoexcitation of an organic molecule from its ground state to the first excited singlet state, ISC by spin-orbit coupling to the first excited triplet state (a spin-selective process) in the molecular frame, transformation to the laboratory frame, and reaction of the spin-polarized triplet state to create free radicals, in this case with net emission. A change in the sign of the zero-field splitting parameters can lead to a change in the phase of the TM to net absorption

1.4.2 The Radical-Triplet Pair Mechanism (RTPM)

The quenching of excited states by molecules has been extensively investigated on photochemical and physical processes, such as energy transfer, triplet-triplet annihilation, and quenching by radicals. In particular, the system which includes excited triplet state quenching by free radicals, shows CIDEP effects which are observable by TREPR.

Two mechanisms have been proposed to explain the polarization associated with triplet-doublet (T-D) systems; one is a radical triplet pair mechanism (RTPM), and the other is an electron spin polarization transfer (ESPT) mechanism.

The radical-triplet pair mechanism (RTPM) of CIDEP, as its name implies, for its polarization requires an interaction between an excited molecular triplet state and a free radical, usually a stable nitroxide structure. The participation of a stable radical is not a requirement for the appearance of the RTPM, nor is the phenomenon restricted to liquid solution. In some photochemical reactions, a large concentration of excited triplet states are produced, leading to spin-spin interactions between the excess triplets and the unstable free radicals produced from previous reactions. The polarization mechanism itself is explained as follows: In free solution, encounters between molecules (M) in their electronically excited singlet ($^1M^*$) or triplet ($^3M^*$) states with radicals (R) in their ground doublet state (2R) result in either enhanced intersystem crossing (EISC) or deactivation of the electronic excitation. The quenching reaction of an electronically excited triplet state with free radicals splits the quartet (Q) and doublet (D) spin states of a “radical-triplet (RT) encounter complex” with exchange interaction, J :





In the non-adiabatic potential surface, where free radicals have no electron spin polarization because four quartet spin states are equally populated after dissociation, but Reaction (1.2) is possible has never been conclusively observed. Relying on numerous transient optical absorption spectroscopy experiments [22–27], it was concluded that quenching reactions (1.3) and (1.4) occur at diffusion-controlled rates if the electronic energy of the excited molecular triplet state is higher than the energy of the doublet excited state of the radical. In other words, quenching is effective when it is followed by energy transfer (reaction 1.4) and is ineffective when energy transfer is impossible (reaction 1.5). Reactions (1.3)–(1.5) are collectively called the EISC processes shown in figure 1.12 and 1.13.

Imamura et al. [28] discovered that stable nitroxide radicals that encounter excited molecular triplet states can develop ESP (electron spin polarization). This phenomenon has been confirmed in numerous other experimental studies [29–33] and is now included in the CIDEP family with two separate abbreviations: RTPM and ESPT (electron spin polarization transfer). These are used to differentiate between two possible mechanisms for the generation of ESP.

The RTPM polarization is determined by the multiplicity of an excited state (S_1 or T_1) and the sign of an exchange parameter, J , between the triplet and the radical. On the other hand, in the case of ESPT, the spin polarization of the excited T_1 state via a spin-selective ISC is transferred to a stable radical via an energy transfer or a spin exchange interaction, and the overpopulation of the higher energy spin level of the stable radical (for TEMPO, α spin level),

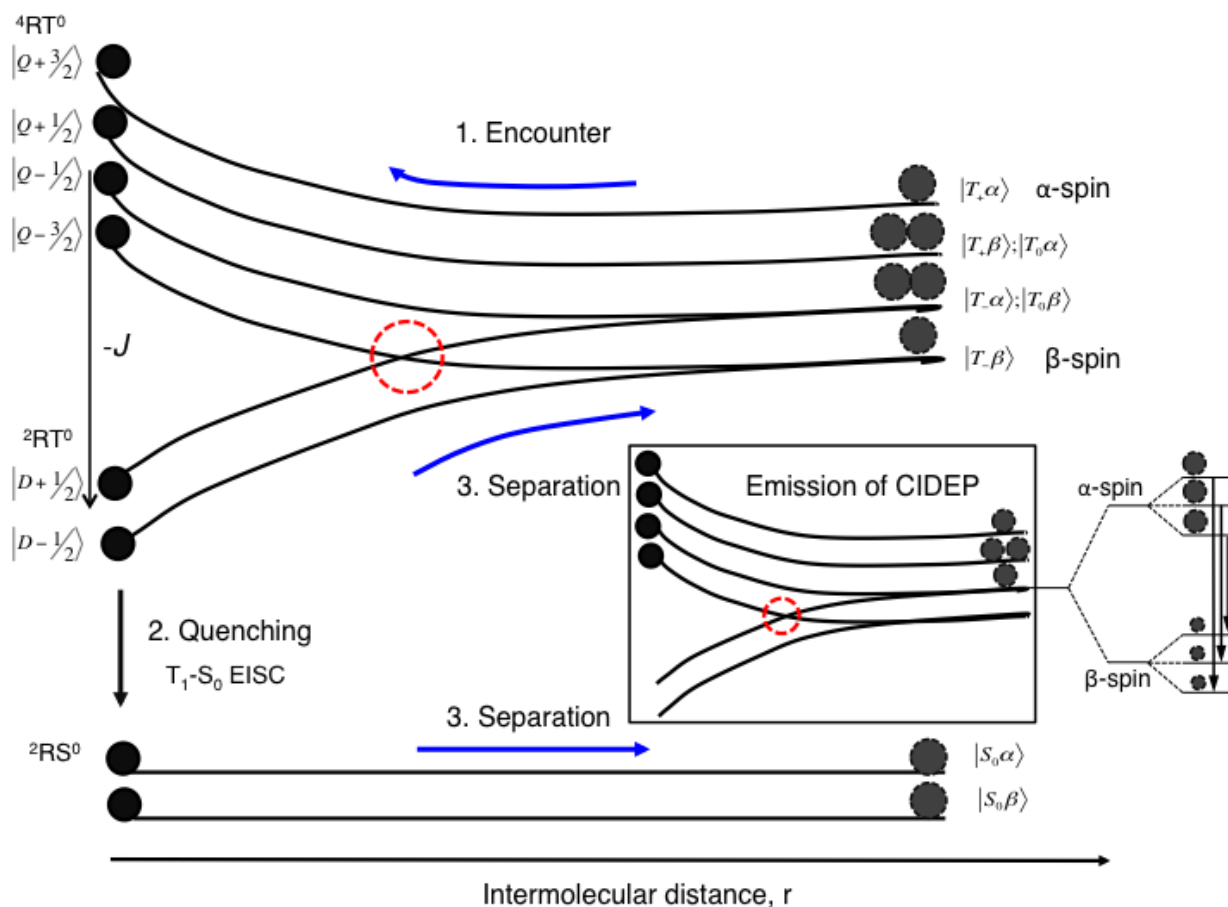


Figure 1.12 Energy levels of a radical-triplet pair as a function of their separation. Schematic explanation of net emission CIDEP created by excited triplet quenching by stable free radical. The red circles show the mixing region where RTPM polarization is generated. The black dots represent the population. 1. Encounter, 2. Quenching and 3. Separation steps. The quartet ($^4RT^0$) and doublet ($^2RT^0$) spin states are energetically separated by intermolecular exchange interaction, J . After the separation of the residual $^4RT^0$ pair, β -spin is enriched on stable radical.

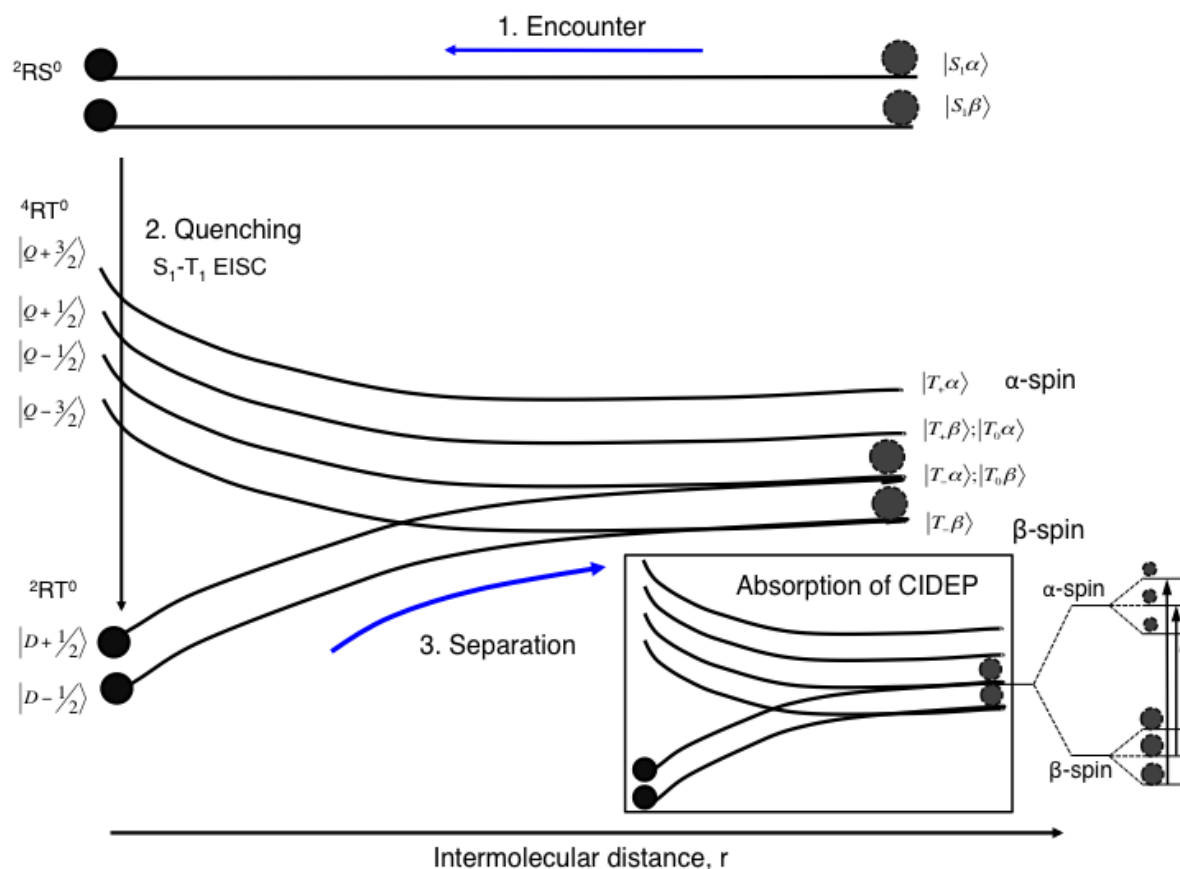


Figure 1.13 Energy levels of a radical-triplet pair as a function of their separation. Schematic explanation of net absorption CIDEP created by excited singlet quenching by stable free radical. The black dots represent the population. 1. Encounter, 2. Quenching and 3. During the separation of the $^2RT^0$ encounter pair, spin state mixings at the level crossings proceed then β -spin is enriched on stable radical

and the overpopulation of the this level results in the observation of emission in the observed TREPR spectrum.

As shown in the figure 1.12, neglecting the Boltzmann spin polarization, we can assume that when a molecular triplet collides with a stable nitroxide radical, the resulting Radical-Triplet (R-T) (or collision complex) pair creates six equally populated electron spin states a molecular triplet collides with a stable nitroxide radical, the resulting Radical-Triplet (R-T) (or collision complex) pair creates six equally populated electron spin states $\{|T_+\alpha\rangle, |T_+\beta\rangle, |T_0\alpha\rangle, |T_0\beta\rangle, |T_-\alpha\rangle, |T_-\beta\rangle$. At the distance of closest approach (R) between the radical and the triplet state, the exchange interaction dominates all of the magnetic interactions in the R-T pair. The electronic spin levels of the system can be labeled according to the total spin $F=T+D$, resulting in four quartet spin states: $|Q_{+3/2}\rangle, |Q_{+1/2}\rangle, |Q_{-1/2}\rangle, |Q_{-3/2}\rangle$ and two doublet spin states $|D_{+1/2}\rangle$ and $|D_{-1/2}\rangle$, the latter two being lower in energy than the former four if the J is negative (Fig. 1.12). The doublet states are depopulated because of quenching reaction (1.4) earlier. If the exchange interaction is the only interparticle interaction, the $|D_{+1/2}\rangle$ spin state of the R-T complex correlates with the $|T_+\beta\rangle$ state of the separated R-T pair, and the $|D_{-1/2}\rangle$ correlates with the $|T_-\alpha\rangle$ state. For this reason, spin-selective quenching does not lead to ESP. However, the spin-spin dipolar interaction between the electron spins located in the triplet (ZFS) does not commute with the Hamiltonian of the R-T pair, the elements of which are coupled by the exchange interaction. This creates mixing of the spin states in the vicinity of the avoided crossings of the spin states, which are the circled points in Fig. 1.12.

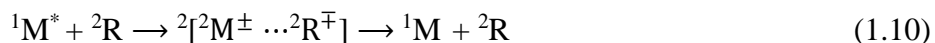
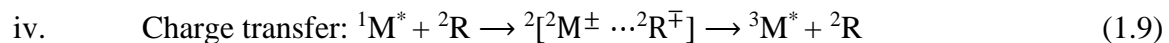
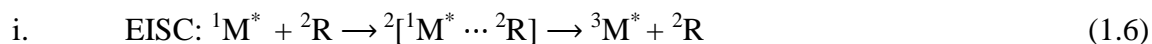
As a consequence, the spin states $|Q_{-1/2}\rangle$ and $|Q_{-3/2}\rangle$ become involved in depopulation because of quenching through mixing with the spin states $|D_{+1/2}\rangle$ and $|D_{-1/2}\rangle$, and the remaining two quartet states $|Q_{+3/2}\rangle$ and $|Q_{+1/2}\rangle$, which correlate with the $|T_+\alpha\rangle$ and $|T_0\alpha\rangle$ spin states,

remain passive.

This increases the population of the $|T_+\alpha\rangle$ and $|T_0\alpha\rangle$ spin states of the separate R-T pair, creating an excess of the $|\alpha\rangle$ spins located in the radicals. In the TREPR experiment, this depopulation process manifests itself as emissive polarization in the three-line nitroxide radical signal. It should be noted that a corresponding correlation diagram for a positive exchange interaction (quartets with lower energy than the doublet spin states) could be constructed in a similar fashion and leads to radicals that have escaped from the R-T encounter with positive polarization (enhanced absorption) as shown in figure 1.13.

Evans [34] was the first to discover that strongly forbidden singlet–triplet UV optical absorptions in aromatic molecules can be induced by paramagnetic substances, particularly oxygen. Later, Hoijsink [35] and Murrell [36] proved that the intermolecular exchange interaction was a driving force for this $^1M^* \rightarrow ^3M^*$ EISC in electronically excited molecules.

There are five general spin-allowed reactions of 2R with electronically excited singlet molecules $^1M^*$:



Among these possible processes, EISC $^1M^* \rightarrow ^3M^*$ (reactions 1.6 and 1.9) are the most effective [37,38]. Reaction (1.7) is followed by the generation of ESP [39,40]. The ESP generated in processes (1.6) and (1.7), they are called QP RTPM and DP RTPM, respectively. For a negative

exchange interaction, QP RTPM always results in emissive net polarization of radicals, and the DP RTPM mechanism results in positive polarization. The notable examples of RTPM will be discussed in Chapter 4. The radical-triplet pair interactions can be used to investigate the dynamics of acrylic polymers in dilute solution. By incorporating a nitroxide into the polymer chain via covalent bonds, we can generate RTPM polarization via *intramolecular* encounters that depend on several structural and physical features of the polymer/solvent system. The magnitude of this polarization is directly proportional to the number of encounters made between the stable radical and the excited triplet state, and is therefore an indirect measure of the rate of intra-chain contact between the two sites.

Chapter 2. Photochemistry of acrylate-POSS block copolymers and dynamic effects in copolymer radicals

2.1 Introduction

As discussed in Chapter 1.4.1, the degradation of acrylic polymers has been a subject of intense study in our laboratory for the past decade, and our TREPR techniques are powerful enough to investigate the photochemical and photophysical properties of acrylic homopolymers. The creation of carbon-centered radicals within the main chain of an acrylic homopolymer provides a means to investigate the conformational energy landscape using a highly localized, minimally perturbative spin probe.

Because the electron-nuclear hyperfine interactions in the main chain radical depend on the dihedral angle between the p orbital containing the unpaired electron and the neighboring C-H sigma bond, the TREPR spectra of these main chain radicals show a strong temperature dependence on both line widths and line positions. Changes in line width are related to the “jump time” between conformations, while changes in line position (at constant width) reflect changes in the populations of certain rotational conformers (“rotamers”). Additionally, alternating hyperfine line width effect is shown in lower temperature spectra of acrylate polymers because system involves dynamic effects due to conformational motion. As mentioned in chapter 1.4.1, polymer tacticity plays a strong role in both the overall spectral appearance and in the temperature-dependent line broadening processes.

For this reason, the observed TREPR spectra are rich in information regarding the

conformational landscape of the polymers. Furthermore, because the photochemistry involved in these studies is destructive, characterization of the observed free radicals can offer insight into the degradation mechanism of acrylates in solution with high spectral resolution and unambiguous assignment of the reactive intermediates involved. However, the photodegradation mechanisms of block copolymers are not yet fully understood because the dynamics of block copolymer chains are expected to be much more complicated than that of the homopolymer.

The polyhedral oligosilsesquioxane (POSS)-based polymers, one of the most studied inorganic-organic hybrid copolymers, are of significant interest, with diverse potential applications such as biomaterial [41], molecular optics [42], electronics [43], and coatings and films [44]. This is because they show unique physical properties such as a high modulus, a high resistance to oxidation and an increased stability to UV light compared to other acrylic structures.

In this chapter, we will discuss the photochemistry of several acrylate-POSS block copolymers that have not been investigated before and we will show novel degradation pathways, the relationship between degradation stability and microstructure, and interesting chain dynamics. Before going into detail regarding the TREPR results of these POSS-based copolymers, it is useful to present some background on previous studies on acrylate-POSS polymer degradation, including the structure of both POSS and POSS based polymers.

2.1.1 POSS and POSS based Polymers

The properties of these hybrid polymers rely on the quality and nature of inorganic fillers (nm or μm) embedded in the polymer matrix and in order to minimize the total surface energy, these nano-scale inorganic particles tend to aggregate in the polymer matrix. Several studies have been conducted to create well-dispersed hybrid polymers and solutions [42,45], e. g.:

- 1) By modifying and incorporating inorganic fillers into organic groups via covalent bonds; or,
- 2) By using melt-mixing or in-situ polymerization to improve compatibility between the inorganic and the polymer matrix

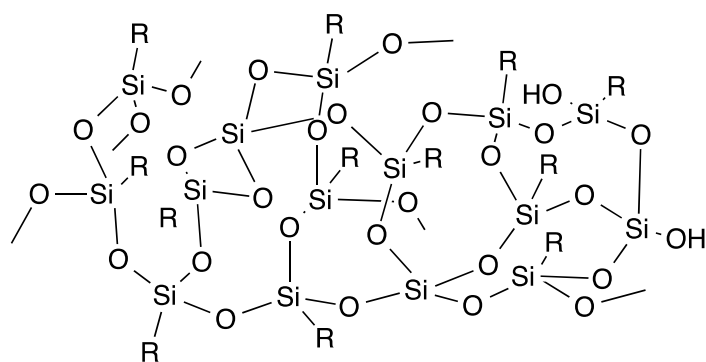
By using the former method, POSS can be produced and the inorganic fillers naturally disperse into the matrix.

POSS is one of many kinds of silsesquioxane molecules. The term silsesquioxane refers to the chemical structures following the basic composition of $(\text{RSiO}_{1.5})_n$, n is typically 8, 10, 12, 16, 17. Here, the R-group, also called the vertex group for polyhedral molecules, may be hydrogen, alkyl, alkylene, and aryl arylene among others⁶.

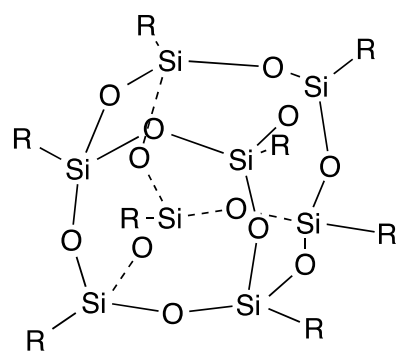
The molecular architecture of silsesquioxanes can be classified into two categories: (a) non-caged structure and (b) caged structure (the most prevalent structure shown in Figure 2.1). Only caged silsesquioxanes are usually called POSS and these are well-defined, highly symmetric molecules. POSS molecules with an inorganic core composed of silicon-oxygen ($\text{R}_8\text{Si}_8\text{O}_{12}$) are the most common structures used in studies of physical and photochemical properties.

The overall performance of POSS base polymers relies on how POSS moieties are incorporated into the polymer chains, and this in turn affects the local molecular interaction and chain mobility. Highly symmetric POSS molecules are tethered to eight organic groups including methyl, isobutyl and phenyl, which surround and are bonded to the silicon vertices [46].

One or more corner groups can be substituted by functional groups, such as methacrylate, butyl methacrylate, acrylate, or styrene to produce POSS based polymers with the structure shown in Figure 2.2 [47,48].



(non-caged structure)



(caged structure)

Figure 2.1 Chemical structures of silsesquioxanes. non-caged (left) vs. caged (right)
silsesquioxanes

In 1946, Scott successfully synthesized well-defined POSS structures, after which the Air Force Research Lab developed a series of linear random and block POSS structures containing copolymers [49]. So far, research on POSS-based polymer and copolymers has continued in several research labs, but especially at the Air Force Research Lab due to an interest in their development as aerospace coatings [50-52].

2.1.2 Degradation studies of POSS-based Polymer

Common polymers such as acrylate polymers can be easily degraded by interactions with UV-light [53] and under high temperature [54], so it can be undesirable to use these polymers in outdoor applications such as architectural coatings or packaging materials that may be exposed to light. Several studies have been undertaken to understand the mechanism of degradation so that the degradation of such polymers can be controlled by means of additives and/or modifications to the structure of polymer. One attempt incorporated inorganic nanofillers in a polymer chain similar to the POSS-based polymer. This approach makes the polymer thermally and chemically robust, to such an extent that one of the promising applications of POSS-based polymers is for use in the highly oxidizing environment of orbiting space vehicles [55,56]. Accordingly, the photo-stability of polyolefin-based nanocomposites including POSS polymers is a very important and desirable asset that may positively contribute to the resolution of a wide range of industrial challenges.

The study of the degradation mechanism in POSS based polymers has been carried out mainly on thin films or solid state under a variety of experimental conditions mostly, focusing on

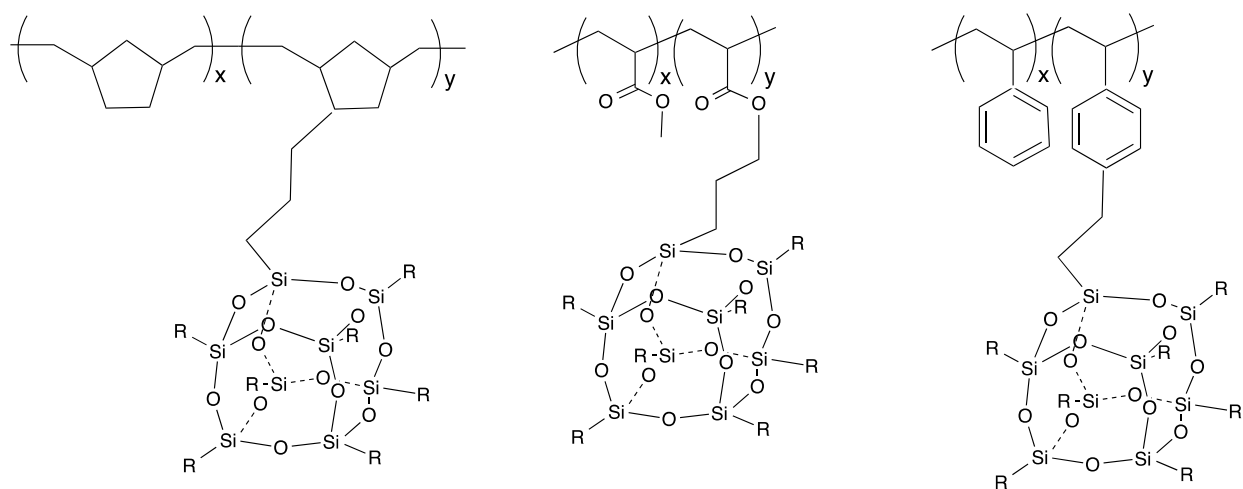


Figure 2.2 Schematic drawing of chemical structures of POSS-based polymeric nanocomposites: (left) norbornyl-POSS copolymers; (middle) methacrylate-POSS copolymers and (right) styryl-POSS copolymers.

the thermal degradation of these polymers.

Bolln et al. [57] found that increasing the substitutes of alkyl (from C₂ to C₁₀) improved the thermal properties of POSS when the polymers were subjected to thermogravimetric analysis (TGA). Fina et al. [58] reported the mechanism of thermal degradations of octa-isobutyl POSS, hydrogen POSS, methyl POSS, phenyl POSS and vinyl POSS. The thermal degradation of octyl trisilanol POSS under conditions where heat was applied and isothermal conditions was studied by Zeng et al. Blanco et al. [59] conducted a thermal study on phenyl, hepta isobutyl-polyhedral oligomeric silsesquioxane/polystyrene nanocomposites by varying POSS concentration (3, 5, and 10%) under both inert (flowing nitrogen) and oxidative (air) atmospheres.

However, there is only one published report of the effect of POSS on the photo-induced oxidation and aging of POSS-containing organic polymeric matrices. In this study, Schwab et al. [60] investigated the photo-oxidation behavior of polystyrene (PS) incorporating several structures of POSS and PS-POSS copolymer and proved that POSS molecules in contact with polystyrene confer the advantages of UV resistance (indeed there is no published report on the photodegradation mechanisms of POSS-base polymers especially, acrylate-POSS copolymers).

In this chapter, results will be presented on the photodegradation of acrylate-POSS copolymers at 248 nm as a function of temperature, side chain structure and POSS concentrations. The dynamic effect that makes the spectra complex and unusual in appearance at high temperature will be presented and discussed. Finally, simulating the spectra will be necessary to complete characterization of the radicals.

2.2 Results and discussion

Figure 2.3 shows the structure of the different POSS-based acrylate copolymers and

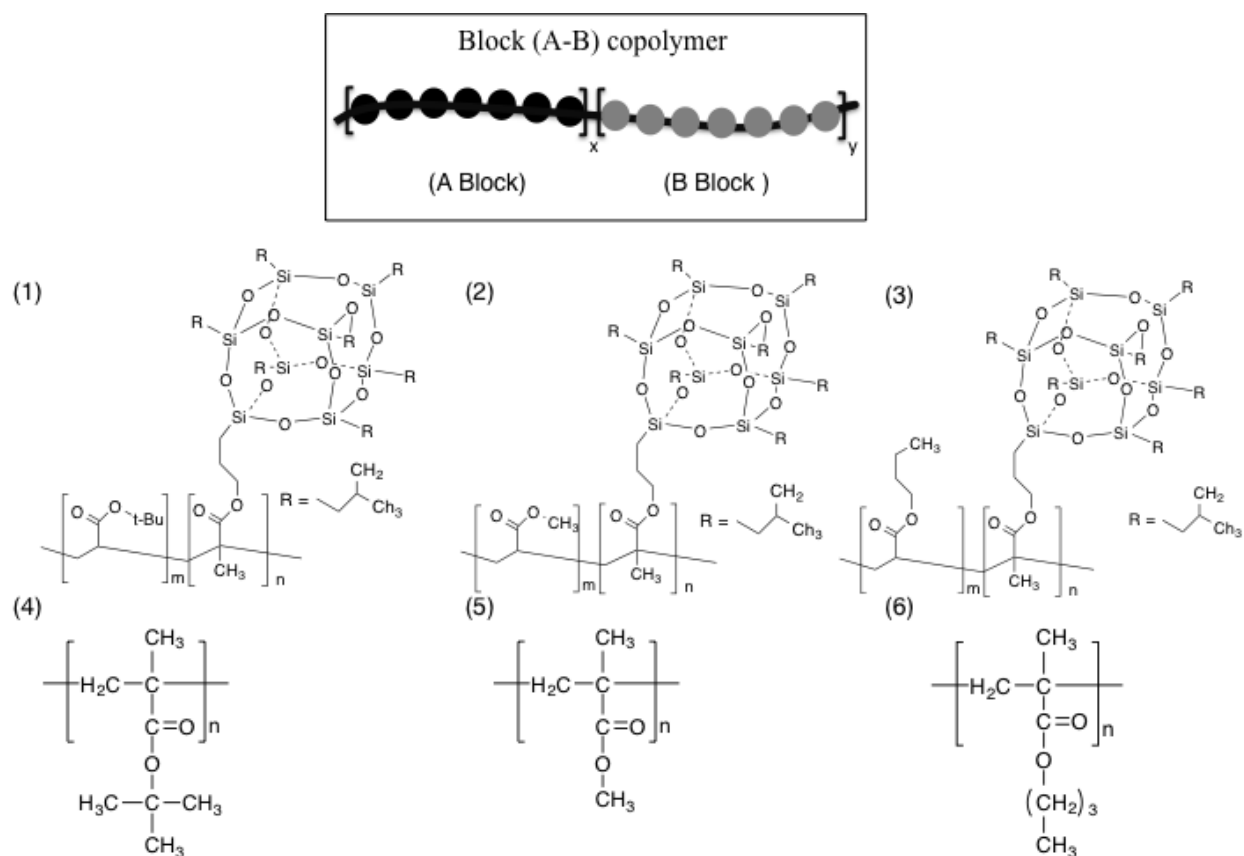


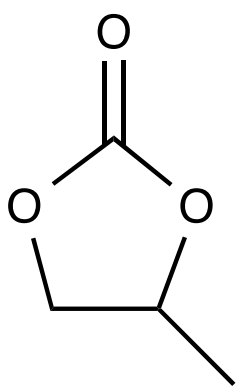
Figure 2.3 Structures of polymers characterized by TREPR: (1) [(propylmethacryl-heptaisobutyl-POSS)-*co*-(*t*-butyl methacrylate)]; (2) [(propylmethacryl-heptaisobutyl-POSS)-*co*-(*n*-butyl methacrylate)]; (3) [(propylmethacryl-heptaisobutyl-POSS)-*co*-(*methyl methacrylate*)]; (4) Poly (*t*-butyl methacrylate); (5) Poly (methyl methacrylate) and (6) Poly (*n*-butyl methacrylate)]

acrylate polymers studied in this work. The first three polymers in this series are all POSS-based acrylate copolymers - while the block (A) of copolymers is different in all three structures, tert-butyl methacrylate (1), methyl methacrylate (2), and n-butyl methacrylate (3), the block (B) is the same for all of the POSS acrylate block copolymers. The three different methacrylates shown here for comparison are poly tert-butyl methacrylate P(t-BMA) (4), poly methyl methacrylate (PMMA) (5), and poly n-butyl methacrylate P(n-BMA) (6).

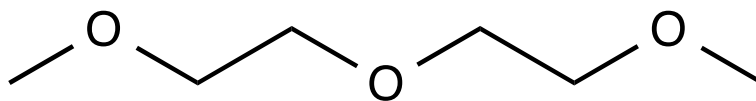
As described in detail in the Chapter 1.2, a special flow apparatus was used to obtain high-temperature TREPR spectra with flowing samples. The choice of solvent is critical for the success of high-temperature experiments; specifically, diethyl glycol dimethyl ether (diglyme) and propylene carbonate (PC), shown in Figure 2.4, is an excellent choices as it is transparent at 248 nm and has a high enough boiling point to withstand the reservoir temperature without evaporating or decomposing.

As discussed in a previous chapter, the several acrylate polymer solutions begin to absorb in the UV light at about 250 nm, and we are exciting them at 248 nm. However, polymers do not absorb very much light and the quantum yield for degradation of acrylic polymers in solution is quite low (about 0.1) [61]. We are therefore just on the edge of the $n-\pi^*$ excitation of the ester carbonyl group thus the photochemistry does not produce very many radicals with each laser flash, but the spectral all show extremely intense chemically induced dynamic spin polarization (CIDEP).

Figure 2.5 shows the TREPR spectra taken in diglyme during 248 nm laser flash photolysis for three different polymers at high temperature, P(t-BMA) (Fig. 2.5C) and Poly [(propylmethacryl-heptaisobutyl-POSS)-*co*-(t-butyl methacrylate)], with POSS 25% (Fig. 2.5A) and 45% (Fig. 2.5B).



Propylene carbonate (PC)



Diethylene glycol dimethyl ether (Diglyme)

Figure 2.4 Two solvents for TREPR experiments at high Temperature

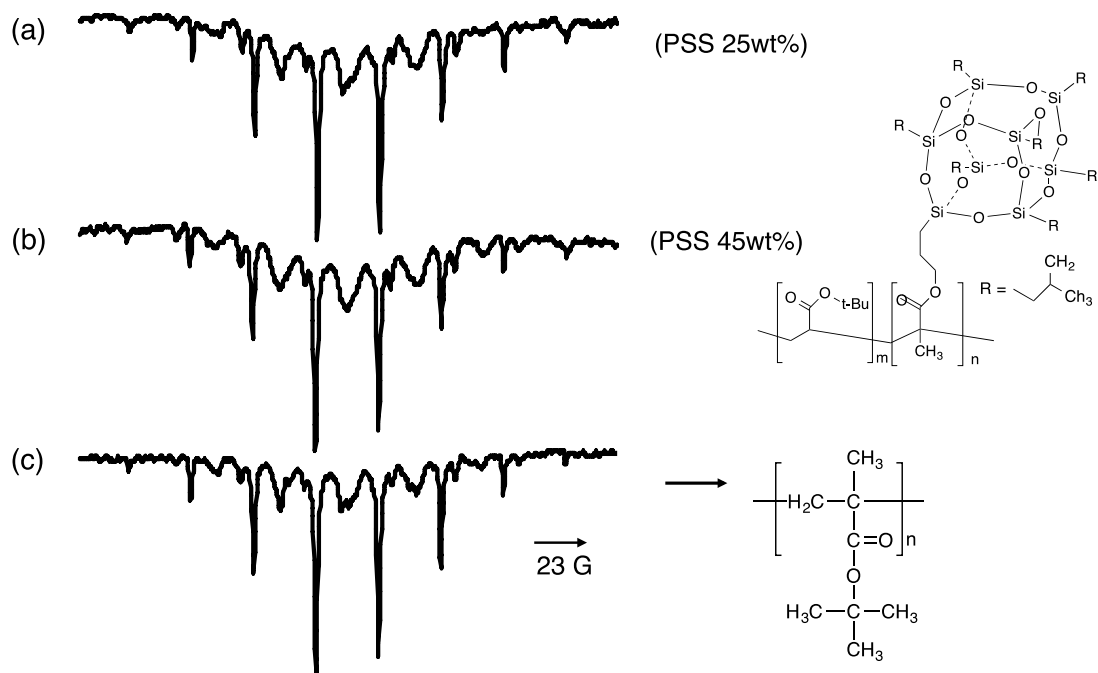


Figure 2.5 Experimental High-temperature TREPR spectra for the main-chain radical from 248 nm irradiation of the following polymers: (A) PSS 25 wt % of Poly [(propylmethacryl-heptaisobutyl-POSS)-*co*-(*t*-butyl methacrylate)], (B) PSS 45 wt % of Poly [(propylmethacryl-heptaisobutyl-POSS)-*co*-(*t*-butyl methacrylate)], (C) P(*t*-butyl methacrylate) in diethyl glycol dimethyl ether at 125 °C, shown for comparison

All of the spectra from polymeric radicals shown here exhibit strong net emissive spin polarization from the TM but none from the RPM or the SCRP mechanism. However, the appearance of the TREPR spectra shown in Figure 2.5 has an interesting feature in its line shape and width although all the TREPR spectra show very intense emission that is similar to the TREPR spectra of acrylate polymers, alternating broad and sharp lines were observed in the spectra. As mentioned in chapter 1.4.1, this is indicative of conformationally induced modulation of hyperfine coupling constants, which is expected for β -hyperfine couplings in polymeric radicals with such bulky substituents on the main chain [62].

At a glance, the TREPR spectra in Figure 2.5 of both Poly [(propylmethacryl-heptaisobutyl-POSS)-*co*-(*t*-butyl methacrylate)] (Fig. 2.5 A and B) and homo P(*t*-BMA) (Fig. 2.5C) in diglyme are quite similar. All appears to have a similar sharp line signal carrier with a single coupling constant (~ 23 G)—at least eight lines are observed and indicated with asterisks in Fig. 2.6. It is suspected that these are actually the innermost eight lines of the 10-line *tert*-butyl radical spectrum from decarboxylation of the oxo–acyl radical, in accordance with the possible mechanism in Figure 2.7, making this the first observation of side-chain radical chemistry in these acrylic polymer photodegradation studies. The evidence of 10-line *tert*-butyl radical spectrum is shown in Figure 2.6. Furthermore, we should consider the fact that a group of broad lines is present in Figure 2.5, which is most likely the (unusual) appearance of the main-chain acrylic polymer radical at high temperature with perhaps an intermediate or even slow motion TREPR spectrum.

The unexpected alternating lines and line width effect in the P(*t*-BMA) spectra could be caused by a number of factors, including the presence of main-chain radicals or propagating radicals as broad lines superimposed on spectra from *tert*-butyl radicals (side chain radical

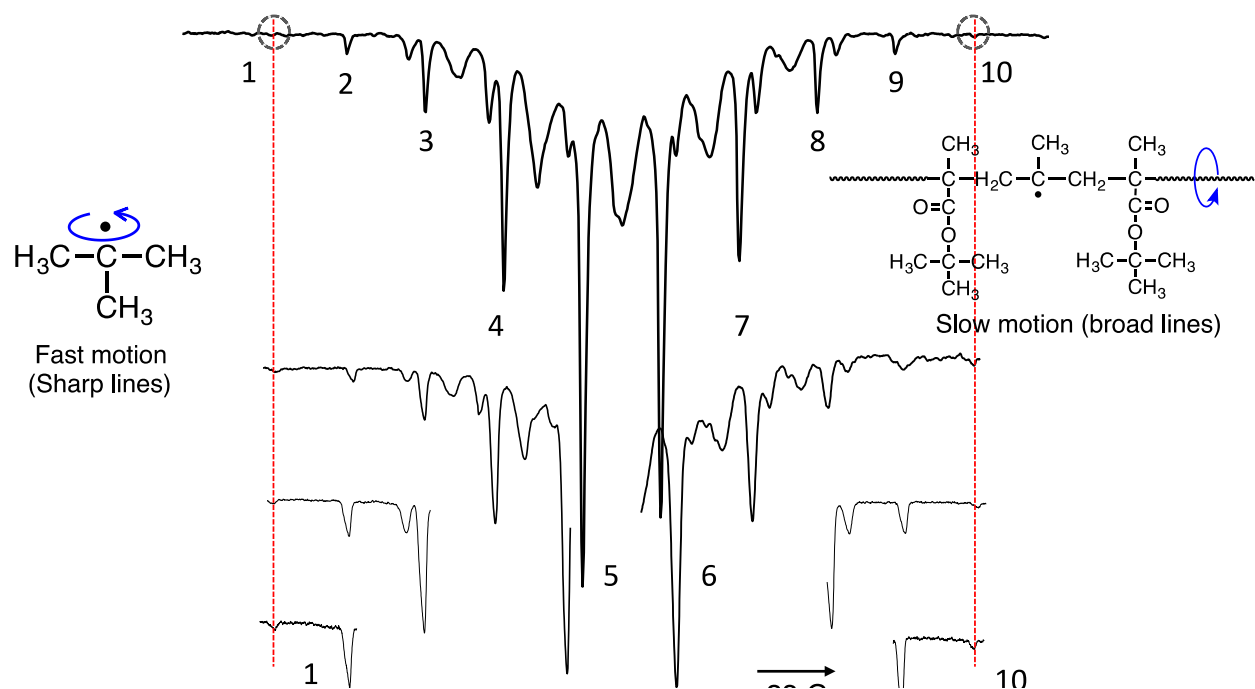


Figure 2.6 The 10-line t-butyl radical spectrum from decarboxylation of poly (t-butyl methacrylate) oxo-acyl radical in diethylene glycol dimethyl ether at 125 °C with following total sweep width: (top) 300 G, 100 G, 50 G, and (bottom) 30 G and delay time: 500 ns

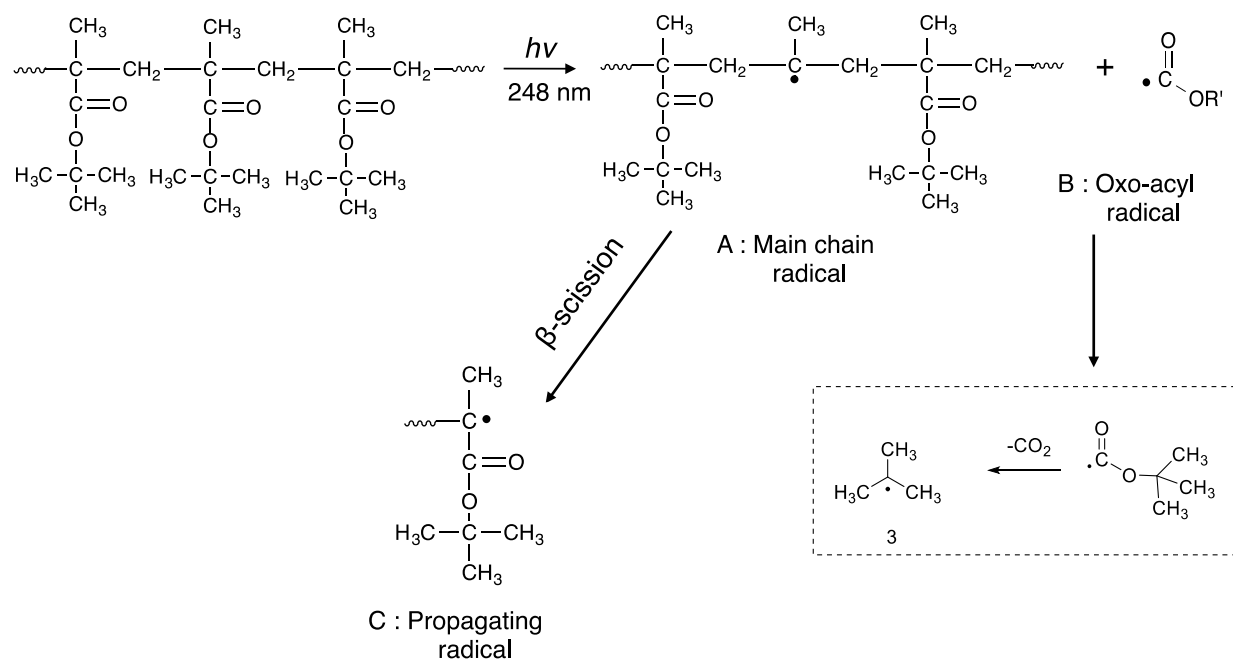


Figure 2.7 Photochemistry and free radicals resulting from 248nm excimer laser excitation of Poly (t-butyl methacrylate) in solution

chemistry), and the influence of polymer conformational changes on the spectra due to the extremely bulky t-butyl side-chain.

The oxo-acyl radicals are not generally observed in high temperature TREPR experiments due to fast spin relaxation (below 10ns in solution) [63], which has two unimolecular decomposition pathways: loss of CO and loss of CO₂. The decarboxylation rate of an oxo-acyl radical from acrylate polymers is about $2.1 \times 10^6 \text{ s}^{-1}$ at 373K, as reported by Griller et al [64]. This means the oxo-acyl radical can be observed in our time scale (500ns) of TREPR, but only at room temperature. However, there is a major exception to this trend in oxo-acyl radical behaviors as observed by TREPR, namely for PFOMA as shown in Figure 2.8. In this case, the polymeric main-chain radical did not show a fast-motion spectrum even at very high temperatures and only the oxo-acyl radical from the side chain was observed. This is understandable because of the steric bulk and conformational rigidity of the perfluoroalkyl ester side chains as well as the much longer rotational correlation time of fluorinated oxo-acyl radical has a than its alkyl analog [10].

TREPR results of poly tert-butyl methacrylate and their copolymer shown in Figure 2.6 has shown a trend similar to that of PFOMA such that it is suspected that the electron spin rotational correlation time of the tert-butyl radical is much slower than the other oxo-radicals so that it can remain long enough to be observed as shown intense and sharp signal carriers by TREPR. However, tert-butyl ester side chains decarboxylation in P(t-BMA) is faster than oxo-acyl radical decarboxylation in PFOMA due to tertiary radical forming so that tert-butyl radical can observe in TREPR spectrum of P(t-BMA)

Also, main-chain radicals or propagating radicals may be present in system with relatively slower conformational motion than the fast motion of tert-butyl radical thus they might

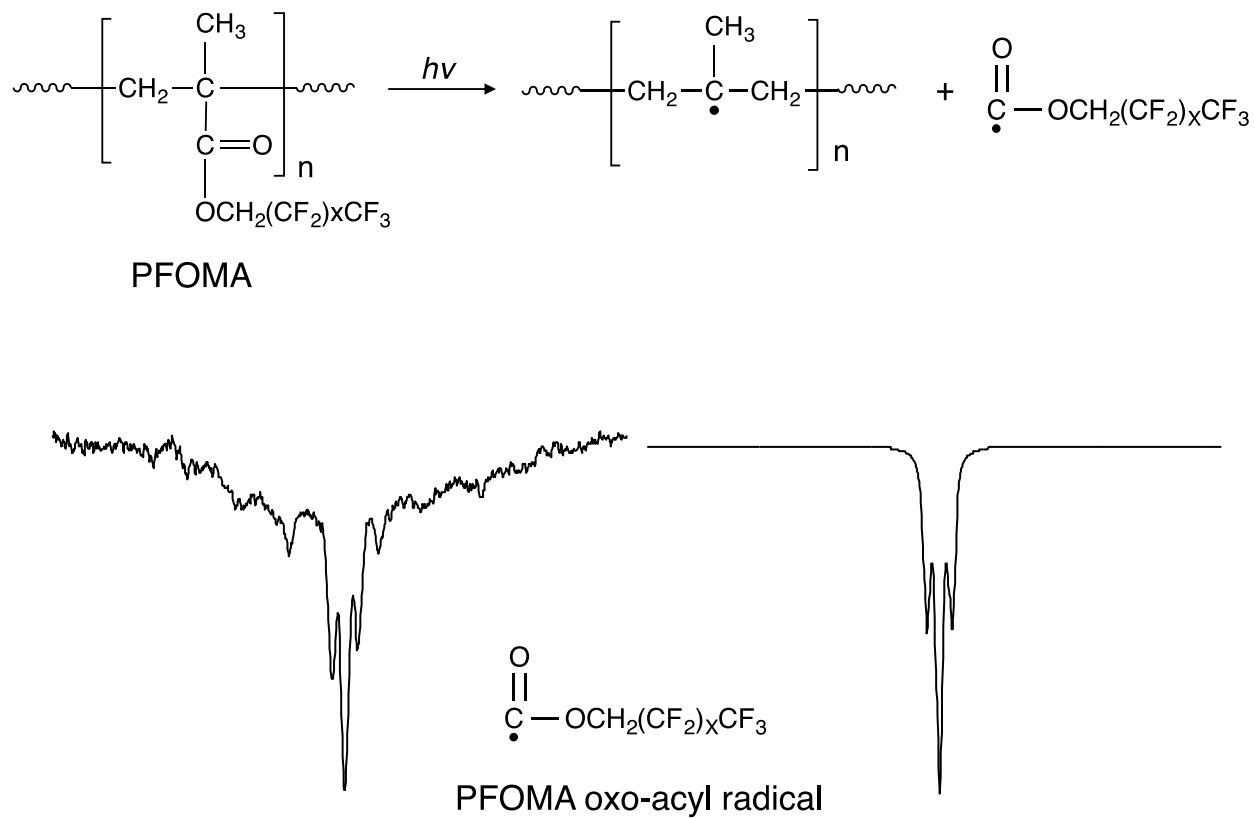


Figure 2.8 (Top) The photochemistry of PFOMA. (Bottom left) experimental and (Bottom right) simulated high temperature TREPR spectra of the oxo-acyl radical from PFOMA in perfluorinated solvent FC-70 at 110 °C and delay time 0.5 μ s. Simulation parameters: $a_F(\text{CF}_2) = 3.2$ G, $a_F(\text{CF}_2) = 0.8$ G from McCaffrey, V. P.; Forbes, M. D. E. *Macromolecules* 2005, 38, 3334.

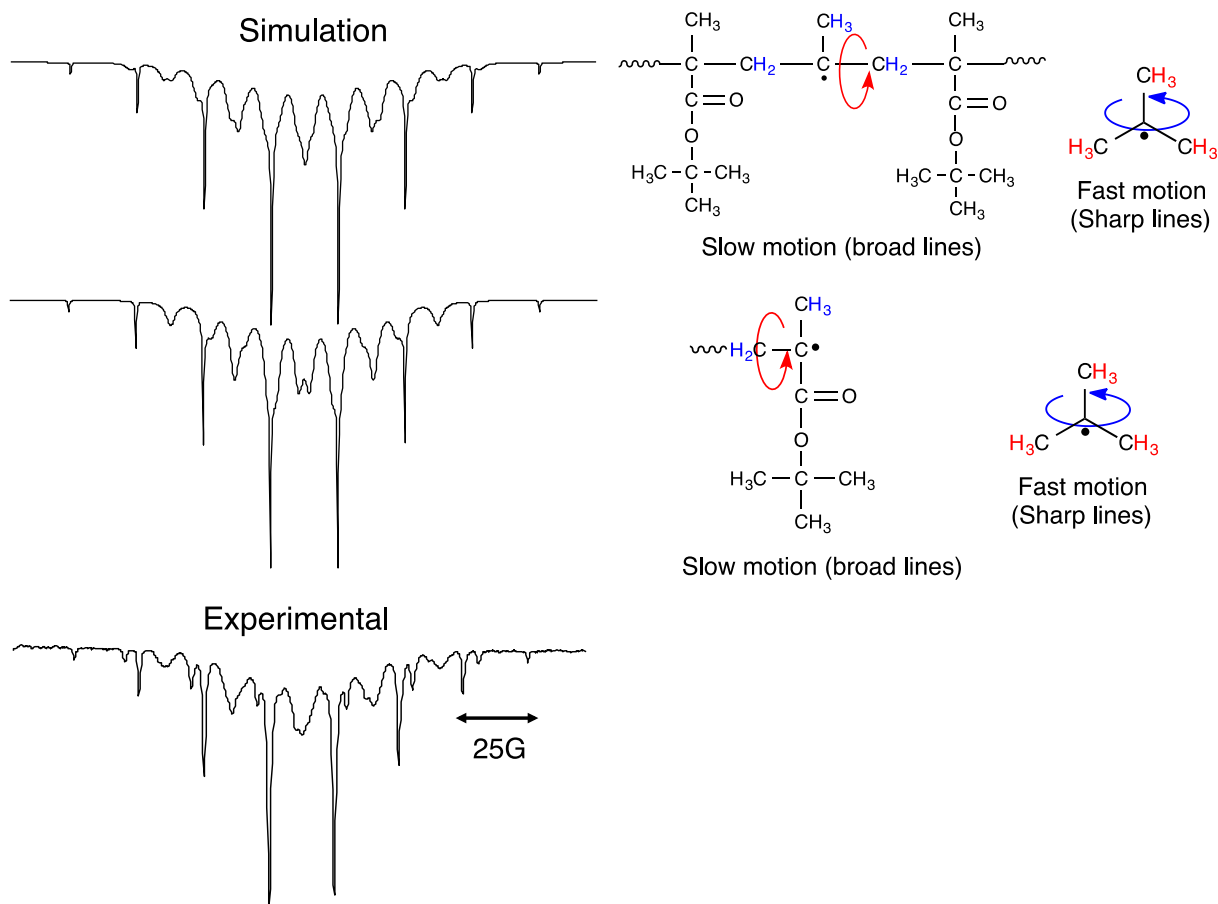


Figure 2.9 Two proposed simulated high temperature TREPR spectra of poly (t-butyl methacrylate) after photolysis at 120°C and delay time of 500ns by using following simulation parameters (Top) $a_{\text{H}}(\text{CH}_3) = 22.8 \text{ G}$, $a_{\text{H}}(\text{CH}_2) = 11.4 \text{ G}$, $a_{\text{H}}(\text{CH}_2) = 14.1 \text{ G}$ LW = 3 (R1) and $a_{\text{H}}((\text{CH}_3)_3) = 22.8 \text{ G}$ (R2); (middle) $a_{\text{H}}(\text{CH}_3) = 21.7 \text{ G}$, $a_{\text{H}}(\text{CH}) = 11.4 \text{ G}$, $a_{\text{H}}(\text{CH}) = 14 \text{ G}$ LW = 3 (R1) and $a_{\text{H}}((\text{CH}_3)_3) = 22.8 \text{ G}$ (R2) (bottom) experimental high temperature TREPR spectrum of poly (t-butyl methacrylate) (1g of polymer in 25ml of diglyme) shown for comparison

be present as broad lines, superimposed with a spectrum from tert-butyl radical in the TREPR spectrum. The alternating line width effect observed in the P(t-BMA) and POSS-P(t-BMA) copolymer TREPR spectra makes it difficult to simulate the experimental data. The two possible simulations of the P(t-BMA) fast motion TREPR spectra are shown in Figure 2.9 along with the corresponding experimental spectrum. The coupling constants used for each simulation are listed in the respective figure captions. At the top of Figure 2.9, two radicals were used for the simulation. For the broad line, which is suspected to indicate the main-chain radical from P(t-BMA) after photolysis, a value of 22.8 Gauss was used for the hyperfine coupling constant for the three β -protons of the methyl group, and values of 14.1 Gauss and 11.4 Gauss were used for the two sets of methylene protons with a huge line width. To create sharp peaks corresponding to the 10-line t-butyl radical spectrum from decarboxylation of the oxo-acyl radical in Figure 2.9 top, a single coupling constant 22.8 Gauss for the protons of tert-butyl was used along with a line width 1.3 Gauss.

The spectrum shown in the middle of figure 2.9 is simulated using hyperfine coupling constants of 14 Gauss for one proton, 11.4 Gauss for one proton, and 21.7 Gauss for three protons of the methyl group from propagating radicals of P(t-BMA) along with a single coupling constant 22.8 Gauss for the protons of tert-butyl radicals.

We concluded from the resulting two simulation spectra that main-chain radicals are present as broad lines, superimposed with a spectrum from tert-butyl radicals. An interesting observation is that the poly [(propylmethacryl-heptaisobutyl-POSS)-*co*-(t-butyl methacrylate)] spectrum shows only photodegradation of P(t-BMA) and, as expected, that another block containing POSS along with their chains does not participate in the photodegradation process because the resistance to photolysis is improved when polymer composites with POSS.

Figure 2.10 shows the temperature dependence of the TREPR signal for poly[(propylmethacryl-heptaisobutyl-POSS)-*co*-(n-butyl methacrylate)] upon 248 nm photolysis in diglyme along with TREPR spectrum of Poly (n-BMA) taken at high temperature (115 °C). As expected, the appearance of POSS-P(n-BMA) is similar to that of P(n-BMA), which indicates that the photodegradation process of POSS acrylate copolymer only relies on polymer (A block), which has no POSS. At room temperature, alternating linewidth pattern is observed, as usual for acrylate polymer as mentioned previously, the presence of the oxo acyl radical is common to the acrylate polymer spectra at room temperature. However, in the POSS-P(n-BMA) and P(n-BMA) high temperature TREPR spectra, the strong signal for the oxo-acyl radical is observed near the center, while in the high temperature TEPPR spectrum of POSS-PMMA is shown in figure 2.11, there is no oxo-acyl radical at high temperature (115 °C) due to fast spin relaxation. The larger and bulkier n-butyl side chain in P(n-BMA) makes the spin rotational relaxation process of side chain slower compared to smaller methyl group in PMMA so that the strong oxo-acyl radical shows in the fast motion TREPR spectra of P(n-BMA). The lower temperature spectra show the same alternation linewidth effect at low temperature as observed with POSS-P(n-BMA). Furthermore, the appearance of high temperature TREPR spectra for POSS-PMMA and PMMA shows as almost identical to other POSS-acrylate copolymers.

2.3 Summary and Implications

The photodegradation mechanism of several methacrylate-POSS block copolymers in solution was investigated by TREPR. The observed photochemical degradation mechanism is quite similar to that previously observed in photolysis of homo poly (methacrylate)s.

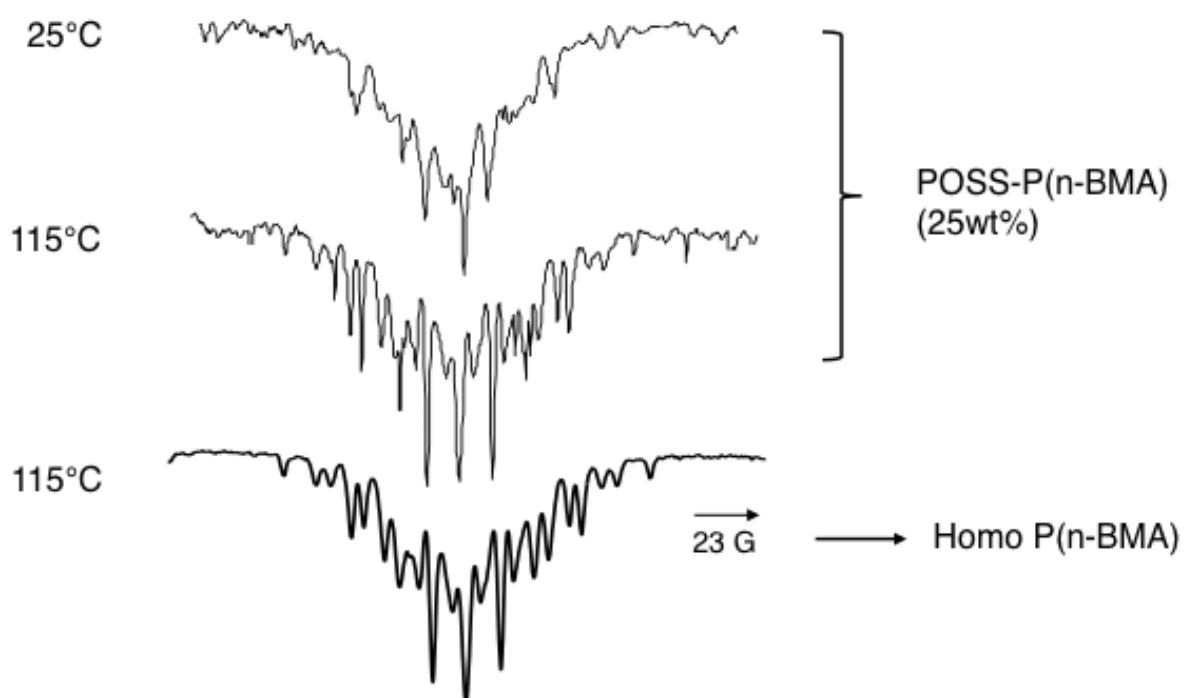


Figure 2.10 The temperature dependence of TREPR spectra for the main-chain radical from 248 nm irradiation of Poly [(propylmethacryl-heptaisobutyl-POSS)-*co*-(*n*-butyl methacrylate)] in propylene carbonate (1g of polymer in 25 ml of solvent) at delay time of 500 ns, and (bottom) P (n-butyl methacrylate) main chain radical TREPR spectrum in diglyme at 115 °C shown for comparison

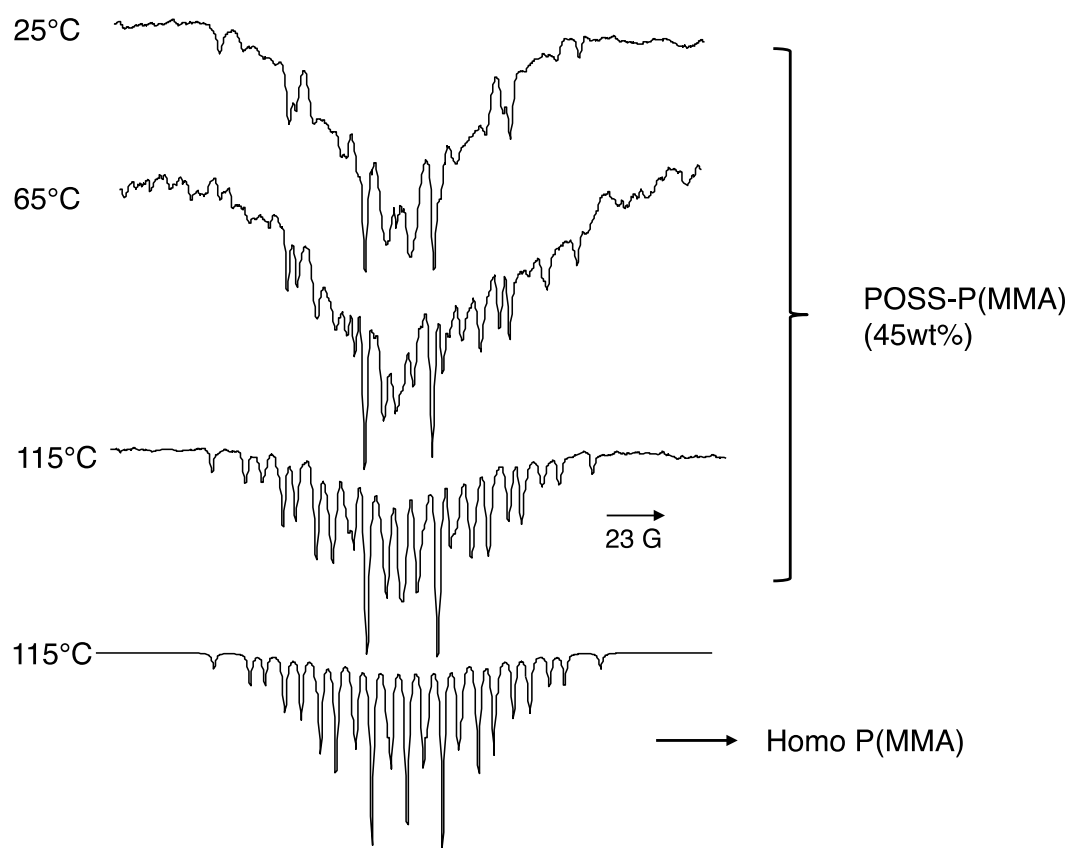


Figure 2.11 The temperature dependence of TREPR spectra for the main-chain radical from 248 nm irradiation of Poly [(propylmethacryl-heptaisobutyl-POSS)-*co*-(*n*ethyl methacrylate)] in diglyme (1g of polymer in 25 ml of solvent) at delay time of 500 ns, and (bottom) P(*m*ethyl methacrylate) main chain radical TREPR spectrum in propylene carbonate at 115 °C shown for comparison

As expected, chromophores with POSS group side chain do not participate in the photodegradation process, which suggests that POSS utilize a beneficial effect against UV light photodegradation in these copolymers. The resulting experimental spectra suggest since all of the investigated methacrylate-POSS copolymers show the same photodegradation phenomena, that POSS could play an important roles in preventing UV degradation and improving photoresistance in such materials. Also of note is that the degradation process does not follow the concentration of POSS within the chain. It is interesting note that alternating line broadening effects due to the modulated hyperfine constant cause by a bulky ester side chain are observed in high temperature TREPR spectra of both POSS-P(t-BMA) block copolymer and P(t-BMA). The excellent fit of the simulations allow for identification of the signal carriers. The spectra show a strong signal from the tert-butyl radical after decarboxylation rate of the oxo-acyl radical. This process is rarely observed in our time scale, which is really rare in high temperature fast limit TPEPR spectra.

The temperature dependence of TREPR spectra of all block copolymers presented here shows similar conformational dynamics to those reported in our previous papers.

2.4 Experimental

Commercial compounds. Poly [(propylmethacryl-heptaisobutyl-POSS)-co-(t-butyl methacrylate)], Poly [(propylmethacryl-heptaisobutyl-POSS)-co-(methyl methacrylate)], Poly [(propylmethacryl-heptaisobutyl-POSS)-co-(iso-butyl methacrylate)], Poly(t-butyl methacrylate), Poly (iso-butyl methacrylate), and poly (methyl methacrylate) were obtained from Aldrich and used as received. Propylene carbonate and diethylene glycol dimethyl ether were used as a solvent for TREPR experiments.

TREPR experiments. Continuous wave TREPR experiments were performed as previously described [10]. All experiments were performed on a JEOL USA Inc. JES-RE1X X-band EPR spectrometer equipped with a wide bandwidth preamplifier and a low-noise GaAsFET microwave amplifier. Samples were typically prepared as solutions of polymer (1 g) in propylene carbonate or diethylene glycol dimethyl ether (diglyme) (25 ml) and circulated through a quartz flat cell (0.4 mm path length) positioned in the center of a Varian TE₁₀₃ optical transmission cavity. The solutions were photolyzed using a Lambda Physik Compex 120 excimer laser (248 nm, KrF) running at 60 Hz with a pulse energy of 100 mJ (~20 mJ per pulse hitting the sample) and a pulse width of 17 ns. Spectra were collected in the absence of field modulation at a fixed delay time after the laser flash using a two-gate boxcar integrator (Stanford, 100 ns gates), while the external magnetic field was swept with a scan time of 4 min.

For high-temperature TREPR experiments, the deoxygenated sample solution under N₂ was circulated using a micropump through Teflon PFA 1/8 in. tubing insulated with polyurethane foam tape. From the pump, the sample tubing passed through a copper coil wrapped with heating tape (Omega Inc.), which was controlled using a feedback circuit between a variable power temperature controller and thermocouples placed at the entrance and exit of the quartz flow cell. The sample was recirculated between the flat cell and the reservoir. Reported temperatures are the average of three measurements from the top and bottom of the flat cell and the reservoir. The maximum temperature gradient at the highest temperatures was 10 °C; therefore, all temperature are reported as ± 5 °C.

Chapter 3. Photodegradation of Acrylic Block Copolymers

3.1 Introduction

The recent development of several controlled and free radical polymerization mechanisms have allowed the synthesis of many types of block copolymers, especially acrylics.

Of interest to the Forbes laboratory is the photophysical and photochemical behavior of acrylic blocks in dilute solution, in particular if site selective photochemistry might be observed. The discovery of such behavior could lead to the design novel materials that degrade in a specified place along the polymer chain. Alternatively, such studies might also suggest ways to make materials that are thermally robust in one section and photochemically sensitive in another (or vice versa). Understanding of a complex correlation between polymer conformational chain dynamics and polymer bulk properties is the key to the polymer design ready to meet new technological requirements such as electro-optical materials, artificial organs, antioxidant surface coatings, membranes and drug delivery devices [65]. As we discussed earlier, the conformational chain dynamics of each acrylates polymers is quite different depending on their structures thus in this chapter will focus on the spin selective and conformational chain dynamics of several acrylate block copolymers as a function of temperature, ester side chain stiffness, and variation of chain length of block chains.

3.1.1 Structure of Block Copolymers

The structure of a block copolymer can be investigated as a melt, a solid, in solution or as a blend. In the case of a melts, if the individual blocks are immiscible, they attempt to separate. Because of the connectivity of each segment, the length scale along with phase separation can occur is restricted. The homogeneity and phase separability of block polymer melts are strongly influenced by temperature [66]. At high temperatures, exceeding the microphase separation temperature (MST), both block chains can mix, but the blocks will separate upon lowering the temperature, resulting in microphase separation.

Before discussing the features of block copolymers in dilute solution, it is useful to present one background information regarding the dilute regime for a polymer solution. The phase diagram for a polymer solution is shown in Figure 3.1. The interaction parameter $\chi = \frac{1}{2}$, and the excluded volume is zero at a special temperature, called the θ temperature. At very low concentrations, the polymer chains in solution are considered to be isolated. When $\phi < \phi^*$, the polymer solution is defined as dilute. With increasing ϕ , the polymer solution can be in the semi-dilute region or in the concentrated region.

This is the overlap concentration ϕ^* , expressed as in eq. 2:

$$\phi^* \cong a^3 N / R_F^3 = N^{1-\frac{3}{v}} \quad (3.1)$$

where N is degree of polymerization, R_F is the end-to-end distance of the chain, a is the polymer segment length and v is the Flory exponent. ($v = 0.558$ in a good solvent and $v = 0.5$ in a theta solvent where the effective monomer and monomer interaction are weak thus polymer coil can consider as ideal chain.) [67]

Above the critical overlap concentration, the chains in the solution become aggregated and densely packed, which can lead to micellization of a block copolymer solution. The phase

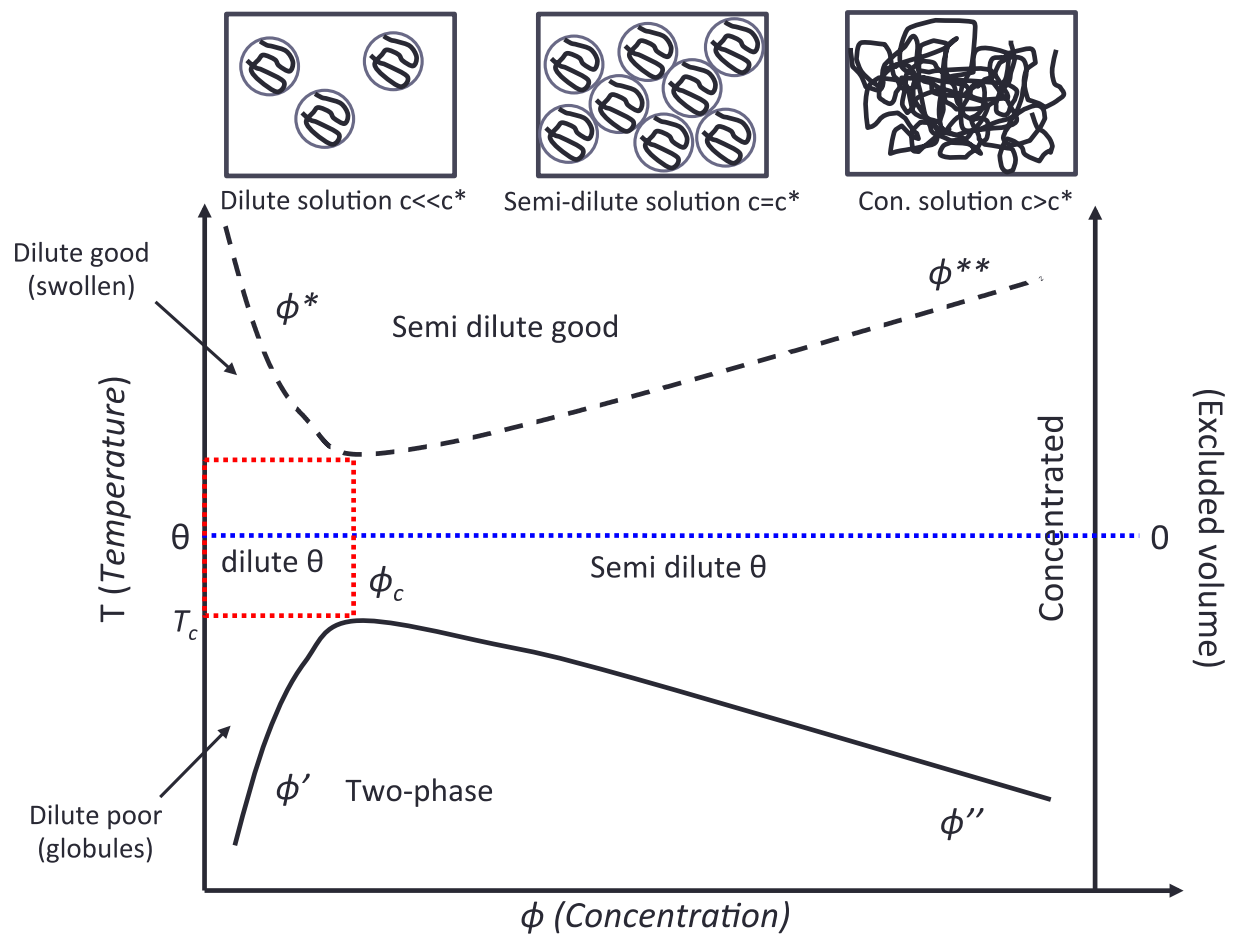


Figure 3.1 Phase diagram for polymer solution. The solid curve denotes the binodal and phase separation occurs for polymer solutions with T and ϕ below the binodal. The dashed curve is the low temperature boundary of the semidilute good solvent regime from Polymer physics by M. Rubinstein and R. H. Colby.

behavior of a block copolymer in solution is therefore quite different from those of melts and they typically form spherical micelles in dilution solution in a selective solvent when the core of the micelle is composed by an insoluble or a selectively soluble block [68]. Also, the shape of the block copolymer micelle (e.g., sphere, ellipse, rod) strongly depends on the concentration.

So far, much of the literature in the field has focused on the self-assembly of block copolymers and microphase separation of block copolymer melts and solutions [68-71]. For block copolymer solutions, the experimental and theoretical study of micellization of an ionic block copolymer is most important in this field because of their industrial applications such as bio-friendly drug delivery systems and membranes. Additionally, most theoretical models and computer simulation studies of block copolymer have used melts and micelle forms. For this reason, much of the literature in this field has focused on the thermodynamics, bulk properties and formation of micelles. However, the theoretical understanding of macromolecular level dynamic in block copolymer melts and solutions has not been well established. There are a few published reports regarding non-ionic block copolymers, which often contain poly(styrene) (PS), using a selective solvent for PS to form a micelle [72]. However, local chain dynamics of non-ionic and non-micelle structures of block copolymers in a dilute “good” solvent for both block chains have not been studied well. A notable example is the work of Tsunashima and Kawamata, who investigated the dynamic modes of motion in a PS-PMMA diblock copolymer in dilute solution using dynamic light scattering (DLS) [73]. A high molecular weight diblock copolymer was used to easily detect the internal motions in the subchain. Benzene was used as a solvent since it is a good solvent for both PS and PMMA. Indeed, understanding of a complex correlation between conformational chain dynamics of block copolymers and their structures in solution is still ambiguous. To the best of our knowledge, there are no publications that detail the macromolecular

level properties of an A-B block copolymer both experimentally and theoretically. The “spin reporter” methodologies developed in this thesis are an excellent way to probe their behavior.

3.1.2 Photochemistry of Acrylic Polymers

Over the past decade, our laboratory has been studying the photodegradation and photochemistry of acrylic homopolymers in dilute solution using time-resolved electron paramagnetic resonance (TREPR) spectroscopy [74-77]. In this chapter, we have extended this work to investigate the chain dynamics of several acrylate block copolymers and create a workable “atom-specific” model for macromolecular chain dynamics that has so far proven elusive for these complex structures.

The conformational properties of copolymers are related to both the structures of their individual chemical unit and their chemical sequence distribution. It is well understood that a block copolymer retains the properties of each of the homopolymers. This often results in improvement to the physical and bulk properties of the copolymers. For example, the mechanical and physical properties of the polymers such as the glass transition temperature (T_g), melting temperature (T_m) and modulus, strongly correspond with the structural arrangement of the molecular units comprising the copolymer structure [78]. The composition and architecture of block copolymers play an important role in the enhancement of their bulk properties. However, there are only few published reports on degradation mechanisms, thermal or photochemical, of acrylic block copolymers [78].

The photodegradation mechanism and chain dynamics of several acrylic homopolymers has been reported [79-82]. In spite of the close structural similarities among several poly(methacrylates) and poly(acrylates), the degradation rates and the chain dynamics of the

ensuing radicals are quite different from each other, especially at high temperature spectrums, as a function of a solvent, nuclear symmetry, rigidity of chain moieties, and molecular weight.

Before going into detail regarding the photochemistry of acrylic block copolymers in dilute solution, it is helpful to have background information about previous work in the Forbes laboratory on acrylic polymer degradation, dynamic effects, and the possible theoretical models available to assist in spectral analysis of both slow and fast motion TREPR spectra [76].

After absorption of UV light by the $n\text{-}\pi^*$ state of the ester chromophore in these polymers, side chain cleavage from the first excited triplet state via the Norrish I process takes place. This leads to a main chain acrylic polymer radical and an oxo-acyl radical from the ester side chain, followed by formation of the propagating radical and a terminal alkene via unimolecular decomposition, specifically β -scission, on a time scale of about 20 μs [63]. It has been determined and well studied by both SSEPR and TREPR techniques; however, the TREPR experiment is unique in its ability to detect these main-chain macromolecular radicals cleanly with high resolution on the sub-microsecond time scale well before any rearrangements take place.

In our recent series of papers, the photodegradation mechanism for PMMA and related polymers with ester side chains have conclusively demonstrated and established the following general principles:

- (1) The carbon-centered main chain radical of an acrylic polymer is a highly localized, minimally perturbative spin probe, allowing investigation the conformational energy landscape near the radical center.
- (2) The temperature dependence of the TREPR spectra of these polymers provides rich in information of the conformational motion of polymers. The lower temperature spectra shows dynamic effects such as an alternating hyperfine line width effect due to conformational

modulation of the hyperfine coupling. Interestingly, this dynamic effect has been only shown in SSEPR spectra of propagating radicals so far, however, in our TREPR spectra at lower temperature show this modulation effects where restricted motion between the $C_\alpha - C_\beta$ bond within polymer main chain radicals due to bulky substituents leading to conformationally slow motion in our system. In contrast, at high temperature, the fast conformational motion alters the hyperfine coupling constants leading to clearer and shaper appearance of spectrum of main-chain radicals. Because the electron-nuclear hyperfine interactions in the main chain radical depend on the dihedral angle between the p orbital containing the unpaired electron and the neighboring C-H sigma bond, the TREPR spectra of these main chain radicals show a strong temperature dependence on both line widths and line positions. Changes in line width are related to the “jump time” between conformations, while changes in line position (at constant width) reflect changes in the populations of certain rotational conformers (rotamers).

As shown in Chapter 1.2, an interesting observation is that β -hyperfine coupling constants between acrylate and methacrylate exhibit quite different values at high temperature. In case of acrylates, the β -hyperfine interaction is quite similar in the spectra at all temperatures due to their conformational flexibility on their chain moieties. On the other hand, methacrylates, especially PMMA, show large differences in their spectrum appearance due to not only conformational motion but also polymer tacticity. Stereochemistry plays a strong role in both the overall spectral appearance (as determined by fast motion hyperfine coupling constants) and in the temperature-dependent line broadening processes [10].

(3) The oxo-acyl radical from the ester group is rarely observed due to fast spin relaxation and extremely different diffusional properties between main-chain radical and acyl radical although they often appear at room temperature, and exhibit a single emissive peak near the center of

spectrum (g-factor for acyl radical is 2.009) [10].

(4) The TM polarization is created within the laser flash and arise from the anisotropic nature of the spin-orbit coupling process from the first excited singlet state to the lowest excited molecular triplet state of the ester side chain. Most likely, the fast rotation of the side chain along one axis and the much slower conformational motion along the polymer chain provide this high degree of anisotropy resulting in very large magnitude of the observed TM polarization in these systems. Several factors can maximize the TM [74,75], including the intersystem crossing rate, the chemical decay rate, and the magnitude of the zero-field splitting parameters of the triplet, but the most important parameter is the rotational anisotropy of the triplet as it tumbles in the applied magnetic field of the EPR spectrometer. The ester side chains have significantly greater freedom of motion along an axis perpendicular to the polymer backbone, but very poor rotational mobility along the backbone axis itself. This difference in rotational mobility allows for greater spin state selectivity in the molecular frame during inter-sytem crossing and will amplify the TM.

(5) The TREPR spectra show a shows strong side chain dependence. For example, in the case of PFOMA, which has fluorinated alkyl groups on the ester side chain, the observed TREPR spectrum is quite different to other acrylate polymers (Figure 3.2). The oxo-acyl radical exhibits a very intense signal and the main chain radical is broad and weak. This broad signal of main-chain radial is most likely due to the slow dynamics of the PFOMA main chain radical. The reason for these abnormal phenomena is that bulky ester side chains make polymer chain more rigid, restring the internal motion of the polymer; thus, the spin relaxation time of the PFOMA

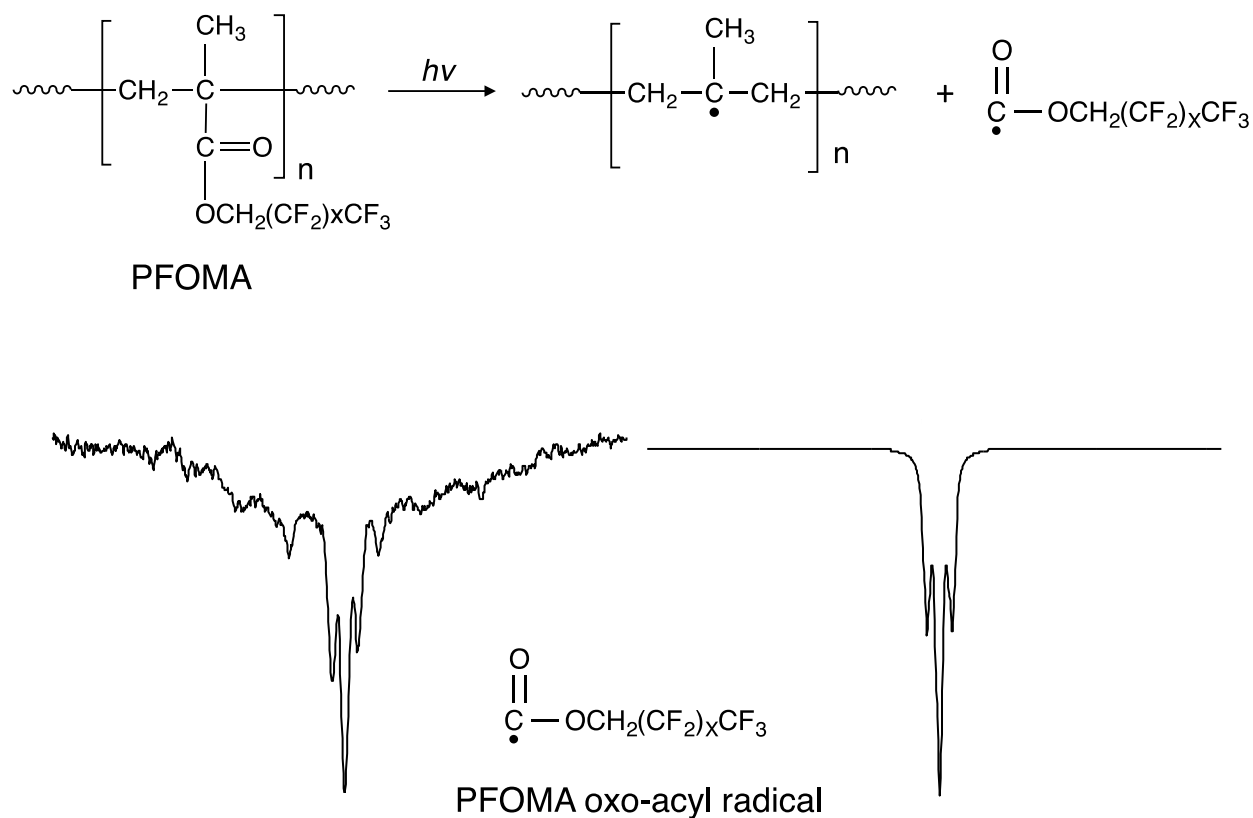


Figure 3.2 (Top) The photochemistry of PFOMA. (Bottom left) experimental and (Bottom right) simulated high temperature TREPR spectra of the oxo-acyl radical from PFOMA in perfluorinated solvent FC-70 at 110 °C and delay time 0.5 μ s. Simulation parameters: $a_F(\text{CF}_2) = 3.2$ G, $a_F(\text{CF}_2) = 0.8$ G from McCaffrey, V. P.; Forbes, M. D. E. *Macromolecules* 2005, 38, 3334.

oxo-acyl radical is longer than usual for an acyl radical. Below we will see this phenomenon in some block copolymers as well.

To model our experimental results using hyperfine modulation, we have applied selective broadening of the lines in the spectrum (in the condition of fast exchange), which occurs according to the equation [83]

$$T_2^{-1} = \gamma_e^2 \tau \langle \delta a^2 \rangle (M_a - M_b)^2 + T_{2,0}^{-1} \quad (3.2)$$

where T_2^{-1} is the line width after broadening, γ_e is the gyromagnetic ratio of the electron, M_a and M_b are the nuclear spin quantum numbers of the transitions, and $T_{2,0}^{-1}$ is the contribution to the line width from other mechanisms. The term τ is the correlation time for the exchange process and can be calculated from where τ_1 and τ_2 are the inverse of the rate constants for jumping the barrier to rotation. The mean-square deviation in the hyperfine splitting is where $(a_1 - a_2)$ is the difference between the fast-motion hyperfine coupling constants. An important note is that this model only works in a system in which the sum of the hyperfine coupling constant always remains constant, like as our carbon-centered main chain radicals with sterically hindered, but still flexible. Because the electron-nuclear hyperfine interactions in the main chain radical depend on the dihedral angle between the p orbital containing the unpaired electron and the neighboring C-H sigma bond, the TREPR spectra of these main chain radicals show a strong temperature dependence on both line widths and line positions.

3.2 Result and Discussion

The structures of the copolymers studied in this chapter are shown in Table 3.1 along with experimental values for their molecular weights, polydispersities (Mw/Mn) and composition

(block and random copolymers). The synthesis, sample preparation, polymer characterization, and spectroscopic methods are all described in experimental section. By using the anionic polymerization, all block copolymers have relatively narrow PDIs, and their degree of polymerization (N) is about 250 ~ 500.

There are three different types of block copolymer with PMMA as the A block for all three structures. For the B block, Poly (ethyl acrylate) (PEA), Poly (n-butyl methacrylate) (P(n-BMA)), and Poly (tert-butyl methacrylate) (P(t-BMA)) are used. However, the synthesis of the PMMA-b-PEA fails to synthesis because the resulting polymer was gel and hard to precipitate in any organic solvents.

The irradiation wavelength in all of the experiments reported here is 248nm, which is a good wavelength with which acrylate polymers. The critical concentration (c^*), same as overlap concentration discussed above of our several acrylate block copolymer solutions can be calculated using the following equation:

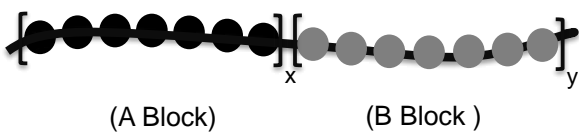
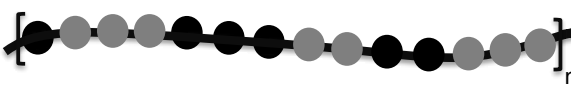
$$c^* \cong \frac{1}{N_A} \left(\frac{3M}{4\pi R_g^3} \right) \quad (3.3)$$

where, M is the Molecular weight of the polymer, N_A is Avogadro's number, R_g is the radius of gyration. The radius of gyration of a polymer in a good solvent varies as follows:

$$R_g^3 \propto M^{3\nu} \quad (3.4)$$

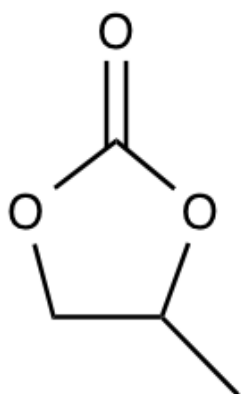
where ν is the excluded volume index. The literature value of the calculated critical concentration, C_{calc}^* of PMMA (Mw: 56,000 ~ 110,000) in good dilute solvent is about 0.025 [84]. The concentration of our samples is about 0.03, which is quite close to the critical

Table 3.1 The structure and molecular weight of block copolymers studied in this chapter

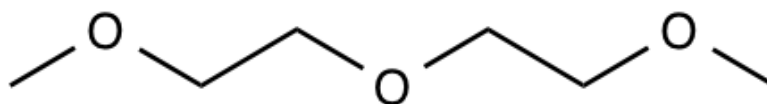
Block (A-B) copolymer		Random (A-B) copolymer	
 <p>(A Block) (B Block)</p>			
Polymer	Structure	Ratio (A: B)	Molecular weight (Mw)
Poly (methyl methacrylate)- <i>b</i> -poly(tert-butyl methacrylate)	$\left[\begin{array}{c} \text{CH}_3 \\ \\ \text{H}_2\text{C}-\text{C} \\ \\ \text{C}=\text{O} \\ \\ \text{O} \\ \\ \text{CH}_3 \end{array} \right]_n \left[\begin{array}{c} \text{CH}_3 \\ \\ \text{H}_2\text{C}-\text{C} \\ \\ \text{C}=\text{O} \\ \\ \text{O} \\ \\ (\text{CH}_2)_3 \\ \\ \text{CH}_3 \end{array} \right]_m$	1:9 1:1(Random and Block) 9:1	50,000 ~ 70,000 (PDI : 1.2)
Poly methyl methacrylate- <i>b</i> -poly(n-butyl methacrylate)	$\left[\begin{array}{c} \text{CH}_3 \\ \\ \text{H}_2\text{C}-\text{C} \\ \\ \text{C}=\text{O} \\ \\ \text{O} \\ \\ \text{CH}_3 \end{array} \right]_n \left[\begin{array}{c} \text{CH}_3 \\ \\ \text{H}_2\text{C}-\text{C} \\ \\ \text{C}=\text{O} \\ \\ \text{O} \\ \\ (\text{CH}_2)_3 \\ \\ \text{CH}_3 \end{array} \right]_m$	1:9 1:1(Random and Block) 9:1	50,000~100,000 (PDI: 1.1) For Random : PDI: 1.45)
Poly methyl methacrylate- <i>b</i> -poly(ethyl acrylate)	$\left[\begin{array}{c} \text{CH}_3 \\ \\ \text{H}_2\text{C}-\text{C} \\ \\ \text{C}=\text{O} \\ \\ \text{O} \\ \\ \text{CH}_3 \end{array} \right]_n \left[\begin{array}{c} \text{H} \\ \\ \text{H}_2\text{C}-\text{C} \\ \\ \text{C}=\text{O} \\ \\ \text{O} \\ \\ \text{CH}_2 \\ \\ \text{CH}_3 \end{array} \right]_m$	1:1 9:1 ?	50,000~100,000 (PDI: 1.3) ?

concentration; however, our polymer chains almost start to overlap between macromolecular chains. Also, it is important to note that where polymer in good solvent, the overlap concentration decreases with increasing temperature. For this reason, our polymers are considered to be dissolved in a good solvent when TREPR spectra are acquired at high temperatures, and we therefore assume that our investigations of the polymer chain dynamics takes place without overlapping chains. The choice of solvent is critical for studying the block copolymer solutions. In the case of PMMA- and PEA- rich block copolymers, propylene carbonate, shown in Figure 3.3, is the favored solvent because of its high boiling temperature and because it is optically transparent at 248nm. Diglyme, shown in Figure 3.3, is a good solvent for the n-BAM, t-BMA rich block copolymers. Before discussing the photochemistry of acrylate block copolymers, it is useful to review the photochemistry of acrylic homopolymers composed of either the A and the B block monomers. In the case of PMMA, the general principles are discussed in introduction. High temperature TREPR spectra acquired during 248 nm photolysis of PEA, P(n-BMA), and P(t-BMA) in diglyme are described below.

Figure 3.4 shows experimental TREPR spectra for the four types of acrylate polymers, and the corresponding computer simulated spectra are shown in Figure 3.5. There are several noteworthy features of these spectra. At first glance, the spectra in Figure 3.4 appear entirely in net emission, due to the Triplet Mechanism (TM) of CIDEP, but the other spectral features such as line shapes and widths are very different from each other. In particular, the P(t-BMA) spectrum shows an TREPR spectra acquired during 248 nm photolysis of PEA, P(n-BMA), and P(t-BMA) in diglyme are described below. Figure 3.4 shows experimental TREPR spectra for the four types of acrylate polymers, and the corresponding computer simulated spectra are shown in Figure 3.5.



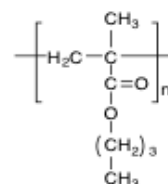
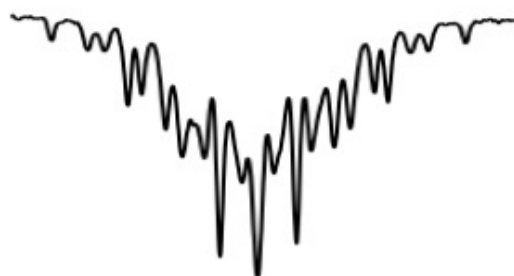
Propylene carbonate (PC)



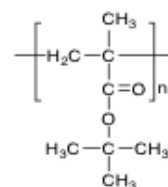
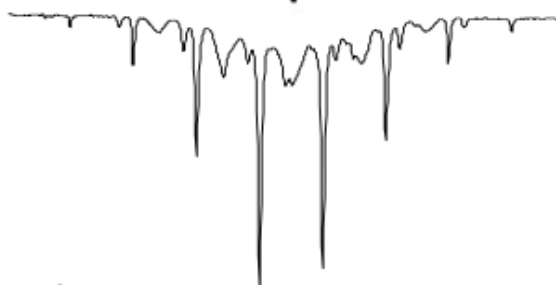
Diethylene glycol dimethyl ether (Diglyme)

Figure 3.3 Two solvents for TREPR experiments at high Temperature

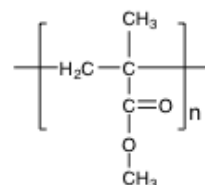
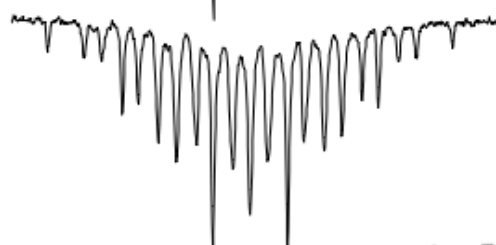
Poly (n-butyl methacrylate)



Poly (t-butyl methacrylate)



Poly (methyl methacrylate)



Poly (ethyl acrylate)

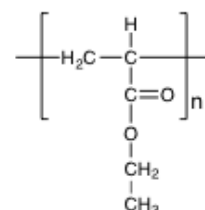
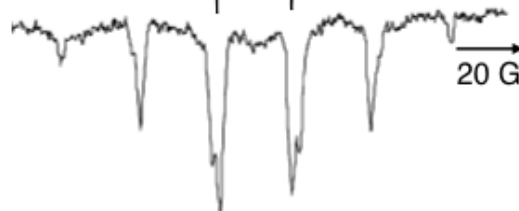


Figure 3.4 Experimental high temperature TREPR spectra for radicals observed after 248 nm laser flash photolysis of the following polymers and their structures: (Top) poly (n-butyl methacrylate), poly (t-butyl methacrylate), poly (methyl methacrylate), and (bottom) poly (ethyl acrylate). The delay time is 500 ns. The PEA spectrum is from McCaffrey, V. P.; Forbes, M. D. E. *Macromolecules* 2005, 38, 3334.

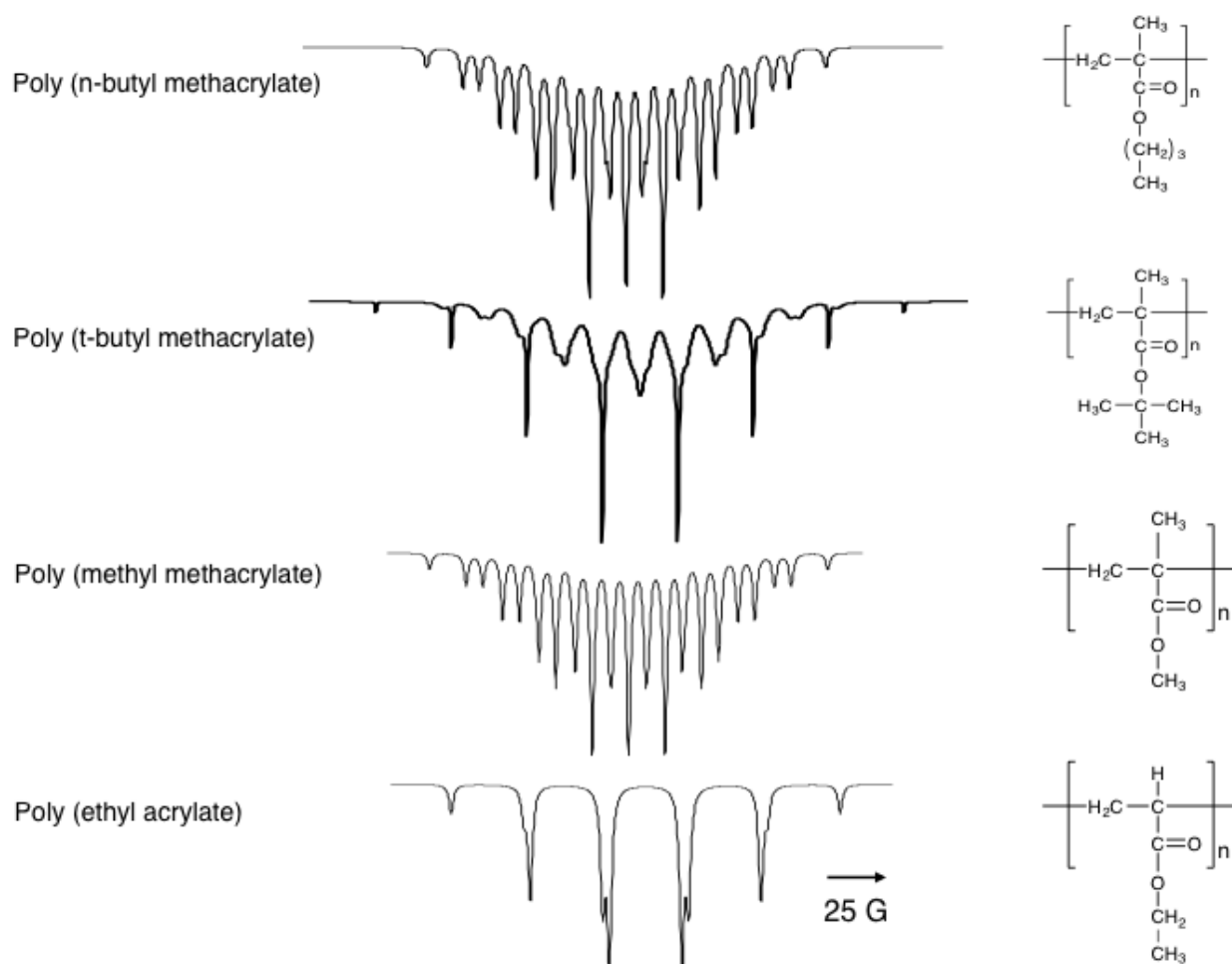


Figure 3.5 Simulated high temperature TREPR spectra for radicals observed after 248 nm laser flash photolysis of the following polymers and their structures: (Top) poly (n-butyl methacrylate), poly (t-butyl methacrylate), poly (methyl methacrylate), and (bottom) poly (ethyl acrylate). The delay time is 500 ns. Except for the spectrum obtained from poly (t-butyl methacrylate), the simulation assigns the signal carrier to main-chain polymer radical. In the case of poly (t-butyl methacrylate), tert-butyl radical after decarboxylation is the dominant signal carrier. Hyperfine value for each simulation are the following: $3a_{\text{H}}(\text{CH}_3) = 22.9 \text{ G}$, $2a_{\text{H}}(\text{CH}_2) = 16.4 \text{ G}$, $2a_{\text{H}}(\text{CH}_2) = 11.3 \text{ G}$ for P(nBMA); $a_{\text{H}}(\text{CH}_3) = 22.8 \text{ G}$, $a_{\text{H}}(\text{CH}_2) = 11.4 \text{ G}$, $a_{\text{H}}(\text{CH}_2) = 14.1 \text{ G}$ LW = 3 (main-chain radical) and $a_{\text{H}}((\text{CH}_3)_3) = 22.8 \text{ G}$ (tert-butyl radical) for P(tBMA); $3a_{\text{H}}(\text{CH}_3) = 22.9 \text{ G}$, $2a_{\text{H}}(\text{CH}_2) = 16.4 \text{ G}$, $2a_{\text{H}}(\text{CH}_2) = 11.7 \text{ G}$ for PMMA; $a_{\text{H}}(\text{H}) = 21.7 \text{ G}$, $2a_{\text{H}}(\text{CH}_2) = 23.5 \text{ G}$, $2a_{\text{H}}(\text{CH}_2) = 23.8 \text{ G}$ for PEA.

There are several noteworthy features of these spectra. At first glance, the spectra in Figure 3.4 appear entirely in net emission, due to the Triplet Mechanism (TM) of CIDEP, but the other spectral features such as line shapes and widths are very different from each other. In particular, the P(t-BMA) spectrum shows an alternating line width effect and line broadening at high temperatures, which is an unusual behavior in the high temperature TREPR spectrum. As mentioned earlier, this is indicative of conformationally induced modulation of hyperfine coupling constants, which is expected for β -hyperfine couplings in polymeric radicals with such bulky substituents on the main chain [10]. A similar sharp line signal carrier with a single coupling constant (~ 23 G) at least eight lines is also observed. These are actually the innermost eight lines of the 10-line t-butyl radical spectrum from decarboxylation of the oxo-acyl radical. This marks the first observation of side chain radical chemistry in acrylic polymer degradation.

In order to simulate the TREPR spectrum of P(t-BMA) in Figure 3.4, values of 22.8 Gauss for the protons for tert-butyl radical with narrow line width along with 22.9 Gauss for the protons of the methyl group, and 15.8 Gauss and 11.2 Gauss were used for the each of the two sets of methylene protons with broad line width. However, The simulation spectrum is not perfectly matched to the experimental data because the alternating line width effect observed in the P(t-BMA) TREPR spectrum. As we discussed in the previous chapter, the presence of the slow conformational motion makes main-chain radicals as broad lines, superimposed with a spectrum from tert-butyl radical in the TREPR spectrum.

It is interesting that the tert-butyl radical created by decarboxylation show high temperature spectrum because even oxo-acyl radical is rarely seen at high temperature because of fast spin relaxation [85]. Furthermore, we should consider the fact that a group of broad lines is present in P(t-BMA) spectrum, which is most likely the (unusual) appearance of the main-chain acrylic

polymer radical at high temperature with perhaps an intermediate or even slow motion TREPR spectrum.

Comparing the main chain radicals of PEA and P(n-BMA), the spectrum of the radical from PEA shows the six lines in Figure 3.4, and can be simulated using values of 21.5 Gauss for the α -proton, 23.5 gauss for two of the β -protons and 24.2 Gauss for the other two β -protons shown in Figure 3.5. On the other hands, the presence of a methyl group in the α -position of P(n-BMA) led to the far more complicated spectrum. The addition of a methyl group on the polymer backbone changes the conformational energies and barriers of the polymer chain. The strong central line, which is an oxo-acyl radical is observed in high TREPR spectrum.

3.2.1 TREPR spectra of Block Copolymers

3.2.1.1 Poly (methyl methacrylate)-b-Poly (tert-butyl methacrylate) Copolymers

One of the hypotheses driving these experiments is that the photophysics, photochemistry, or radical chain dynamics would be site-selective, i.e., one might see different TREPR intensities or line shapes and widths depending on the point of excitation in a block copolymer. Figure 3.6 shows TREPR spectra taken in either propylene carbonate or diglyme during 248 nm laser flash photolysis for three PMMA-b-P(t-BMA) copolymers with different PMMA/PtBMA chain length ratios. In this section, we discuss the following PMMA-b-P(t-MBA) copolymers: (PMMA)₉-b-(P(t-BMA))₁, (PMMA)₁-b-(P(t-BMA))₁ and (PMMA)₁-b-(P(t-BMA))₉ copolymer. Their average molecular weights and PDIs are shown in Table 3.1.

As similar to TREPR spectra of acrylate polymers, the spectra in Figure 3.6 show strong emission from the TM of CIDEP. As discussed in the previous section, the polymer rotational motion along the main axis occurs on a slower time scale than rotation of the individual ester

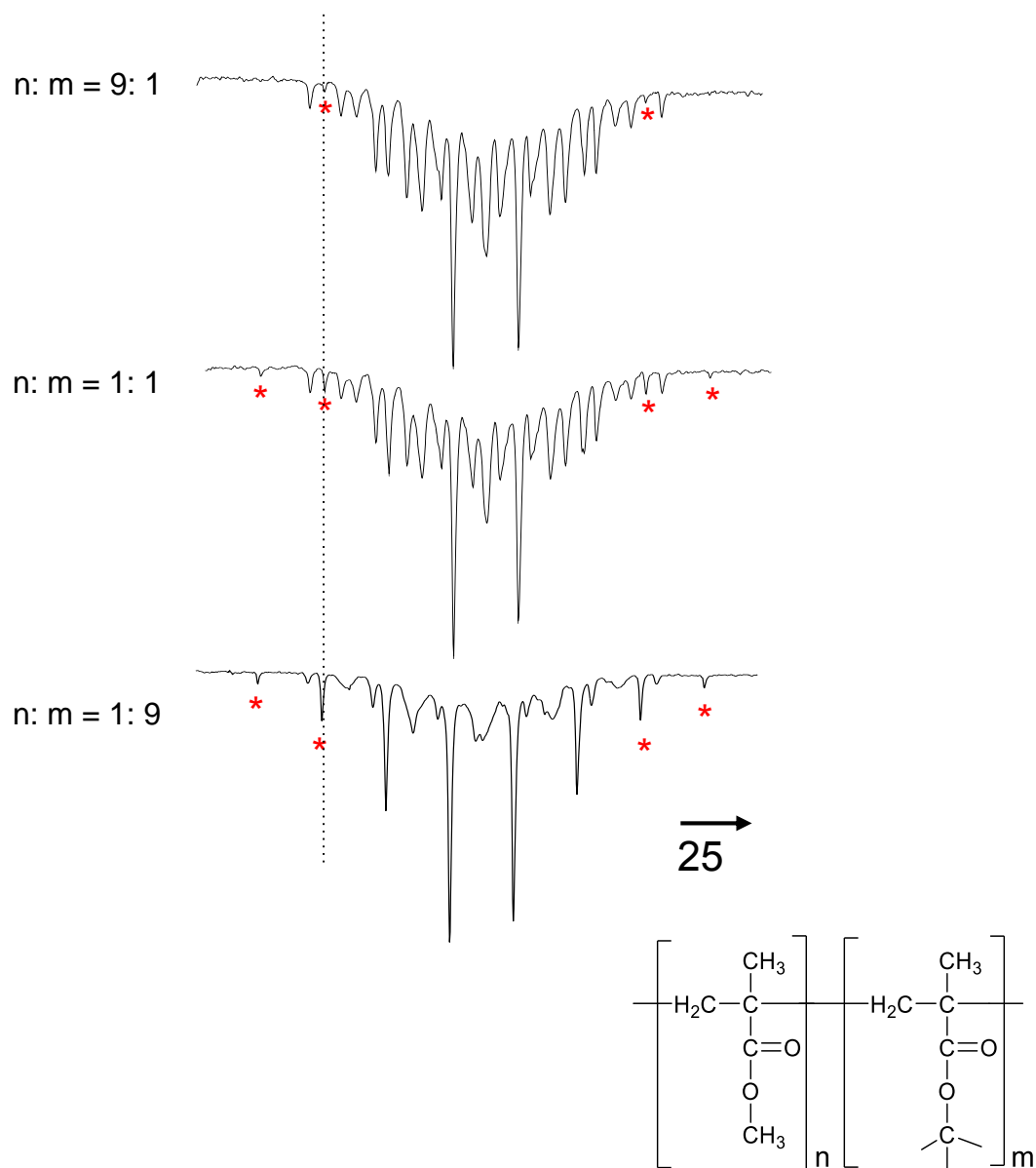


Figure 3.6 Block chain length ratio dependence of Poly (methyl methacrylate)-b-poly (t-butyl methacrylate) copolymer TREPR spectra in diglyme at 500 ns at 125 °C. (Top) 1:9, (middle) 1:1, and (bottom) 1:9. The magnetic field sweep width for all spectra is 200 G. Tert-butyl radical is marked with an asterisk

side chain groups, this asymmetric motion leads to higher selectivity in the intersystem crossing process, a somewhat slower relaxation time of both the excited triplet state and the ensuing polymeric radical exists for the same reasons, and the overall effect leads to an optimal situation for the creation of strong TM polarization.

In Figure 3.6A, the TREPR spectrum is shown for the main chain radical from photolysis of (PMMA)₉-b-P(t-BMA)₁ at high temperature, at a first glance, the spectrum looks very similar to PMMA main chain radicals in terms of the spectral widths and line positions, but the subtle differences become apparent on closer examination, exists. The fast motion TREPR spectrum no longer consists of 21 lines and there are unknown 2 more unknown lines in the spectrum (see red asterisks) whose intensity ratio increase with the increasing ratio of P(t-BMA) chain length within the three block copolymers (compare to Figures 3.6B, and 3.6C). These new lines are assumed to arise from the side chain radical of P(t-BMA). Additionally, the TREPR spectrum of (PMMA)₉-b-P(t-BMA)₁ mostly arises from the main chain radical of PMMA because of its longer chain length. However, when both block chain lengths are same, the signal intensity of PMMA main-chain radical is stronger than that from P(t-BMA). Although, some peaks from P(t-BMA) are overlapping with those of PMMA main chain radicals, two more new lines can be clearly seen in Figure 6.B, which is tentatively attribute to the outmost peak of tert-butyl radical from P(t-BMA).

Figure 3.6C shows the TRERP spectrum from photolysis of (PMMA)₁-b-P(t-BMA)₉ in diglyme at 120 °C. The main feature of this spectrum is the similar large emissive sharp line signal carrier with a single coupling constant (~ 23 G) at least eight lines on a broad emissive background. The sharp lines are actually the innermost eight lines of the 10-line t-butyl radical spectrum from decarboxylation of the oxo-acyl radical shown in Figure 3.7. The broad emissive

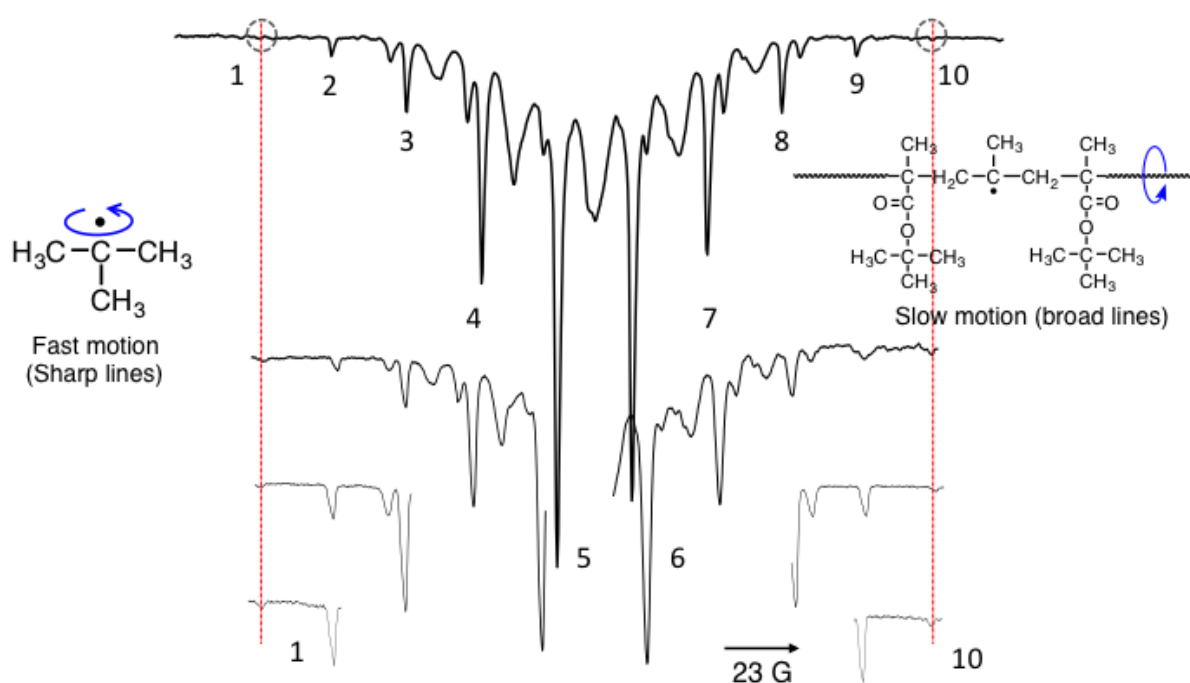


Figure 3.7 The 10-line t-butyl radical spectrum from decarboxylation of poly (t-butyl methacrylate) oxo-acyl radical in diethylene glycol dimethyl ether at 125 °C with following total sweep width: (top) 300 G, 100 G, 50 G, and (bottom) 30 G and delay time: 500 ns

signal in the background is from the main radical from P(t-BMA). The opposite relative intensities were observed for (PMMA)₁-b-P(t-BMA)₉ photolysis. The peak signal of tert-butyl radical is stronger and sharper, broad signal that has similar features to the room temperature spectra was collected for the PMMA main-chain radicals. To make sure of the origin of alternating line width spectrum, we simulated spectrum by using tert-butyl radical with main-chain radical of P(t-BMA), and propagating radical of P(t-BMA). As indicated earlier, conformationally induced modulation of hyperfine coupling constants is usually shown in propagating radicals of polymer after photolysis. The simulated EPR spectra of propagating radical of P(t-MBA) at 150 °C in Figure 3.8, the value of hyperfine coupling constants used here was reported by Kaiwara et al [86]. However, the spectrum is quite different suggesting that the TREPR spectrum of (PMMA)₁-P(t-BMA)₉ mainly from tert-butyl radical not propagating radical. It is also important to note that rich P(t-BMA) on block copolymer will make the polymer chain more rigid which leads to slow conformational dynamics of P(t-BMA) main chain radical.

Figure 3.9 shows the temperature dependence of the TRPER spectra obtained upon photodegradation of all three PMMA-b-P(t-BMA) block copolymers in PC or diglyme. Clearly, all three block copolymers show large changes in both line width and shape upon heating. As we discussed before, the large changes are related to the conformational dynamic motion of β -hyperfine coupling because the mechanism of this interaction is dependent on the dihedral angle between the unpaired p orbital of carbon centered radical and the C-H σ bond adjacent to it. At the highest temperature (~120 °C), all three samples show motionally narrowed spectra with very sharp line widths representing an average of the hyperfine coupling constant via fast chain dynamics. In addition, the alternating line width effect appears in the lower temperature

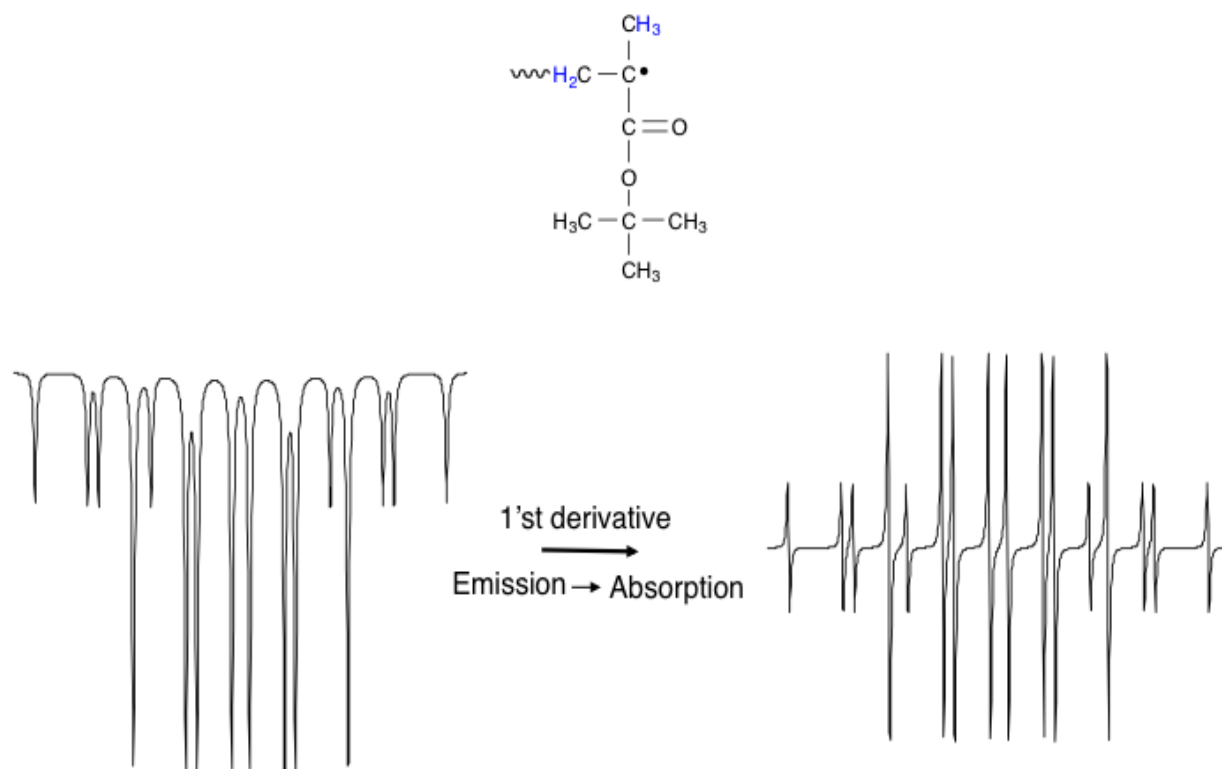


Figure 3.8 Structure of propagating radical of poly (t-butyl methacrylate) and simulated EPR spectra of the propagating radical of poly (t-butyl methacrylate) (left) direct detection and (right) 1'st derivative at 150 °C. The magnetic field sweep width for all spectra is 200 G. Simulation parameters: $3 a_{\text{H}}(\text{CH}_3) = 21.7 \text{ G}$, $a_{\text{H}}(\text{CH}) = 14 \text{ G}$, and $a_{\text{H}}(\text{CH}) = 11.6 \text{ G}$ from Kajiwara, A.; Maeda, K.; Kubo, N.; Kamachi, M. *Macromolecules* 2003, 36, 526–528.

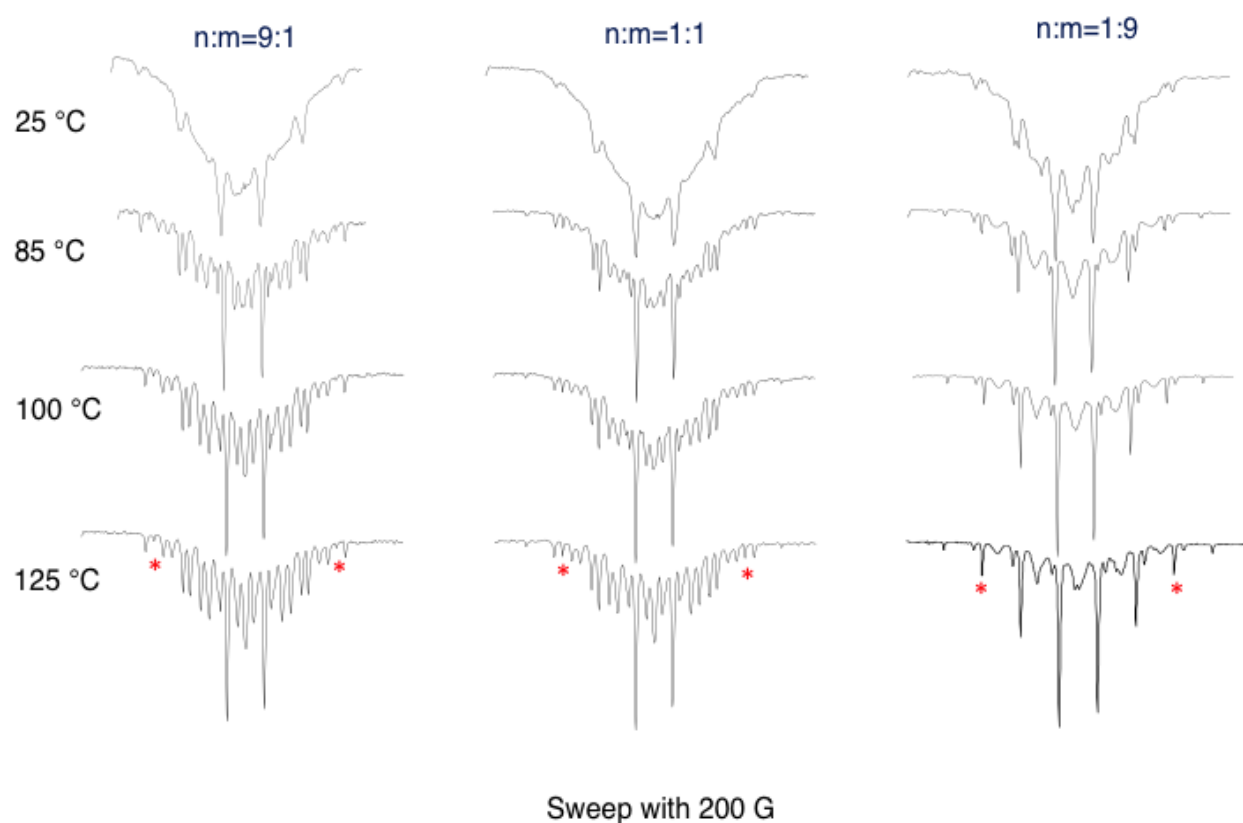


Figure 3.9 The temperature dependence of TREPR spectra for the main-chain radical from 248 nm irradiation of all three Poly (methyl methacrylate)-b-poly (t-butyl methacrylate) copolymer in either diglyme or propylene carbonate (1g of polymer in 25 ml of solvent) at delay time of 500 ns. The temperature for spectra is shown in °C and the magnetic sweep width is 200 G for all spectra. Tert-butyl radical is marked with an asterisk

spectra because of slow motion conformational motion in polymer chain [87]. Restricted and slow chain dynamic allows detection of all possible conformations resulting in broad line width of spectra similar to lower temperature and even frozen EPR spectra of the propagating radical of the polymer [88].

In order to compare chain dynamics between PMMA-b-P(t-BMA) block copolymers and random copolymers, a random copolymer is synthesized. However the random copolymer did not dissolved either PC or diglyme and show phase separation even at high temperature. Therefore the TREPR spectrum of PMMA-P(t-BMA) random copolymer was not obtained.

It is interesting to note that TREPR spectra of main-chain radical of both (PMMA)₉-b-P(t-BMA)₁ and (PMMA)₁-b-P(t-BMA)₉ looks similar to the i-PMMA main chain radical which has shown faster chain dynamics than those two other PMMA polymers. (a- and s- PMMA)

3.2.1.2 Poly (methyl methacrylate)-b-Poly (n-butyl methacrylate) Copolymers

In Figure 3.10, experimental TREPR spectra and the simulations are shown from the photolysis of (PMMA)₉-b-P(n-BMA)₁, (PMMA)₁-b-P(n-BMA)₉ and random PMMA-co-P(n-BMA) (1:1 wt%) at 120 °C. Molecular weight and PDI of these copolymers report in Table 3.1. All spectra in Figure 3.10 looks almost identical with regard to the number of transition, line position and spectral width, however on a closer view (box), it is suspected that central line in (PMMA)₁-b-P(n-BMA)₉ spectrum has split into doublet. It is interesting note that the observed P(n-BMA) TREPR spectrum also shows a large central line, which is distinguishable from TREPR spectrum of PMMA. The simulation of n-butyl radical using literature values supports this feature because the simulated n-butyl spectrum also has a large central line [89].

Additionally, the doublets observed in both TREPR spectrum of P(n-BMA) at high

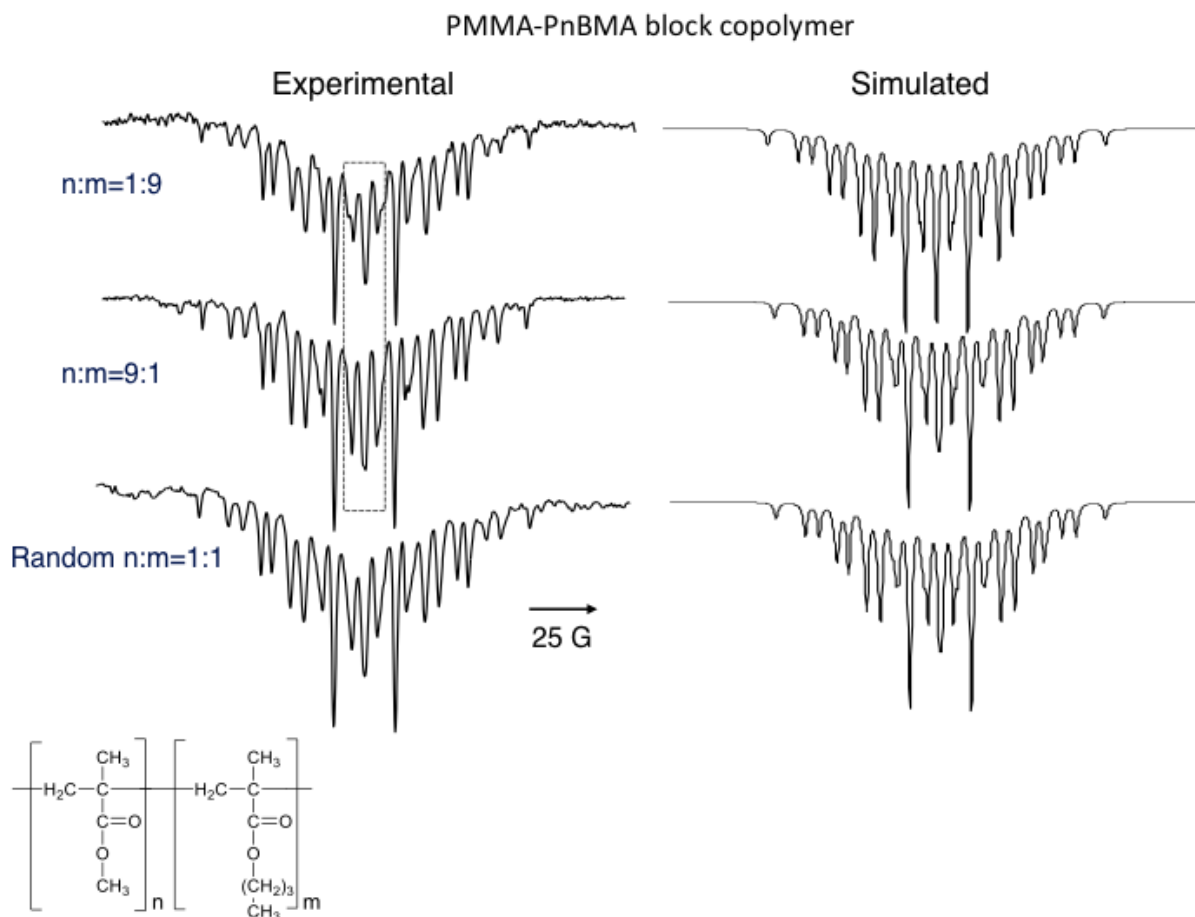


Figure 3.10 Block chain length ratio dependence of Poly (methyl methacrylate)-b-poly (n-butyl methacrylate) copolymer TREPR spectra in diglyme at 500 ns at 115 °C. (Top) 1:9, (middle) 9:1, and (bottom) random 1:1. The magnetic field sweep width for all spectra is 200 G. Computer simulation of the fully converged, high temperature limit spectra are shown side by side with the experimental data, and hyperfine values for each copolymer are following: $3a_{\text{H}}(\text{CH}_3) = 22.9 \text{ G}$, $2a_{\text{H}}(\text{CH}_2) = 16.1 \text{ G}$, $2a_{\text{H}}(\text{CH}_2) = 10.9 \text{ G}$ for $(\text{PMMA})_9\text{-b-}(\text{PnBMA})_1$ and random PMMA-b-P(nBMA) ; $3a_{\text{H}}(\text{CH}_3) = 22.9 \text{ G}$, $2a_{\text{H}}(\text{CH}_2) = 16.4 \text{ G}$, $2a_{\text{H}}(\text{CH}_2) = 11.3 \text{ G}$ for $(\text{PMMA})_1\text{-co-}(\text{PnBMA})_1$

temperature and simulated n-butyl radical would be positioned in the middle of lines spectrum. Similar to $(\text{PMMA})_1\text{-b-P}(\text{t-BMA})_9$ copolymer (Figure 3.6), this might be the first observation of side chain radical in high temperature TREPR spectrum. Although for the $(\text{PMMA})_1\text{-b-P}(\text{t-BMA})_9$, the signal from the t-butyl radical dominates the spectrum due to its high intensity packed into just a few transitions. The n-butyl radical shows a similar intensity to main-chain radical from $\text{P}(\text{n-BMA})$. Thus it is likely that both radical is superimposed.

In contrast to TREPR spectrum of $(\text{PMMA})_1\text{-b-P}(\text{n-BMA})_9$ and, $(\text{PMMA})_9\text{-b-P}(\text{n-BMA})_1$, the spectrum from random $\text{PMMA-co-P}(\text{n-BMA})$ (1:1 wt%) does not show any special features, and showing only the main-chain radical from PMMA.

Computer simulations of the fully converged, high temperature limit spectra are shown side by side with the experimental data in Figure 3.10. The hyperfine coupling constants used for each simulations are listed in the figure caption. The simulation of three samples is straightforward. A value of 22.9 G, standard values for free rotating methyl group, [90-92] was used for the hyperfine coupling constant for the proton of the methyl group, which is identical to all three spectrum. For the two sets of methylene group, 16.1 G and 10.9 G were used for $(\text{PMMA})_9\text{-b-P}(\text{n-BMA})_1$, and random $\text{PMMA-co-P}(\text{n-BMA})$ (1:1 wt%). However, In order to simulate the experimental TREPR spectrum of $(\text{PMMA})_1\text{-b-P}(\text{n-BMA})_9$, the values of 16.4 G and 11.3 G were used for the each of β -protons of the two methylene group. The additional splitting in the TREPR spectrum was simulated by modifying the hyperfine coupling constants for the methylene protons. As we discussed our early papers, changing side ester chain methyl to ethyl leads to change the relative energies of the conformation and the barrier heights thus resulting in hyperfine constants. In the same manner, when the $\text{P}(\text{n-BMA})$ is rich in block copolymer, hyperfine coupling constants are more related with $\text{P}(\text{n-BMA})$ conformation and their barrier thus the appearance of TRERP

between $(\text{PMMA})_1\text{-b-P(n-BMA)}_9$ and $(\text{PMMA})_9\text{-b-P(n-BMA)}_1$.

Figure 3.11 shows the temperature dependence of the TREPR spectra of $(\text{PMMA})_1\text{-b-P(n-BMA)}_9$ and $(\text{PMMA})_9\text{-b-P(n-BMA)}_1$ at a variety of temperature. As the temperature was increased from 28 °C to 115 °C, the alternating sharp and broad lines become sharper and show motional narrowing. The lower temperature spectra showed the same alternating line width effect as observed with PMMA at low temperature. However, in the case of $(\text{PMMA})_1\text{-b-P(n-BMA)}_9$ at higher temperature, the center line become a strong singlet unlike the spectrum at lower temperature.

It is a rather unexpected result in that the lines in the $(\text{PMMA})_1\text{-b-P(n-BMA)}_9$ spectrum at 28 °C was not broader than $(\text{PMMA})_9\text{-b-P(n-BMA)}_1$. From our previous study [10], the dynamics of the ester group (β -relaxation) can couple to the motion of the polymer backbone (α -relaxation) and influence the R-relaxation rates. Additionally, relaxation is related with T_g of polymer. For example, the PEMA polymer chain backbone is much more rigid than PMMA due to bulkier ester side chain thus TREPR spectrum of PEMA shows broader line at lower temperature than in PMMA because the larger ethyl group in PEMA makes the β -relaxation processes of the side chains slower by an order of magnitude. Although the structure of P(n-BMA) looks more complicated than PMMA, the T_g of P(n-MBA) (25 °C) is much lower than PMMA (115 °C). Therefore, TREPR spectrum P(n-BMA) rich block copolymer at lower temperature do not show broader lines compared to that of $(\text{PMMA})_9\text{-b-(P(n-BMA))}_1$.

3.2.1.3 Poly (methyl methacrylate)–b–Poly (ethyl acrylate) Copolymers

So far, we have discussed only methacrylate types of A-B block copolymer. In this

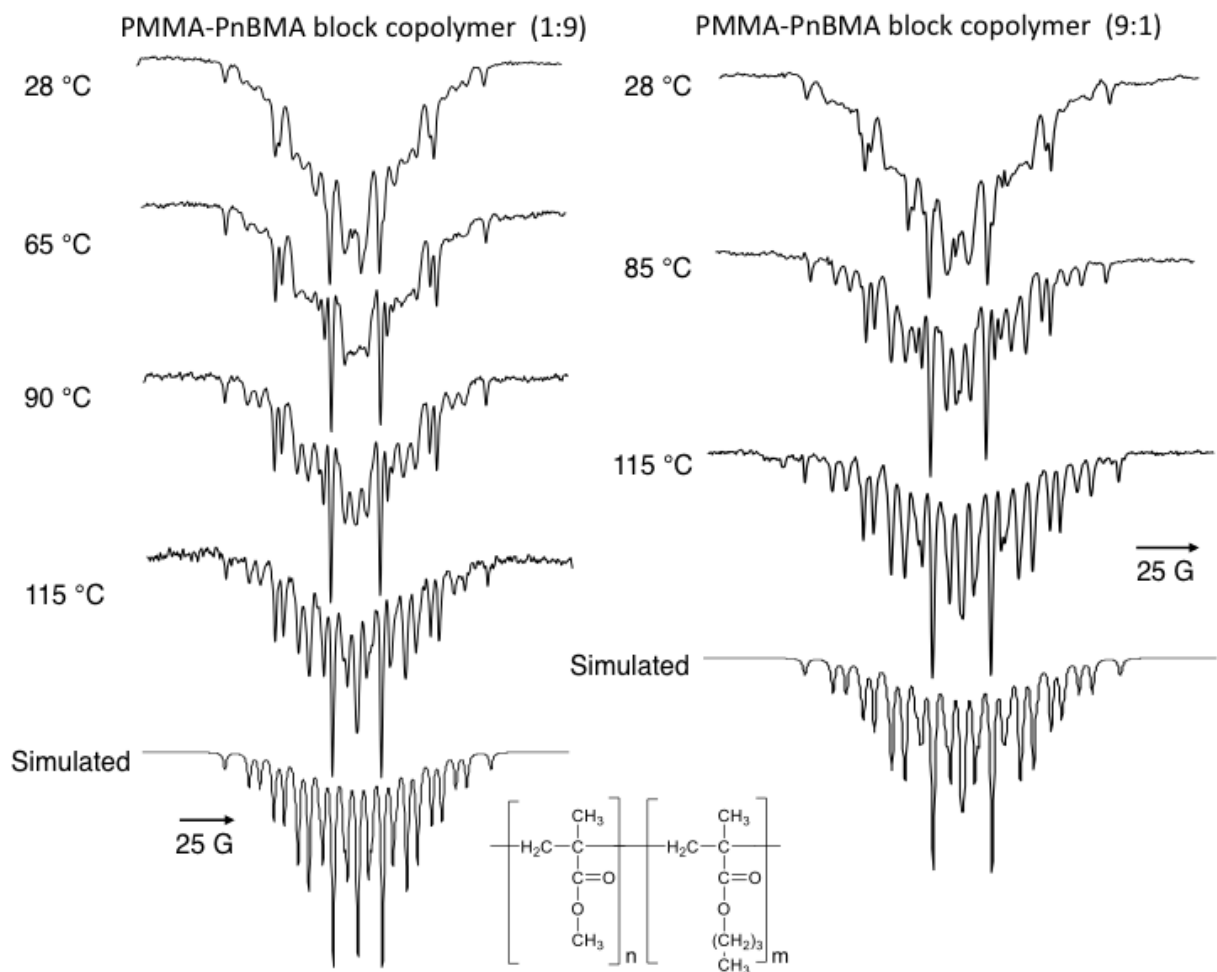


Figure 3.11 The temperature dependence of TREPR spectra for the main-chain radical from 248 nm irradiation of all two Poly (methyl methacrylate)-b-poly (t-butyl methacrylate) copolymer in either diglyme or propylene carbonate (1g of polymer in 25 ml of solvent) at delay time of 500 ns. The temperature for each spectrum is shown in °C and the magnetic sweep width is 200 G for all spectra. (Bottom) The simulated high-temperature TREPR spectra for each copolymer. Hyperfine values for each copolymer are the following : $3a_{\text{H}}(\text{CH}_3) = 22.9 \text{ G}$, $2a_{\text{H}}(\text{CH}_2) = 16.4 \text{ G}$, $2a_{\text{H}}(\text{CH}_2) = 11.3 \text{ G}$ for $(\text{PMMA})_1\text{-b-}(\text{PnBMA})_9$ and $3a_{\text{H}}(\text{CH}_3) = 22.9 \text{ G}$, $2a_{\text{H}}(\text{CH}_2) = 16.1 \text{ G}$, $2a_{\text{H}}(\text{CH}_2) = 10.9 \text{ G}$ for $(\text{PMMA})_9\text{-b-}(\text{PnBMA})_1$

section we present result on A-block is methacrylate polymer with B-block is acrylate copolymer.

TREPR spectrum of PEA and PMMA are quite different in terms of number of line, line position and line width as shown in Figure 3.12. In the case of PEA, main chain radical shows six major transitions with the doublets of the innermost lines attributed to two β -methylene hyperfine couplings of 23.0 and 24.7 G and one α -hyperfine coupling of 21.5 G, which were comparable to the reported literature values for radicals of similar chemical structure. The oxo-acyl radical from PEA was not observed at high temperature because the signal from this radical decays rapidly due to fast spin relaxation. As we discussed earlier chapter, the different symmetry relationships between PEA and PMMA main chain radical resulted in the large difference between PEA and PMMA spectra. In addition, methacrylate polymers show a strong tacticity dependence unlike in PEA.

Figure 3.12 shows the experimental spectra and the corresponding simulation of the TREPR spectra from photolysis of $(\text{PMMA})_9\text{-b-(PEA)}_1$, $(\text{PMMA})_1\text{-b-(PEA)}_1$, PEA and PMMA in propylene carbonate solution. PEA and PMMA spectrum is also shown here for comparison. Similar to other PMMA rich block copolymers, the TREPR spectrum shows intense emission from the TM of CIDEP. Also the appearance of TREPR spectra is identical in each case. Even the $(\text{PMMA})_1\text{-b-(PEA)}_1$ block copolymer has same features as PMMA main chain radical after photolysis. The temperature dependence of the TREPR spectra from the $(\text{PMMA})_9\text{-b-(PEA)}_1$ and $(\text{PMMA})_1\text{-b-(PEA)}_1$ main chain radicals are shown in Figure 3.13. The same alternating line width effect at lower temperature are observed for both $(\text{PMMA})_9\text{-b-(PEA)}_1$ and $(\text{PMMA})_1\text{-b-(PEA)}_1$. With increasing temperature, a large transformation takes place in both figure and full convergence motionally narrowed spectrum is clearly observed.

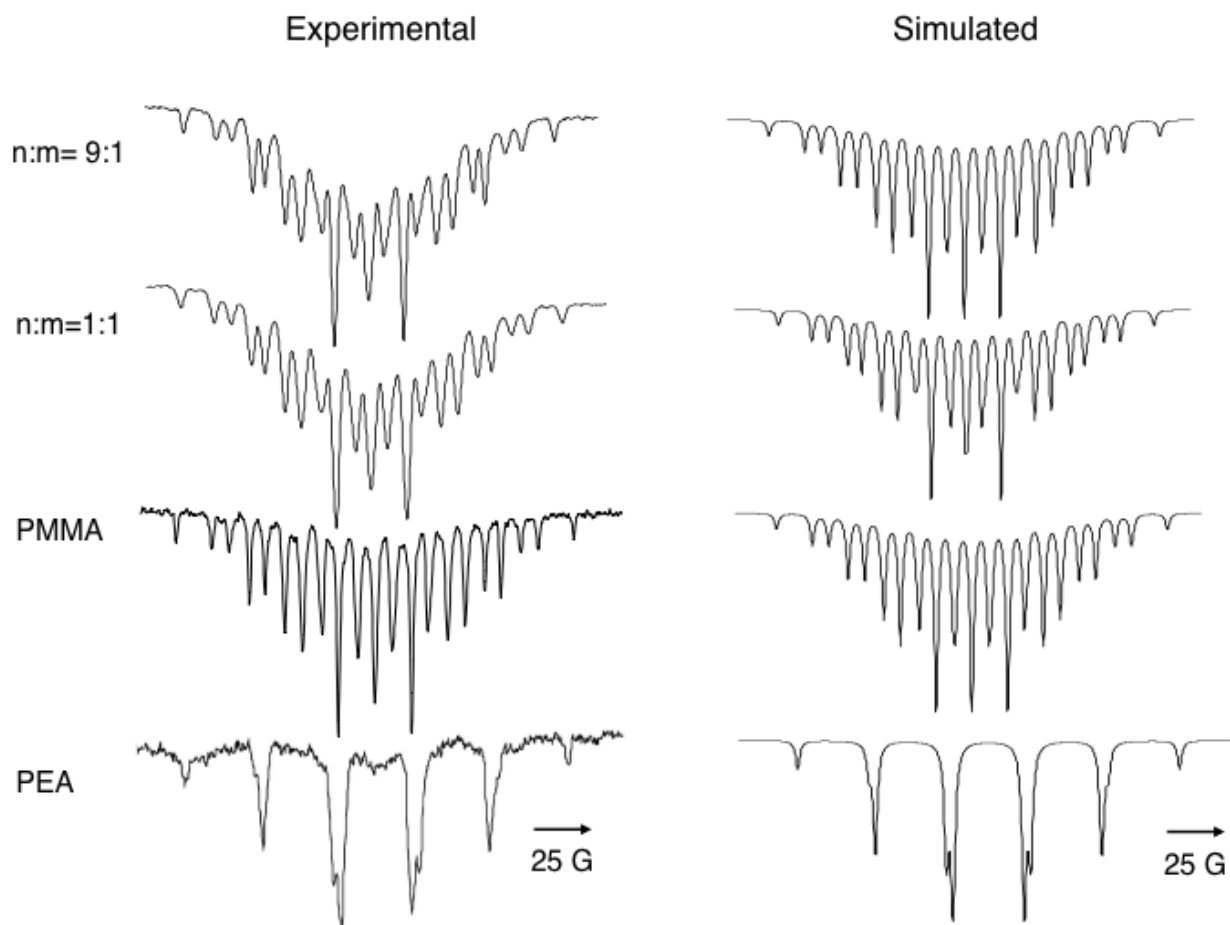


Figure 3.12 (Left) Experimental high temperature TREPR spectra and (Right) simulated spectra for main-chain radicals observed at 500 ns after 248 nm laser flash photolysis of the following polymers: Poly (methyl methacrylate)-b-poly ethyl acrylate) copolymer (Top) $n:m = 9:1$, $1:1$, poly methacrylate , and (bottom) poly ethyl acrylate for comparison in propylene carbonate (1g polymer in 25 ml solvent). The magnetic sweep for all spectra is 150 G. The simulated high-temperature TREPR spectra for each copolymer. Hyperfine values for each copolymer are the following: $3a_H(\text{CH}_3) = 22.9$ G, $2a_H(\text{CH}_2) = 16.4$ G, $2a_H(\text{CH}_2) = 11.7$ G for PMMA and $(\text{PMMA})_9\text{-b-}(\text{PEA})_1$; $3a_H(\text{CH}_3) = 22.9$ G, $2a_H(\text{CH}_2) = 16.4$ G, $2a_H(\text{CH}_2) = 11.0$ G for $(\text{PMMA})_1\text{-b-}(\text{PEA})_1$; $a_H(\text{H}) = 21.7$ G, $2a_H(\text{CH}_2) = 23.5$ G, $2a_H(\text{CH}_2) = 23.8$ G for PEA.

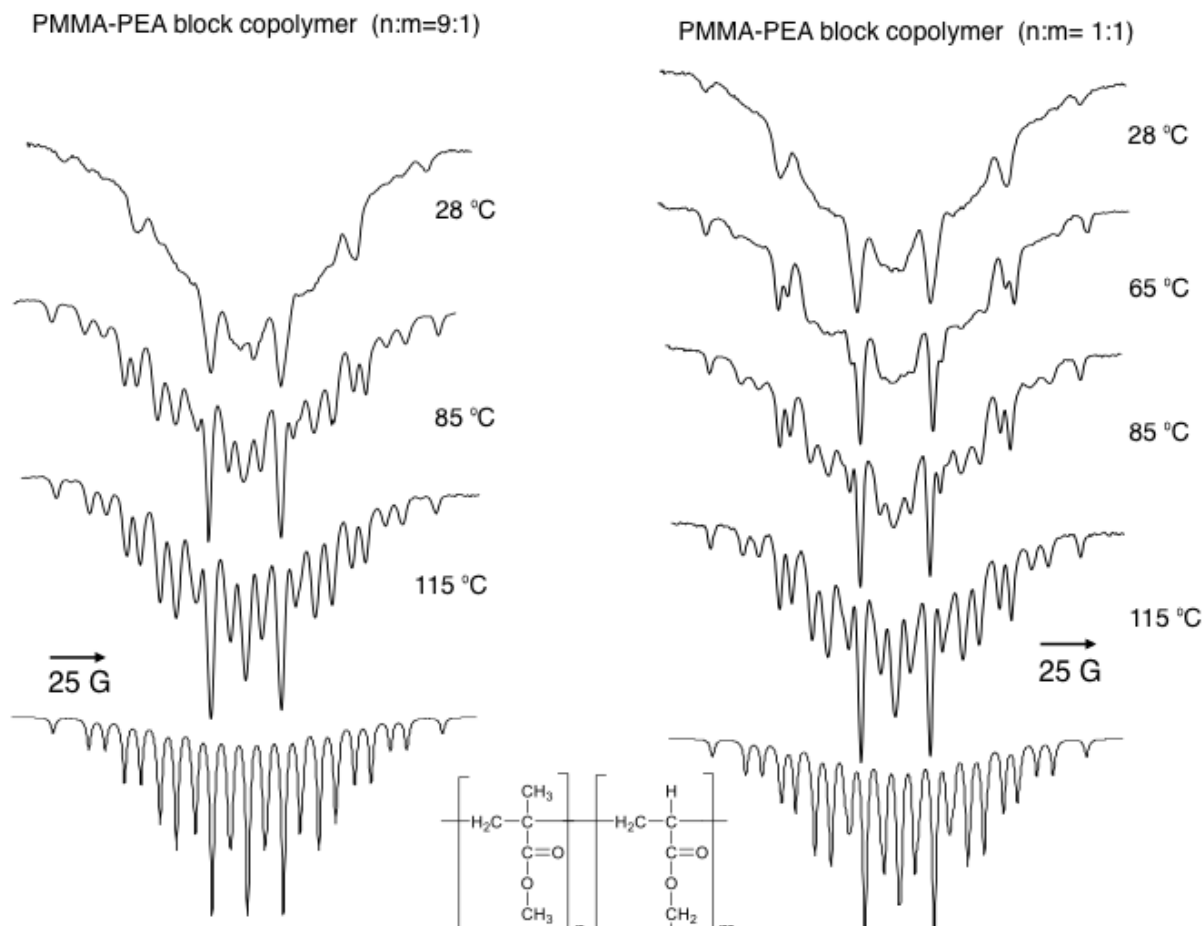


Figure 3.13 The temperature dependence of TREPR spectra for the main-chain radical from 248 nm irradiation of all two Poly (methyl methacrylate)-b-poly (ethyl acrylate) copolymer in propylene carbonate (1g of polymer in 25 ml of solvent) at delay time of 500 ns. The temperature for each spectrum is shown in °C and the magnetic sweep width is 150 G for all spectra. (Bottom) The simulated high-temperature TREPR spectra for each copolymer. Hyperfine values for each copolymer are the following: $3a_{\text{H}}(\text{CH}_3) = 22.9 \text{ G}$, $2a_{\text{H}}(\text{CH}_2) = 16.4 \text{ G}$, $2a_{\text{H}}(\text{CH}_2) = 11.7 \text{ G}$ for $(\text{PMMA})_9\text{-b-(PEA)}_1$; $3a_{\text{H}}(\text{CH}_3) = 22.9 \text{ G}$, $2a_{\text{H}}(\text{CH}_2) = 16.4 \text{ G}$, $2a_{\text{H}}(\text{CH}_2) = 11.0 \text{ G}$ for $(\text{PMMA})_1\text{-b-(PEA)}_1$

3.3 Summary and Outlook

The TREPR spectra presented in this chapter are rich in information about the spin selective and conformational chain dynamics of several acrylate block copolymers as a function of temperature, ester side chain stiffness, and variation of chain length of block chains. The excellent visual fit of the simulations at high temperature TREPR spectra of several block copolymers lead us to the unambiguous identification of the photochemical and photophysical events of these acrylates copolymers. As we expected that the conformational dynamics e.g., fast or slow conformational of the each blocks plays important role on line shapes and appearances of spectrum. In particular, the P(t-BMA) rich block copolymer spectrum shows an alternating line width effect and line broadening at high temperatures, which is an unusual behavior in the high temperature TREPR spectrum. This is indicative of conformationally induced modulation of hyperfine coupling constants, which is expected for β -hyperfine couplings in polymeric radicals with such bulky substituents on the main chain. The simulations of all block copolymers at higher temperature are well matched to the experimental data except for P(t-BMA) rich block copolymer spectrum. Because the anisotropic motion between t-butyl radicals (fast motion) and main-chain radicals (slow motion), it is hard to produce the perfect fit simulated spectrum.

Future work to produce the better fit of the simulation of P(t-BMA) rich copolymers at high temperature. In order to better understand of dynamics of these block copolymers in terms of variation of block chain lengths, we will measure the spin-lattice relaxation rates by kinetic profiles at a constant magnetic field. By using the triplet quenchers such as a sorbic acid, we can be measured of the life times of the ester side chains. The E_a can be calculated to measure the rotational correlation times of these block copolymers by using spin-probe methods or two-jump model.

3.4 Experimental

3.4.1 Materials

MMA, t-BMA, n-BMA and EA (Aldrich) were passed through columns of activated basic alumina and stored at -20 °C prior to use. Extra dried, and stabilized THF (99.5%) was purchased from Aldrich. n-Butyllithium (n-BuLi) (Aldrich, 2.5M solution in cyclohexane), 1,1-diphenylethylene (DPE, Aldrich, 97%), α -methylstyrene (α -MeSt, Aldrich, 99%), and Cyclohexane were used as received. 2,2-Azoisobutyronitrile (AIBN, Aldrich 98%) was doubly recrystallized from methanol. LiCl (99.9%, Aldrich) was dried under vacuum overnight at 130 °C.

3.4.2 Synthesis

3.4.2.1 Anionic Polymerization

The block copolymers used in this paper were synthesized by the anionic polymerization [93]. At the beginning, LiCl was first introduced into a flamed Schlenk Flask and purged with N₂. THF and DPE or α -MeSt were transferred into the Flask by using glass syringes and needles, then the initiator solution (n-BuLi) was added dropwise. (dark red) Finally, the solution was cooled down to -78 °C and added with the required amount of MMA. The polymerization was conducted at -78 °C for 6h. Once MMA was added to the mixture solution, the deep red color of the initiator immediately disappeared due to start initiation. Sequential addition and polymerization of the desired amount of t-BMA, n-BMA and EA were carried out under the same experimental conditions. The copolymerization product was quenched by degassed methanol and the final solution was concentrated before being precipitated into an excess of 90:10 (v/v) methanol–water mixture under stirring. The copolymer was dried under vacuum at 70°C overnight.

1. MMA and t-BMA (Mole ratio 9:1, 1:1 and 1.9)

LiCl/DPE or α -MeSt / n-BuLi + 2 . MMA and n-BMA (Mole ratio 9:1 and 1.9)

(-78 °C, N₂)

3. MMA and EA (Mole ratio 9:1 and 1:1)

3.4.2.2 Free radical Polymerization

To compare photo degradation mechanism between linear block copolymer and random block copolymer, the random block copolymers were also prepared by the free solution radical polymerization. First, cyclohexane was introduced into a flamed glass round bottom flask with magnetic stirrer and purged with N₂, then added inhibitor free MMA and t-BMA, n-BMA or EA by using syringe. While stirring, AIBN as initiator was transferred into solution. The solution degassed with N₂ for 30 min before immersed in an oil bath at 65 °C. After 24h, copolymer was diluted by methylene chloride and precipitated in cold methanol. The crude polymer was dried under vacuum at 70 °C overnight.

3.4.3 Analysis of polymer samples

3.4.3.1 Gel Permeation Chromatography (GPC)

Molecular weights, relative to narrow poly methyl methacrylate standards, were measured using a Waters GPC system consisting of a Waters 510 pump, a Waters 717 autosampler, a Wyatt Optilab DSP refractometer, and a Wyatt Dawn EOS light scattering detector. THF was used as the mobile phase at a flow rate of 1 mL/min with a sample injection volume of 100 μ L. The concentration of sample 5mg/ml. The molecular weights and molecular weight distributions were determined by GPC.

3.4.3.2 High temperature TREPR set-up

Continuous wave TREPR experiments were performed as previously described [10]. All experiments were performed on a JEOL USA Inc. JES-RE1X X-band EPR spectrometer equipped with a wide bandwidth preamplifier and a low-noise GaAsFET microwave amplifier. Samples were typically prepared as solutions of block copolymer (1g) in propylene carbonate or dimethyl ethyl ether (diglyme) (30 ml) and circulated through a quartz flat cell (0.4 mm path length) positioned in the center of a Varian TE₁₀₃ optical transmission cavity. The solutions were photolyzed using a Lambda Physik Compex 120 excimer laser (248 nm, KrF) running at 60 Hz with a pulse energy of 100 mJ (~20 mJ per pulse hitting the sample) and a pulse width of 17 ns. Spectra were collected in the absence of field modulation at a fixed delay time after the laser flash using a two-gate boxcar integrator (Stanford, 100 ns gates), while the external magnetic field was swept with a scan time of 4 min.

To obtain high-temperature TREPR spectra with flowing samples, a special flow apparatus insulated with polyurethane foam can provide stable laminar flow of liquids through the EPR resonator at temperatures up to 150 °C. From the pump, the sample tubing passes through a copper coil wrapped with heating tape (Omega, Inc.), which is controlled using a feedback circuit between a variable power temperature controller and two thermocouples, one placed at the entrance and the other at the exit of the quartz flow cell. Reported temperatures are the average of measurements taken from these thermocouples. The maximum temperature gradient at the highest temperature is about 10 °C but can be as little as 2 °C if the flow rate is fast enough. Very often, the micropump head gets very hot and its internal thermal interlock can switch it off. We have found that wrapping the pump motor casing with copper tubing and circulating cold water through it, using a

submersible pump and ice water bath, is sufficient to avoid this problem.

The choice of solvent is critical for the success of high-temperature experiments. The solvent must (1) dissolve the sample to a concentration that achieves the desired absorbance at the flat cell path length, (2) have a high enough boiling point so that it can withstand the reservoir temperature without evaporating or decomposing, and (3) be optically transparent at the laser excitation wavelength being used. For very high temperatures, diglyme and propylene carbonate are excellent choices as they are transparent at 248 nm and high boiling. If temperatures above 100 °C are desired for aqueous samples, small amounts of ethylene glycol can be added to the solution to raise the boiling point.

Chapter 4. Radical-Triplet Pair Interactions as Probes of Long-Range Polymer Motion in Solution

4.1 Introduction

The molecular dynamics of polymer chains is a topic of great interest in many areas of chemistry and materials science [94-97]. Polymer solutions can be classified as dilute, semi-dilute and concentrated, and of course polymer melts in the absence of solvent can form a bulk liquid state. Above the glass transition temperature and melting point, the viscoelastic (mechanical) properties of polymer melts (neat polymeric liquids), are of interest, but a particular challenge in understanding macromolecular motions is to separate intrinsic polymer properties (e.g., conformational energies) from interchain interactions (entanglements) in the bulk polymer melt state [98,99]. In this regard, physical measurements of polymer conformational dynamics in dilute solution can be very informative. Conformational motion of molecules has been studied by many techniques. The study of Steady-State electron paramagnetic resonance (SSEPR) spin-labeled polymers provides useful information about the molecular dynamics of polymers [100]. The mobility of covalently jointed spin labels, such as nitroxide is sensitive to the flexibility or rigidity of the polymer chain backbone, and its mobility can be quantified by the rotational correlation times in polymer systems. Over the past decade, our laboratory has been studying local chain dynamics in acrylic polymers in dilute solutions using time-resolved electron paramagnetic resonance (TREPR) spectroscopy [101,102].

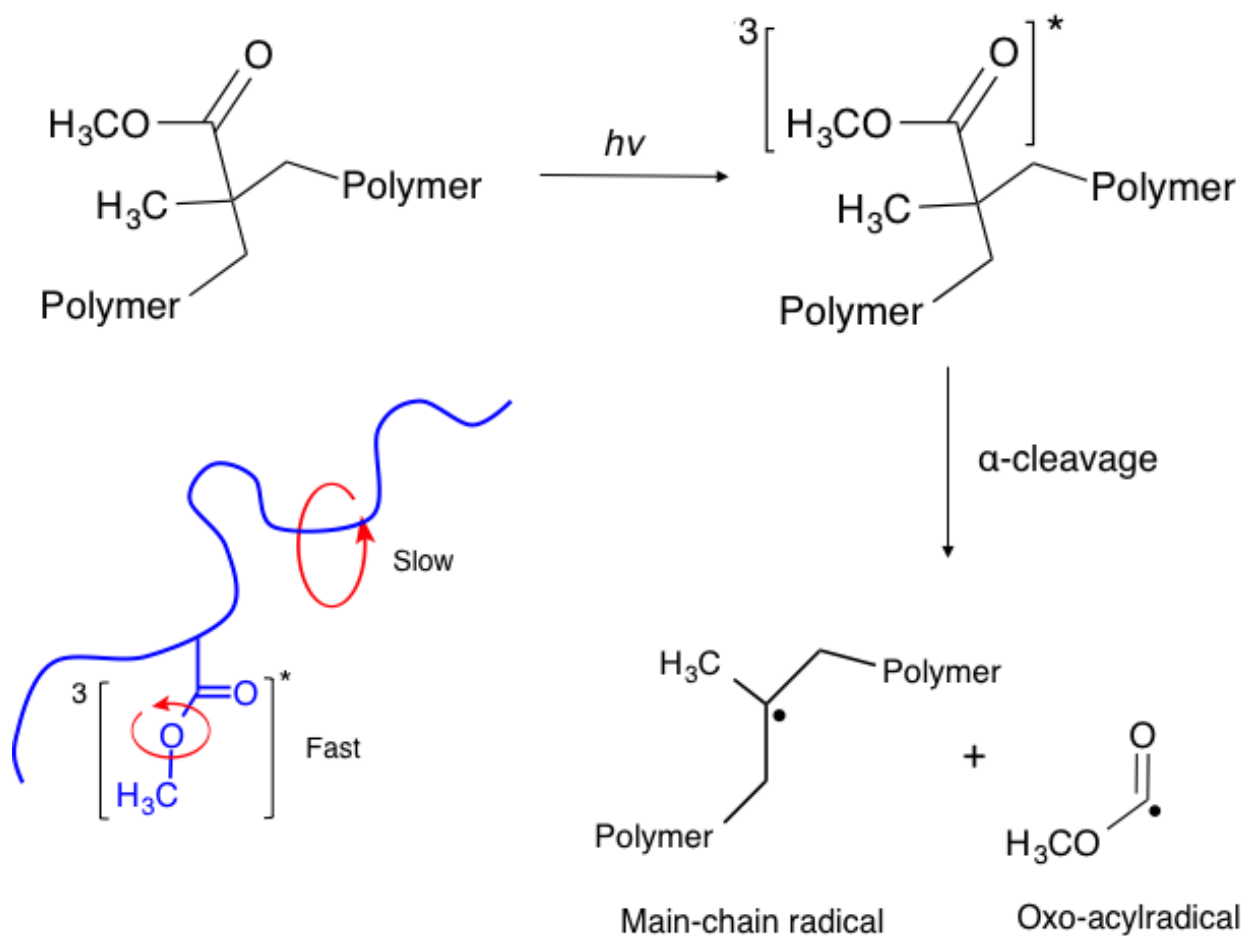


Figure 4.1 Norrish I α -cleavage reaction of poly(methyl methacrylate) (PMMA) and graphical representation of the fast rotation of the side chain along one axis and the much slower conformational motion along the polymer chain.

For example, Figure 4.1 shows the Norrish I α -cleavage reaction of poly(methyl methacrylate) (PMMA) [103], leading to a main chain polymeric radical. The radical center functions as a very small spectroscopic probe of the internal polymer chain dynamics, and the TREPR spectra from such radicals have been shown to be sensitive to solvent, temperature, ester side chain structure, and the stereochemistry of the neighboring carbon atoms.

An often informative feature of TREPR spectra is chemically induced dynamic electron spin polarization (CIDEP), which produces non-Boltzmann electron spin state populations in the radicals⁹ and gives information regarding the spin state of the excited state precursor, diffusive encounters between paramagnetic species, and other dynamic effects such as conformational motion.

In this chapter, by using SSEPR, we characterize the rotational mobility of nitroxide attached PMMA copolymer in dilute solution. The Microscopic Order–Macroscopic Disorder Model model and simulated rotational correlation times allow us to study the local segmental dynamics in our nitroxide attached polymer sample. Also, we examine the RTPM in acrylic polymer/nitroxide systems under different conditions of nitroxide mobility. By comparing TREPR spectra when the nitroxide radical is free to move in solution to those obtained when it is tethered via covalent bonds to the polymer backbone, the influence of intramolecular chain dynamics can be qualitatively assessed. Additionally, the dependence of the RTPM polarization in the covalently linked system as a function of nitroxide incorporation (mol%), temperature, solvent, and acrylic polymer ester side chain structure will be presented.

4.2. The Microscopic Order–Macroscopic Disorder Model (MOMD)

Spectral fitting of nitroxides exhibiting slow rotational motion or ordering are regularly

Spectral fitting of nitroxides exhibiting slow rotational motion or ordering are regularly carried out using a fitting program described extensively by Budil et al. [104] Commonly referred to as the Freed program, it is based on least-squares fitting of experimental spectra using the stochastic Liouville equation. Model parameters for the calculation of slow motion spectra include the magnetic and structural parameters of the radical, dynamic parameters including rates of rotational diffusion, and ordering potentials that describe the influence of anisotropic fluids like liquid crystals or frozen polymer solutions. On the whole, this makes the program useful for examining the dynamic motion of nitroxide radicals in macromolecular structures. However, because a large number of parameters can contribute to the observed line shape of a slow motion EPR spectrum and least-squares fitting is particularly sensitive to over fitting, it is common practice to obtain the magnetic parameters for a spin probe from a rigid limit spectrum and fit only the dynamic parameters and ordering potential.

There are several important coordinate systems to model nitroxide diffusional motion in supramolecular aggregates. These include the magnetic tensor frame of the molecule (x_M, y_M, z_M), the rotational diffusion tensor frame (x_R, y_R, z_R), the director frame (x_D, y_D, z_D), and the laboratory frame of reference (x_L, y_L, z_L). The relationship between these frames of reference is illustrated in Figure 4.2. The first two coordinate systems are based on the molecular frame of reference, and describe the orientation of the magnetic tensor and the rotational diffusion tensor of the molecule relative to the molecular geometry. In the case of a nitroxide molecule like those studied here, the magnetic frame and rotational diffusion frame are identical, and axially symmetric spin probes like DSA. However, if necessary, the two frames of reference can be related to each other through a set of Euler angles, $\Omega_D = (\alpha_D \beta_D \gamma_D)$. In some cases, the magnetic frame and rotational frame of DSA spin probes are offset, and the inclusion of a value of β_D is

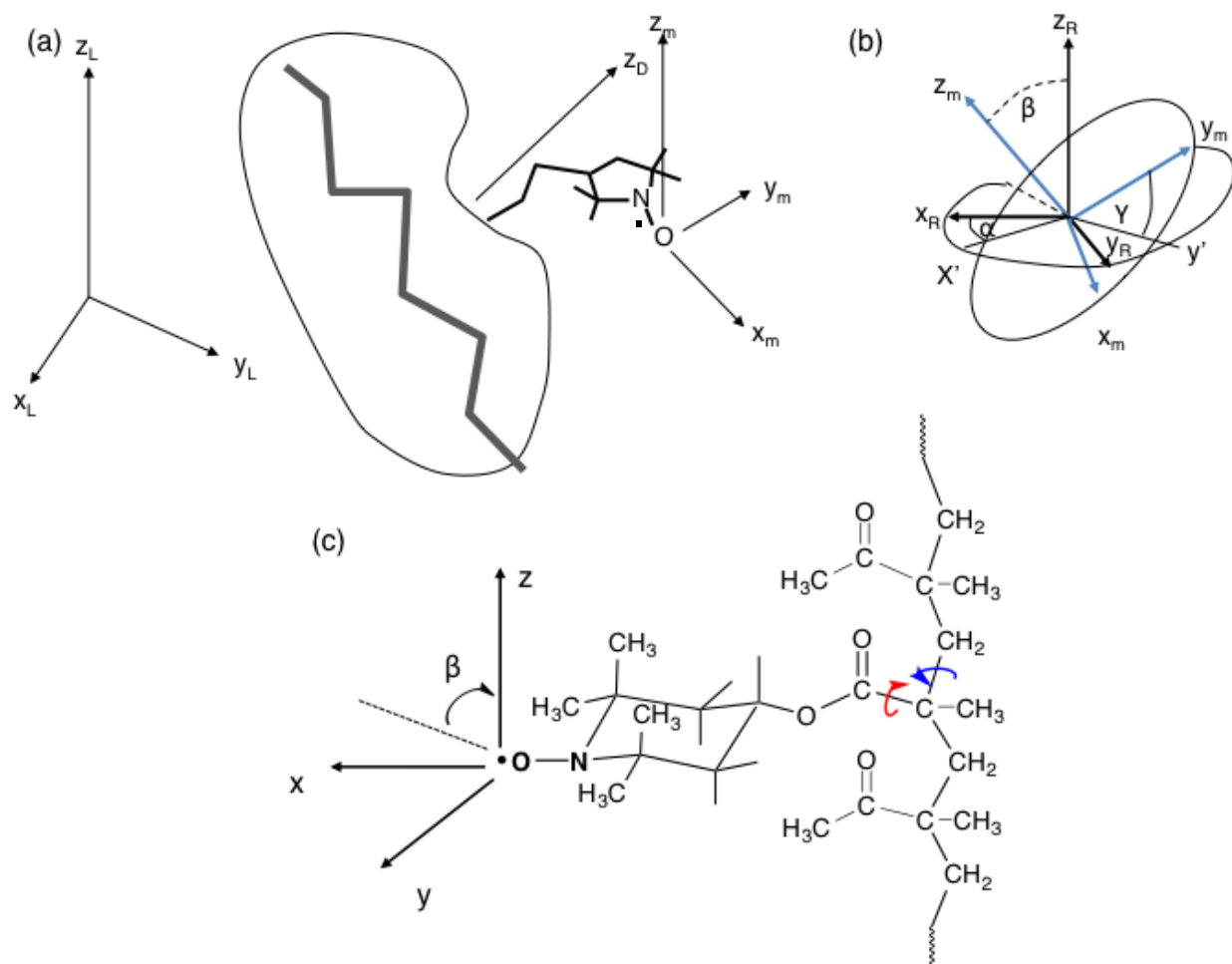


Figure 4.2 (a) Different coordinate systems (laboratory: L, director: D, and magnetic: m) used to define motion parameters for a nitroxide spin label. (b) Diffusion rotation angles used to define the magnetic axes relative to the diffusion axes. Note that the reference system for these angles is the diffusion frame. (c) Structure of spin-labeled PMMA with 2,2,6,6-tetra-methyl-4-hydroxypiperidiny-1-oxyl and the assumed conformation of spin label bounded at the end of the side chain (ref. 104, 105)

necessary to relate the two frames of reference and more accurately fit the experimental data. This angle has been related to the presences of gauche bonds in the alkyl chain of the spin probe [106], which alters the rotational diffusion of the molecule and the orientation of the nitroxide moiety relative to the axis of molecular symmetry. A value of $\beta_D = 65^\circ$ has been regularly used simulations of SSEPR spectra of nitroxides covalently attached to polymers [107].

The final two frames of reference are both related to the laboratory axis system [104]. The director frame describes the orientation of the molecule in anisotropic fluids, and the laboratory frame describes the direction of the applied magnetic field, which lies along the z_L axis. The director frame is related to the laboratory frame by a series of angles $\Psi=(0,\psi,0)$. Only one angle is required to relate the two reference frames because the orienting potential is axially symmetric. This angle ψ is referred to as the director tilt angle, and represents the angle between the director imposing the ordering in an anisotropic fluid and magnetic field.

In terms of simulating experimental spectra in vesicle or lamellar phases, the director tilt angle is particularly important because they exhibit microscopic order with macroscopic disorder (MOMD). In certain supramolecular and macromolecular systems where there are domains of local ordering of the spin probes, but these ordered domains are distributed randomly and isotropically with respect to the laboratory frame, special care must be taken in simulating the SSEPR spectra. Because the EPR experiment is sensitive to the ordering of a spin probe, it is necessary to account for this local ordering to accurately reproduce the experimental spectrum. This is accomplished by integrating the spectral line shapes over the director tilt angle ψ . This MOMD model has been extensively and successfully applied to numerous polymeric systems that exhibit impose a preferential orientation on the spin label. In this chapter, the MOMD model is used to simulate SSEPR spectra of spin labeled copolymers, but an isotropic rotation model

was used for spectra of TEMPO dissolved in solutions of unlabeled polymer.

4.3 Studies of Segmental Rotational Dynamics of Spin-labeled PMMA in Dilute Solution

The mobility of spin-labels depends on the flexibility of the tether connecting it to the backbone, and on tumbling of the macromolecules. Therefore, the calculated rotational correlation time, τ_c of spin-labels provides useful information about the local segmental motions of spin-labeled polymer. When $\tau_c < 10$ ps, the nitroxide spectrum shows three lines with equal widths and amplitudes (fast motion) and $\tau_c < 4$ ns exhibit a liquid-type spectrum and considered mobile [108].

The structure of the polymer system of interest is outlined in Figure 4.3. Random copolymers with molecular weight, $M_w \sim 120,000$ ($PDI \sim 2$) were synthesized as predominantly atactic PMMA with 0, 0.5, 1.0, or 2.0 mole% of the nitroxide moiety incorporated into them. This small amount of added monomer is initially incorporated as an amine (the monomer side chain contains the tetramethylpiperidine skeleton), which is then oxidized, post-polymerization, to the nitroxide using the peroxyacid meta-chloroperoxybenzoic acid (m-CPBA) [109].

Figure 4.4 shows the (dark) steady-state EPR (SSEPR) spectrum of the synthesized polymer (Figure 4.3) at room temperature in three different solvents, along with computer simulations based on the Freed model. These solvents are generally described as “good” or “bad” for a particular polymer based on the balanced of attractive vs. repulsive van der Waals forces between the solvent molecules and the polymer chain. Based on this balance of forces, a “good” solvent generally provides for more extended chains in solution and a “bad” solvent leads to more coiled conformations. This will manifest itself in the EPR spectrum through changes in spectral features such as line broadening and intensity difference.

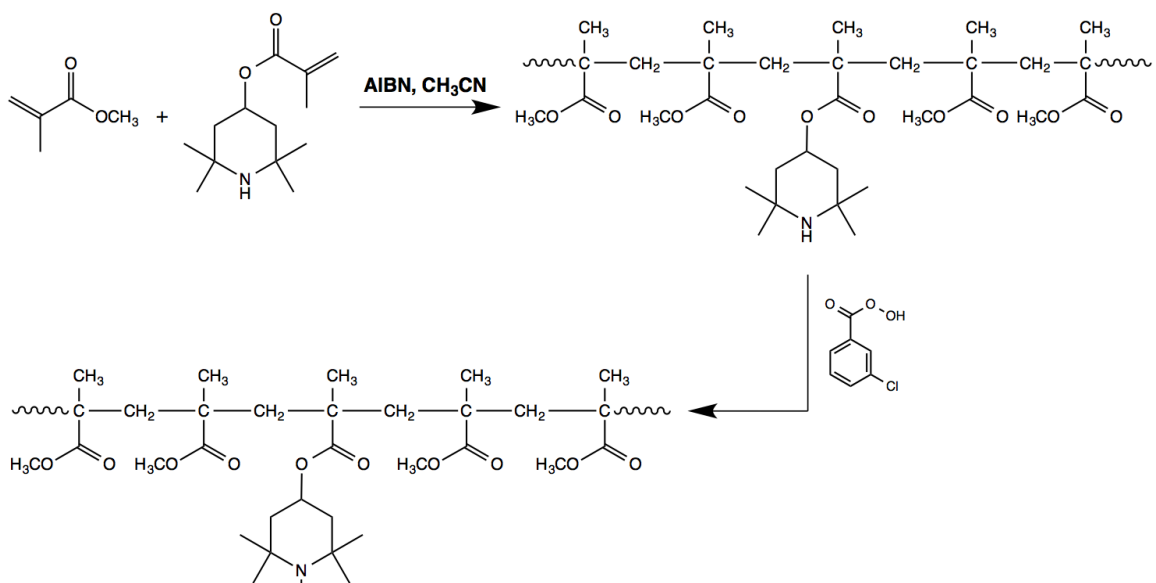


Figure 4.3 The structure of nitroxide containing random PMMA copolymer studied in this chapter

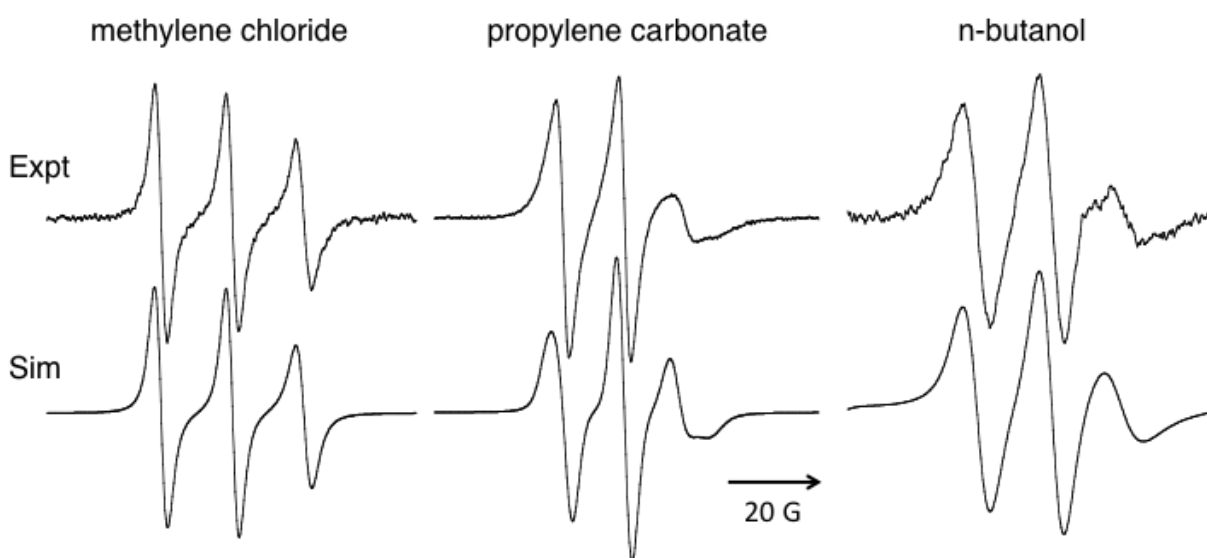


Figure 4.4 Top: X-band SSEPR (dark) spectra of the nitroxide-doped copolymer from Figure 4.3, acquired at room temperature in the solvents indicated. Bottom: Computer simulations using the Freed model REF with rotational correlation times of (left to right) 0.18 ns, 0.45 ns, and 0.72ns respectively

In Figure 4.4, the three line spectrum of the stable nitroxide free radical is evident in all three solvents, arising from a single electron-nuclear hyperfine coupling constant of about 15 Gauss from the ^{14}N nucleus (total spin $I = 1$). The SSEPR spectrum is collected using 100 kHz field modulation, which means the observed signals are detected with a first derivative line shape. The slightly lower intensity and larger line width of the high field line in the spectrum taken in methylene chloride indicates that the nitroxide is experiencing some (mild) constraint in its rotational motion, which is expected if it is covalently bound to the polymer chain. Overall this is still considered to be a “fast motion” spectrum. In the other two solvents, where the polymer chain is more coiled than extended [110,111] the anisotropic motion of the spin label is amplified. The line widths increase and all three lines in the SSEPR spectrum acquired in 1-butanol and propylene carbonate have different intensities. These changes are supported quantitatively by the increased rotational correlation time required the best fit of the spectra in figure 4.4 from the worst solvent (n-butanol, 0.72 ns) to the much better solvent (methylene chloride, 0.18 ns). In fact, Nitroxide radicals with $\tau_c < 4$ ns exhibit a liquid-type spectrum and considered mobile from the simulated nitroxide spectrum [108].

In the absence of an NMR spectrum, the SSEPR spectra in Figure 4.4 provide strong evidence that both steps in the synthesis (polymerization and oxidation) of the polymer were successful, and that the nitroxide radical line shape is sensitive to polymer chain conformation, mobility, and solvent structure.

Next we monitored the effect of nitroxide rotational dynamics on EPR line shape as a function of temperature and inter- and intramolecular system. Figure 4.5 shows the temperature dependence of the SSEPR spectra for the 1 mol % nitroxide copolymer sample in propylene carbonate (on the left side) and with the same mol % nitroxide (TEMPO) and PMMA in the

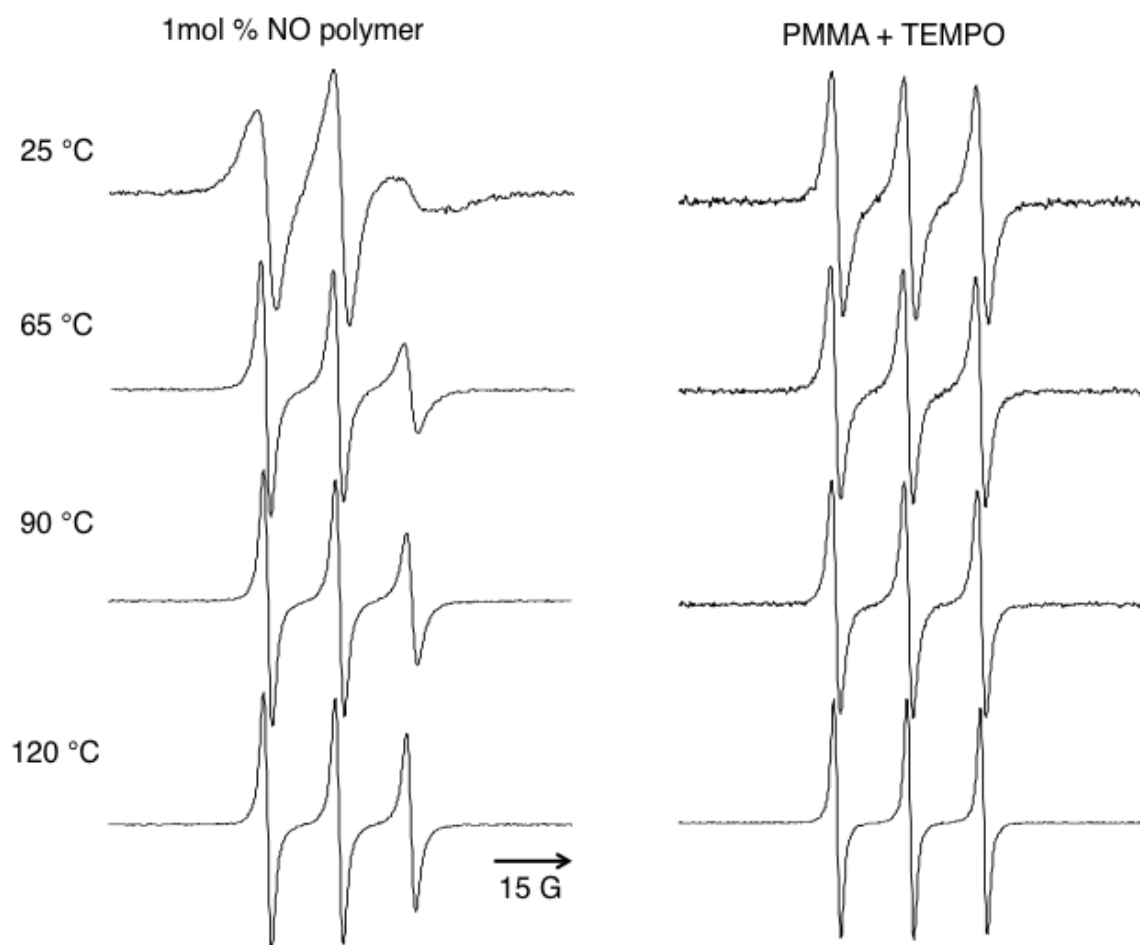


Figure 4.5 (Left) X-band SSEPR spectra of the nitroxide-doped copolymer and (Right) the same mol % nitroxide (TEMPO) and PMMA in PC at the given temperature

same solvent, but the radicals were not covalently linked to the polymer. The SSEPR spectrum of both the spin-labeled polymer and TEMPO mixed with PMMA in PC is clearly resolvable couplings from both the ^{14}N nucleus ($I = 1$).

Although some inhomogeneous broadening (about 3 Gauss) indicates in SSEPR spectrum of TEMPO mixed with PMMA in PC at lower temperature, the SSEPR spectrum exhibit fast motion and three lines are almost identical in terms of line widths and amplitude in Figure 4.5 (right). According to the simulated τ_c (0.2 ns) for TEMPO mixed with PMMA in PC at various temperatures is identical as well. We do not figure out the origin of the inhomogeneous broadening yet, but we assume that there are intermolecular processes due to restricted chain mobility below T_g of PMMA leading to change the rotational motion of nitroxide.

In Figure 4.5 left, at the room temperature, both fast and slow components are present in the SSEPR spectrum of the 1mol % nitroxide copolymer sample in PC, however slow motional effects should not be large. As the temperature increases the SSEPR spectra of the 1mol % nitroxide in copolymer sample, the motionally broad spectrum at R.T undergoes motionally narrowed spectrum eventually at higher temperature. However even at 120 °C, the nitroxide motion is not isotropic for this structure.

The rotational correlation times determined by the fitting process of experimental spectra of 1mol % nitroxide in copolymer sample in PC at all temperatures are listed in Table 4.1. These correlation times were used to determine an activation energy of the conformational changes in this copolymer in PC using the Arrhenius equation with the rate constant k equal to $1/\tau_c$. The slope of a plot of $\ln(\tau_c)$ vs. $1/T$ will be positive and give the activation energy (E_a) directly. Figure 4.6 shows the Arrhenius plot of the correlation times found for the 1mol % nitroxide in copolymer sample at different temperature in PC.

Table 4.1 Parameters used in the simulation Temperature Dependence of the SSEPR spectra 1 mol% nitroxide copolymer sample in PC shown in Figure 4.5 (Left)

Temp (°C)	A_{zz} (G)	A_n (G)	order parameter	τ_c (s)
25	34.52	16.04	0.21	4.55×10^{-9}
65	33.11	15.57	0.17	1.22×10^{-9}
90	32.90	15.50	0.19	6.61×10^{-10}
120	32.77	15.46	0.14	4.64×10^{-10}

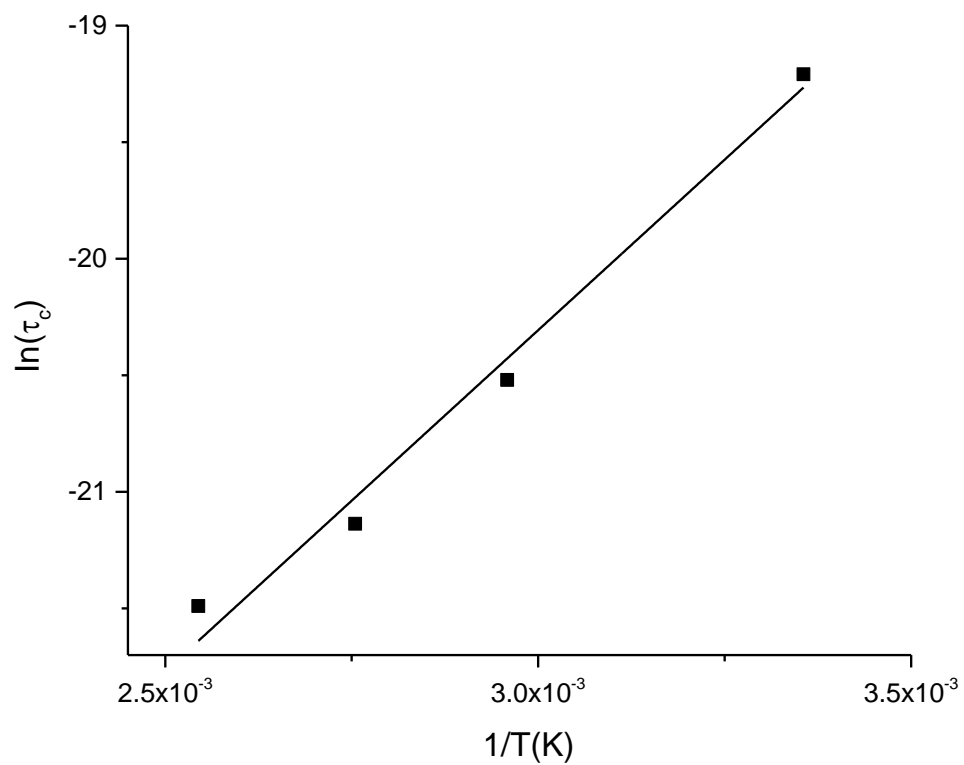


Figure 4.6 Arrhenius plot for rotational correlation time data from nitroxide-doped polymer (Figure 4.5). Squares are the simulated data, and the solid line is the linear fit with $E_a = 23$ KJ/mol

The E_a determined from the slope of this plot is 23 kJ/mol. This value is very close to those measured for d₃-PMMA main chain radical in PC using a two-site jump model for hyperfine modulation (22.2 kJ/mol) [102].

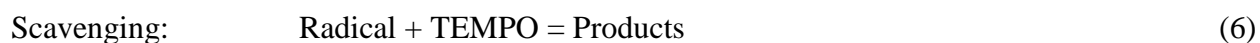
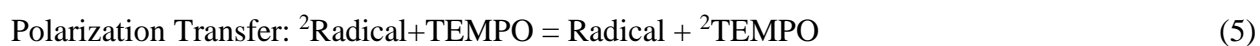
4.4 TREPR Studies of Chain Dynamics of Spin-labeled Polymers in Dilute Solutions

The top right of Figure 4.7 shows a typical high temperature (~100°C) TREPR spectrum of the main chain polymeric radical from isotactic PMMA in propylene carbonate solution, exhibiting net emissive electron spin polarization from the triplet mechanism [112,113] (TM) of CIDEP. The 21-line spectrum, acquired in dilute propylene carbonate solution, is assigned to 3 sets of electron-nuclear hyperfine coupling constants from a total of 7 β -protons. Simulation and extensive interpretation of such spectra are given in several previous publications [102,114,115]. Because hyperfine coupling constants in the main chain radical depend on the dihedral angles between the p-orbital containing the unpaired electron and the C–H σ bonds on the adjacent () carbon, they are very sensitive to local conformational motion and the stereochemistry near the radical center. The coupling constants for the fast motion (high temperature) TREPR spectra are therefore both temperature and tacticity dependent. The other member of the radical pair produced in this reaction is an oxo–acyl radical that is not normally observed in our experiments at high temperatures due to fast spin relaxation. The TM polarization is created within the laser flash and arises from the anisotropic nature of the spin-orbit coupling process from the first excited singlet state to the lowest excited molecular triplet state of the ester side chain. Most likely, the fast rotation of the side chain along one axis and the much slower conformational motion along the polymer chain provide this high degree of anisotropy. (Figure 4.1)

If a stable free radical such as a nitroxide is present either in the solution or covalently

linked to the polymer and makes contact with the photoexcited triplet state of the ester, net polarization in the 3-line nitroxide spectrum will result. At the bottom right of Figure 4.7, this is shown as net emissive polarization and is called Radical-Triplet Pair Mechanism (RTPM). There is no TREPR signal observed after excitation of the nitroxide by itself (a Boltzmann population cannot be detected), i.e., contact with an excited triplet state is required for this net polarization to be detected. Also, the ester triplet state is not detectable in this experiment due to its fast spin relaxation and broad transitions in solution. The 3-line emissive TREPR spectrum on the bottom right of Figure 4.7 arises from physical encounters (on the order of 5-20 Å separation) and electronic spin state mixing between the nitroxide radical and the triplet state during the first few nanoseconds (perhaps as long as 10 ns) after the creation of the triplet state by the laser flash. The RTPM polarization can be thought of as the "spin memory" of those encounters, and the polarization survives for about 1 μs, which is the normal electron spin relaxation time of the monoradical. On the other hands, direct electron spin polarization transfer (ESPT) from the spin polarized triplet state of ester onto the neighboring radical. These and other important reactions are outlined in Scheme 4.1 (here the RTPM is reaction 2 and ESPT is reaction 3). In either case, these events manifest themselves as net polarization in the 3-line nitroxide spectrum (in the bottom right of Figure 4.7 this is shown as net emissive polarization).

Scheme 4.1



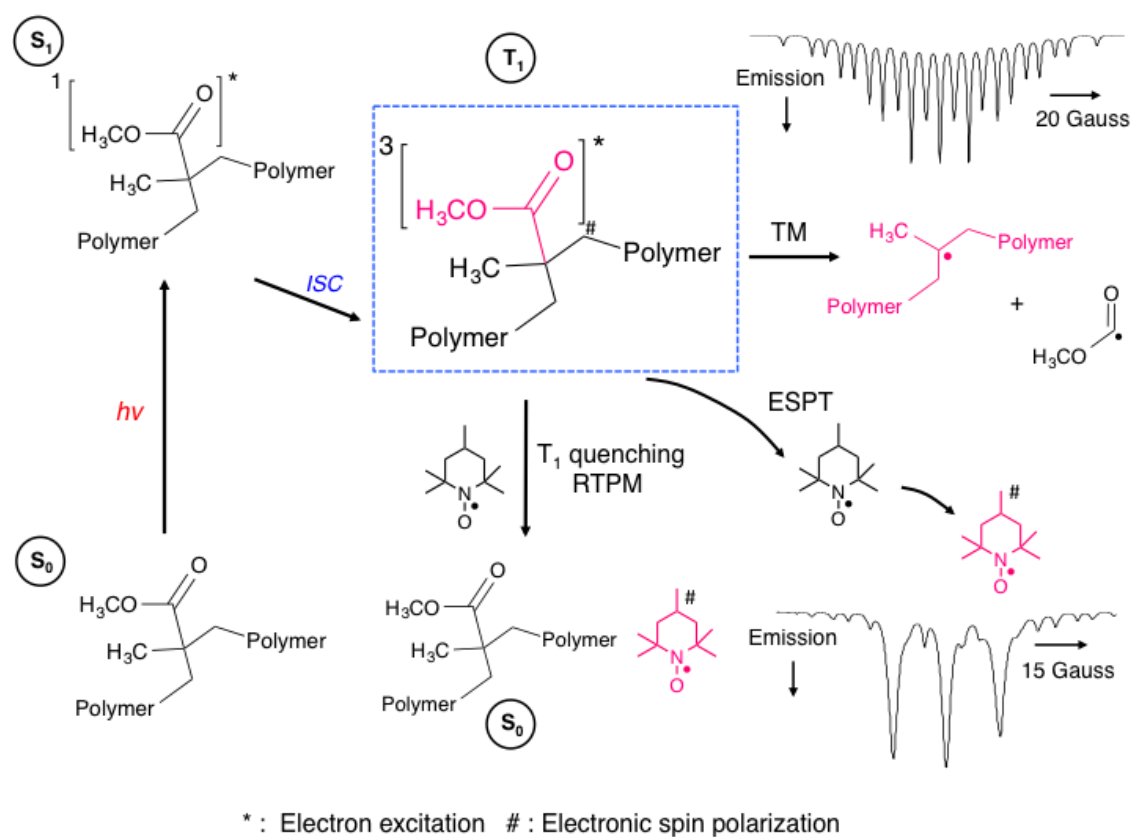


Figure 4.7 Graphical representation of spin polarization created by TM, RTPM and ESPT

The RTPM and ESPT mechanisms are well-established both experimentally [116] and theoretically [117]. Both processes require close contact ($\sim 6\text{--}8 \text{ \AA}$) to provide overlap of the HOMO of the electronically excited triplet ester and the SOMO of the radical in its ground double state. While the RTPM is followed by quenching of the electronic triplet excitation (reaction 2) and can, therefore, compete with the dissociative route of the energy dissipation (reaction 1), the appearance of polarization via ESPT does not necessarily imply that the electronically excited state has been quenched (reaction 3). Therefore, ESPT does not compete with the dissociation reaction. However, the ESPT process creates triplet states that no longer provide electron spin polarization in the resulting radicals. In this sense the ESPT quenches the TM polarization in radicals in a similar fashion to the RTPM.

There are two other important processes in these systems that should be noted. At small distances between radical and electronically excited molecule there is a possibility that electronic excitation can be transferred to the radical due to exchange or by the Förster mechanism of energy transfer (reaction 4) which can be effective at much longer distances ($\sim 15 - 20 \text{ \AA}$) between the radical and the triplet state if the electron dipolar spin-spin interaction is effective. This energy transfer event may or may not be followed by the creation of polarized TEMPO radicals. At the same time, the radicals created due to dissociation of the polymer can transfer (reaction 5) their TM polarization to the nitroxide radicals. In other words, the electron spin polarization observed in the TEMPO molecules may not necessarily arise from competition between dissociation and quenching. Consumption of TEMPO during photolysis would be evidence in favor of either reaction (4) or reaction (6), which is the scavenging of radicals by TEMPO. The latter suggests contribution of reaction (5), which demands contact of radicals (polarized and non-polarized) with TEMPO.

We will refer the emissive TREPR signal of the electron spin polarized TEMPO as “RTPM” with the understanding that the mechanism of generation of polarization can involve several processes. It should be noted that net emission is characteristic for this particular ester triplet state, but the electron spin polarization might be opposite in phase for an excited state created in a different polymer structures.

The competitive nature of the TM and RTPM processes outlined in Figure 4.7 suggests an experimental strategy for expanding our previous polymer chain dynamics studies to a different range of polymer motions. By incorporating a nitroxide into the polymer chain via covalent bonds, as outlined in Figure 4.3, we can generate RTPM polarization via *intramolecular* encounters that depend on several structural and physical features of the polymer/solvent system.

The ester side chain can be photoexcited at a random point along the polymer chain, and the TREPR signal is then detected at a fixed delay time after the laser flash. Because of the much larger concentration of the ester side chain groups, and the known fast relaxation of excited doublet states, the dominant photophysical process leading to electron spin polarization will be the creation of isolated ester triplet excited states on the macromolecule. The absorbance of the nitroxide at 248 nm is somewhat reduced when attached to the polymer chain. However, it should be noted that even if the nitroxide moiety absorbs more light at 248 nm, its molecular excited state will relax very quickly to the ground state and no chemical reactions from nitroxide excited states are known, so it is unlikely to interfere with TM/RTMP competition, except perhaps for reducing overall signal intensity. In order to determine the life times of excited triplet of ester side chain in PMMA, we monitored the quenching of the excited triplet state of ester side chain in PMMA by the sorbic acid (Quencher) in THF as a function of increasing concentration of the sorbic acid then the results were interpreted in terms of the Stern-Volmer model [118].

$$I_0/I = 1 + K_{sv}[Q] = 1 + k_q\tau_0[Q] \quad (4.1)$$

The integral emission intensities of I_0 and I in the absence and in the presence of quencher are related to the quencher concentration $[Q]$ by eq 4.1, where K_{sv} is the Stern-Volmer constant, k_q is the bimolecular quenching constant, and τ_0 is the lifetime of the chromophore in the absence of quencher. The measured value of τ_0 was found to be about 32 ns using the k_q of $5 \times 10^9 \text{ m}^{-1}\text{s}^{-1}$.

The TREPR signal from the system will arise from either the two competing processes described in Figure 4.7. The partitioning of the two spectral signatures will depend on the ability of the attached stable nitroxide to engage in encounters with the excited triplet. A particular advantage of measuring RTPM/TM competition is that the nitroxide is the only radical species detected in a "pure" RTPM experiment (Figure 4.7, bottom center), and its spectral signature is very different from the main chain radical. Polymer chain motion in the dilute condition can also be studied using fluorescence quenching techniques [119], but these probes tend to be large organic molecules with large rotational anisotropies. While the sensitivity and time response of optical methods are favorable for such investigations, the degree of influence of the probe molecules on the macromolecular motion is often quite substantial, and difficult to untangle from the intrinsic properties of the polymer itself.

Figure 4.8 shows X-band TREPR spectra acquired at the same delay time (500 ns) after the laser flash, at the same temperature (120°C) and in the same solvent (propylene carbonate) for polymers with mol% nitroxide values of 2, 1, 0.5 and 0.1 incorporated into the polymer chain. An emissive RTPM pattern is observed for the highest mole fraction (2 mol %), and it is the only signal present (at all delay times) studied. The line shapes are no longer first derivatives because field modulation is bypassed in TREPR (direct detection). Similar to Figure 1, the TREPR signal of the nitroxide shows a small amount of anisotropy in its line shape, with the

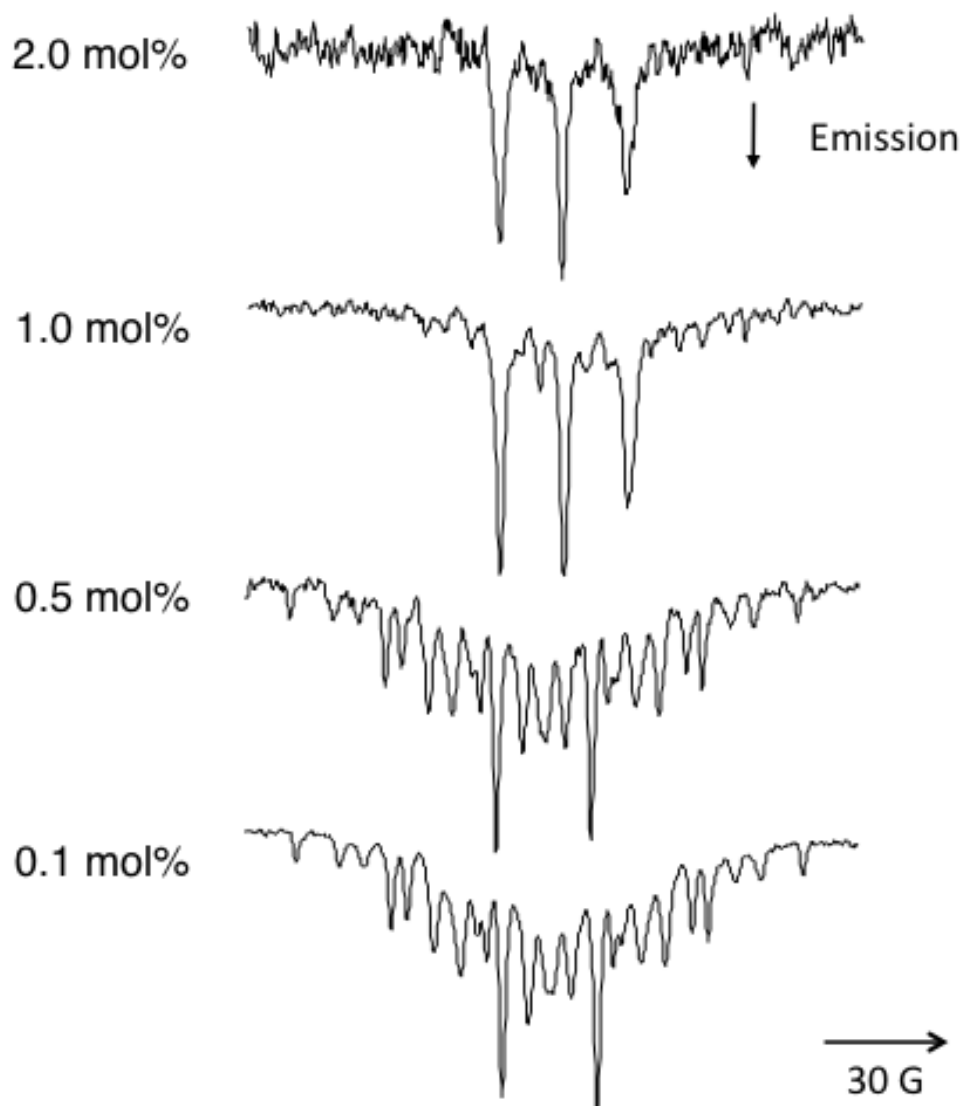


Figure 4.8 TREPR spectra of the nitroxide-containing copolymer shown in figure 4.3, acquired in propylene carbonate solution at 120°C, as a function of nitroxide incorporation (in mol %) the indicated to the left. Asterisks in the 1.0 mole % spectrum indicate transitions from the main chain polymeric radical of PMMA that is dominant in the 0.5 and 0.1 mol % spectra

high field line slightly less intense and broader than the other two. When the amount of incorporated nitroxide is lowered to 1 mol %, the three line nitroxide RTPM spectrum is much more intense (note the higher S/N ratio), and there is evidence for the presence of another signal underneath it, which we assign to the main chain polymeric radical (marked by asterisks in the 1 mol % spectrum). This spectrum also appears to be slightly sharper than the 2 mol % spectrum, (and also note the more equal intensities of the two lower field lines), which suggests that the mole fraction of the nitroxide incorporated into the polymer chain affects the dynamics. The increase in RTPM intensity with the lower nitroxide incorporation is interesting and most likely reflects a change in the amount of direct quenching of the ester triplet state by energy transfer at the lower concentrations.

At 0.5 mol % there is almost no trace of the nitroxide RTPM spectrum and instead the TREPR spectrum shows the main chain radical with TM polarization, albeit very weakly. Thus the crossover between the competition for RTPM generation by radical-triplet pair interactions and the Norrish I α -cleavage reaction of the excited molecular triplet state of the ester side chain is quite sensitive to the loading level of the nitroxide in the polymer. At even less loading (0.1 mol %), the TREPR spectrum is completely dominated by the TM polarized main chain polymeric radical. Figure 4.8 shows that even in a random copolymer arrangement at very small loadings of nitroxide, large changes in the quenching pathways are observed. It should be noted also that we cannot select the position along the chain where the light is absorbed, so the precise location of the excited triplet state is unknown. The spectrum is not identical to that shown at the Top right in Figure 4.7 because the two spectra arise from polymers with different tacticities – there are more lines in the main chain polymer radical spectrum acquired here because of fewer accidental degeneracies in the hyperfine splitting pattern.

The time scale for the encounters needed to create the RTPM polarization must be on the order of the bond cleavage rate in order to compete with it. The triplet lifetime of the ester in the polymer has not been determined, and a thorough search of the literature reveals that triplet lifetimes for small aliphatic esters have not been reported. Presumably this is due to difficulties involved in measuring deep UV absorbances in transient optical experiments. However, the Norrish I α -cleavage reaction is known to be facile in aliphatic esters [120], and similar radicals (alkyl and oxo-acyl) have been detected in high concentrations by SSEPR [121], suggesting a fast cleavage rate at least comparable to aliphatic ketones ($5 \times 10^8 \text{ s}^{-1}$ at room temperature) [122]. In spite of a lack of detail regarding the specific time scale of the radical-triplet encounter events, the results in Figure 4.8 are intriguing with regard to polymer chain dynamics, and so other parameters that can affect the polymer chain mobility were also investigated.

The ester side chain excited molecular triplet state is itself EPR silent in liquid solution due to fast spin relaxation caused by modulation of its electron dipole-dipole interaction. The stable nitroxide radical has a Boltzmann population of spin states in the dark, but this is not observed in the TREPR experiment (the experiment is not, except in rare cases of very high radical concentrations, sensitive to Boltzmann levels – CIDEP is essentially required for observation of direct detection TREPR signals) [123]. If nitroxide radicals and photoexcited triplet states are the only paramagnetic species that exist in a particular solution, and the triplet state does not react to make radicals, no TREPR signal is observed unless they make collisional encounters within the excited triplet state lifetime.

The magnitude of the observed TM polarization in these systems is very large and its origin is worthy of further discussion. Although we cannot quantitatively correlate TREPR signal intensities to radical concentrations, we note the following: very little degradation of the polymer

chains is observed even after many scans and thousands of laser shots. This implies that the number of free radicals produced per laser shot is low ($\sim 10^{-6}$ M). However, the signal intensities are some of the largest we have ever encountered in experiments with samples having similar absorbances. Therefore, the TM polarization, created during the intersystem crossing process that creates the excited triplet state, must be very large indeed. Several factors can maximize the TM [112,113], including the intersystem crossing rate, the chemical decay rate, and the magnitude of the zero-field splitting parameters of the triplet, but the most important parameter is the rotational anisotropy of the triplet as it tumbles in the applied magnetic field of the EPR spectrometer. The ester side chains have significantly greater freedom of motion along an axis perpendicular to the polymer backbone, but very poor rotational mobility along the backbone axis itself. This difference in rotational mobility allows for greater spin state selectivity in the molecular frame during inter-system crossing and will amplify the TM.

Figure 4.9 shows the temperature dependence of the RTPM spectrum for the 1 mol % nitroxide copolymer sample in propylene carbonate, acquired at a delay time of 500 ns. The highest temperature spectrum (Figure 4.9, bottom) is the same as the one shown for 1 mol % in Figure 4.8. There are only minor changes in the spectra as the temperature is lowered from 120°C to 90°C (bottom three spectra in Figure 4.9) but it is interesting that the magnitude of the RTPM polarization remains about the same but the signal from the main chain radical (TM polarized, just left of center) decreases by almost a factor of two over this small temperature range, without significant broadening. This trend continues (data not shown) until the much broader spectrum at room temperature is obtained (Figure 4.9, top). This spectrum is essentially an emissive direct detection analog of the steady-state spectrum shown in Figure 1. The width and anisotropy exhibited by the spectrum at the top of Figure 4.9 suggests that propylene

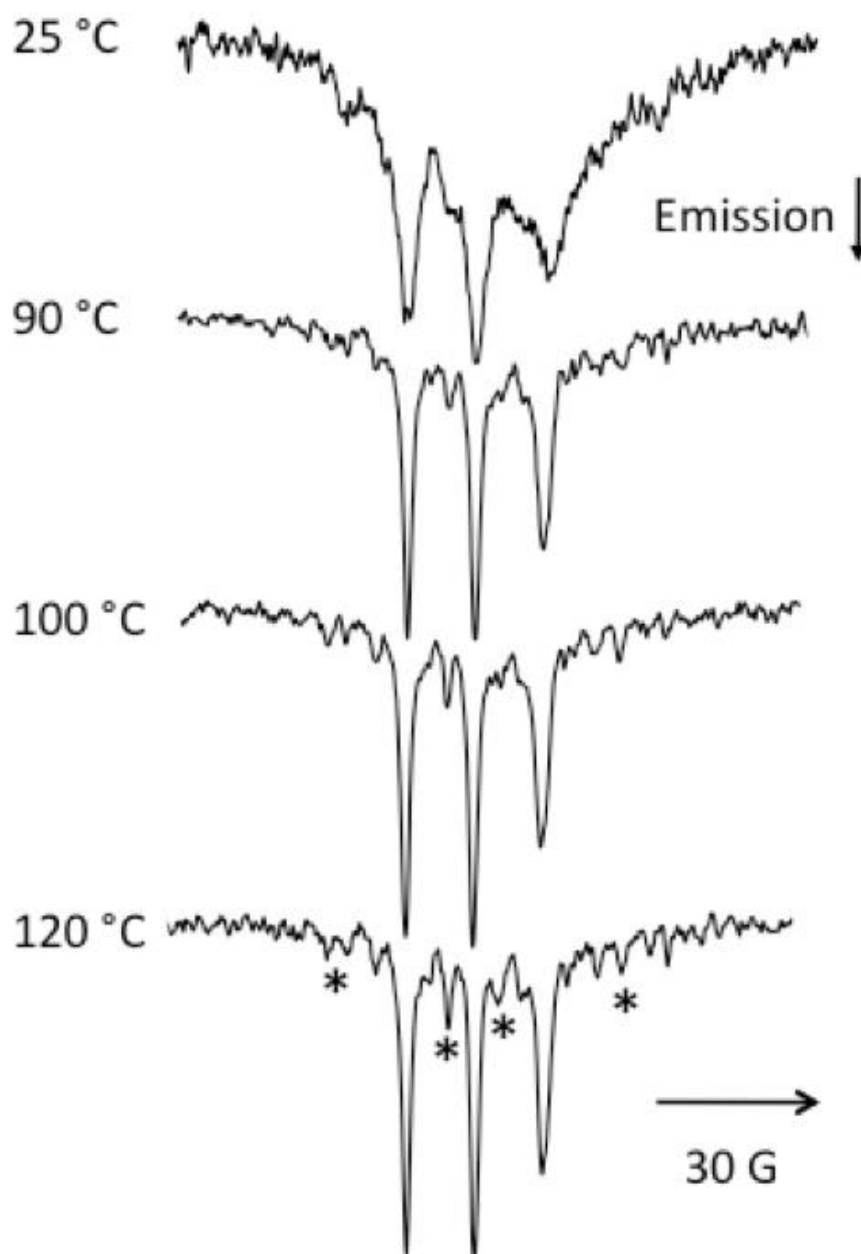


Figure 4.9 TREPR spectra of the nitroxide-containing polymer shown in Figure 4.3 (1 mol % nitroxide) in propylene carbonate solution at the temperatures indicated. Asterisks in the 120°C spectrum indicate transitions from the main chain polymeric radical of PMMA, which is very broad but still observable in the 25 °C spectrum (top). The delay time is 500 ns and the sweep width is 150 G in each spectrum

carbonate may not be a "good" solvent for these copolymers at room temperature, but it becomes a better solvent (as evidenced by the fast motion spectrum) at higher temperatures. Also, it is clear that the room temperature spectrum still contains a contribution from a substantially broadened main chain polymer radical, indicating that both pathways are affected by temperature, although the nitroxide RTPM polarization seems to have decreased in intensity much faster with decreasing temperature than the main chain radical from the Norrish I reaction. At room temperature, there may also be a small contribution from the oxo-acyl radical, just to the high field side of the center of the spectrum.

Figure 4.10 shows a comparison between inter- and intramolecular RTPM pathways. The "benchmark" spectrum, taken again from the 1 mol % nitroxide copolymer at 120 °C, is presented in the bottom spectrum in the Figure to show the intramolecular RTPM for comparison. The top spectrum in Figure 4.10 was acquired with the same mol % nitroxide (TEMPO) and PMMA in the same solvent and at the same temperature, but the radicals were not covalently linked to the polymer. When the nitroxide is free to move in solution, two things are immediately apparent: the TREPR signal is much more isotropic (sharp line widths, with almost equal intensities), and the RTPM polarization is much more intense (the vertical scale is 5x for the bottom spectrum). Figure 4.10 demonstrates that the polymer chain dynamics of the copolymer limit the contact between the ester side chain triplet states and the stable radicals. On the other hand, The RTPM is so intense in the intermolecular case that the main chain radical is barely visible.

Figure 4.11 shows the TREPR experiment for the 1 mol% copolymer at different concentrations. This experiment was run to see if intra-chain interactions (entanglements) exert any influence on the spectra. Somewhat surprisingly, there is very little change in the TREPR

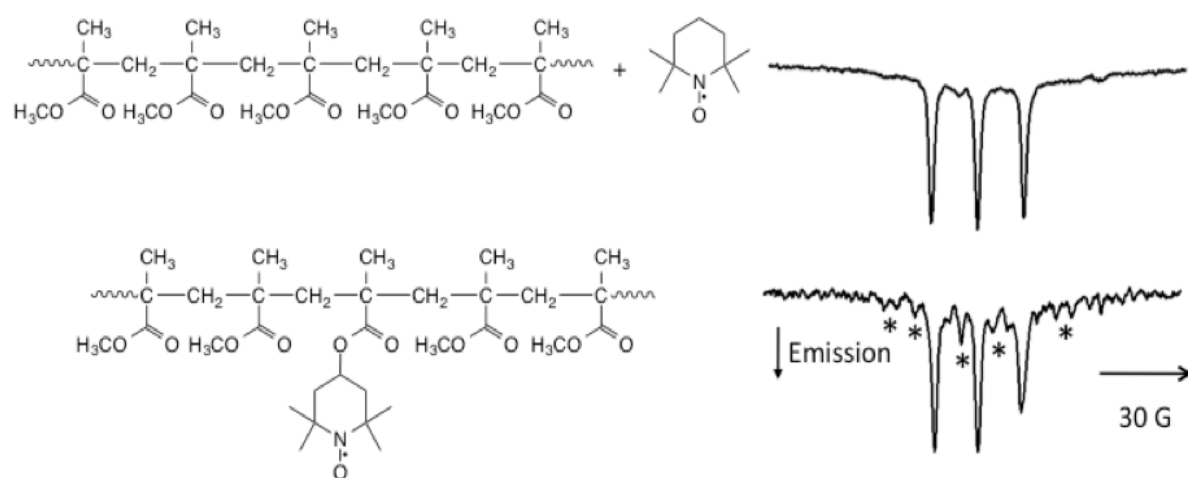


Figure 4.10 Inter- vs. intramolecular competition between TM and RTPM. (Top) TREPR spectra of unattached TEMPO (1.5mM) and PMMA (5 wt %) in propylene carbonate after 248 nm laser excitation at 120°C. (Bottom) TREPR spectrum of the nitroxide containing PMMA copolymer (loading level is 1 mol %) under the same conditions. Asterisks in the bottom spectrum indicate transitions due to the main chain polymeric radical of PMMA. The delay time is 500 ns and the sweep width is 150 G in both spectra.

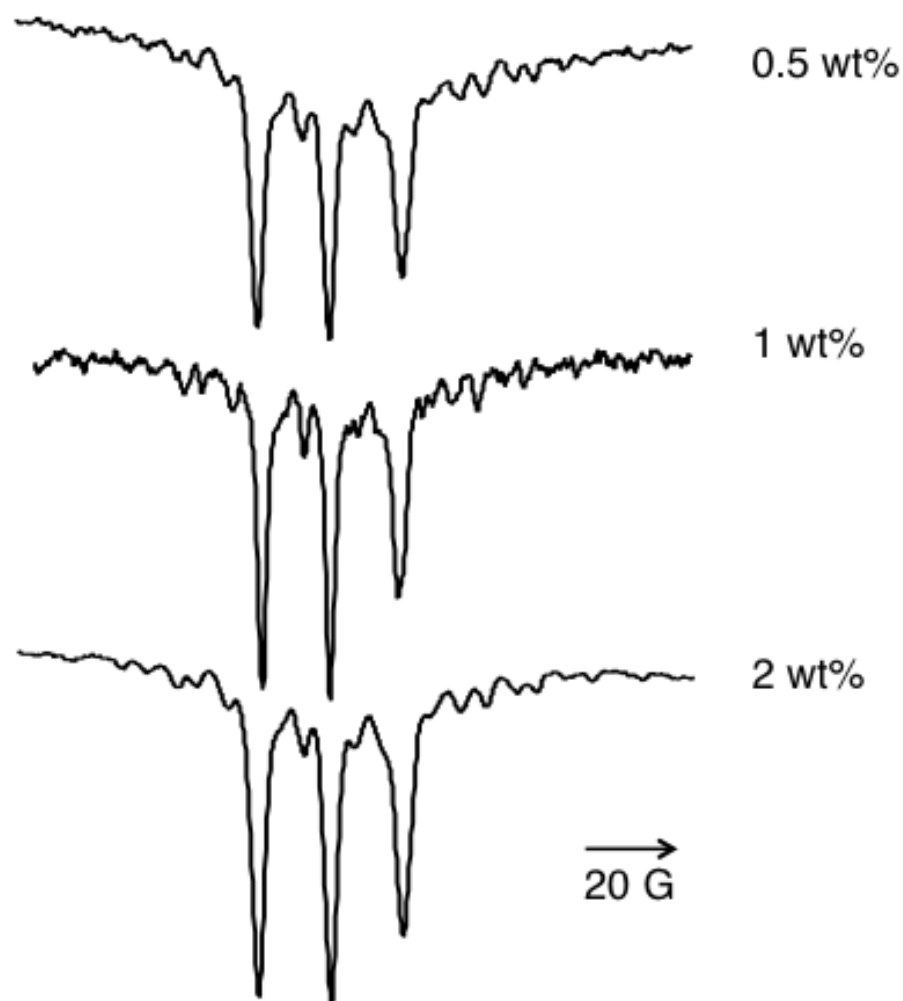


Figure 4.11 TREPR spectra of the 1 mol% of nitroxide-containing PMMA polymer as a function of concentration. The spectra were acquired in propylene carbonate solution at 120 °C. Asterisks in the bottom spectrum indicate transitions due to the main chain polymeric radical of PMMA. The delay time is 500 ns and the sweep width is 150 G in both spectra

spectra of the copolymer as the concentration is increased. The ratio of the main chain radical signal to the nitroxide signal remains about the same, while the overall signal intensity increases. There are slight increases in the line widths of both radicals, but little change in the anisotropic shape of the nitroxide signal. This control experiment demonstrates that generation of the RTPM polarization in the copolymers is dominated by intramolecular polymer chain dynamics and does not arise from chain entanglements, intermolecular quenching, or poor solvation of the polymer.

The ester side chain structure can be varied, although it should be noted that the photochemistry and photophysics of the side chain might change in addition to the copolymer chain dynamics. We selected two methacrylic polymers whose structures should provide different conformational energies in dilute solution with only minimal perturbations of the triplet excited state of the ester side chain. Figure 4.12 shows high temperature TREPR spectra obtained for two copolymers containing 1 mol % nitroxide: n-butyl ester side chains (P(n-BMA), top of Figure 4.12)) and tert-butyl ester side chains (P(t-BMA), bottom of Figure 4.12). In both cases the RTPM is completely absent. It seems that with larger side chains the polymer chain dynamics are slower and so the Norrish I pathway always dominates (too few collisions between the excited esters and the nitroxides). Unfortunately, we cannot increase the mol% of nitroxide incorporation much further without getting weaker signals (recall Figure 4.8, top) and or observing direct excitation and degradation of the nitroxide.

The side chain dependence was investigated further by returning to the intermolecular RTPM experiment described in Figure 4.10, but using a polymer with larger side chains (Pn-BMA). The results are shown in Figure 4.13. At elevated temperatures at 1 mol % TEMPO in diglyme, no intermolecular RTPM is produced in this mixture (top and middle spectra in Figure 4.11). However, if the concentration of TEMPO in the solution is increased to 2 mol %, strong

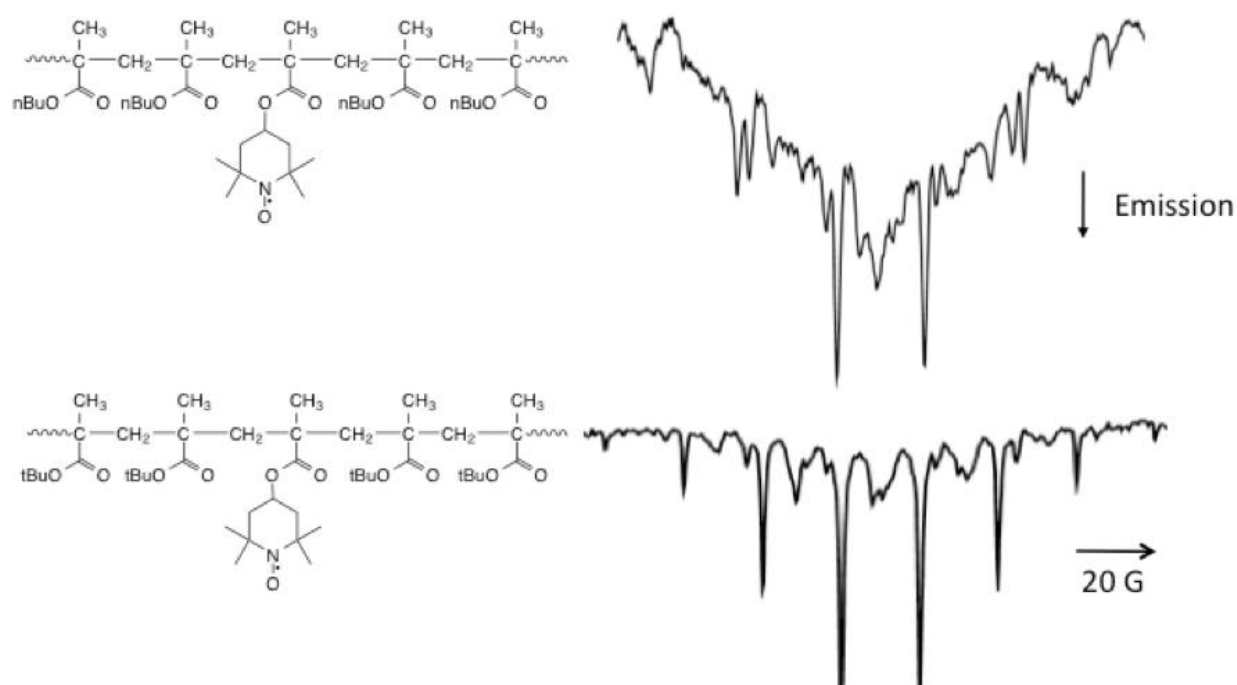


Figure 4.12 TREPR spectra of nitroxide-containing poly(n-butyl methacrylate) at 70°C (top) and poly(tert-butyl methacrylate) at 130°C (bottom) in diglyme. The sweep width is 200 G and the delay time is 500 ns in both spectra. The degree of nitroxide incorporation is 1 mol % for both polymers. Both signals are attributed to the respective main chain polymeric radicals, i.e., RTPM/quenching involving the nitroxide is not taking place

RTPM is observed even at room temperature (Figure 4.13, bottom). This suggests that the side chains of these polymers exert control of our observation of RTPM polarization in two ways: First, larger side chains can influence the polymer chain dynamics such that intramolecular collisions are significantly reduced (Figure 4.13), and second, the bulkier side chains can "shield" the more mobile nitroxide in solution from making sufficient contact with the ester functionality to carry out effective quenching of the excited state.

4.5 Conclusions

We have presented here a "proof-of-principle" series of experiments demonstrating that RTPM and β -cleavage (TM) processes can be observed competing in the copolymers shown in Schemes 2. Furthermore, with this minimally invasive probe method, we have found that the partitioning of these processes is strongly affected by polymer side chain structure, nitroxide concentration, temperature, and intramolecular vs. intermolecular encounters. The time dependence of the signals is somewhat unremarkable, suggesting that the time scale for the formation of the RTPM polarization is fast, on the order of a few tens of nanoseconds. A striking feature of the data presented here is the sensitivity to loading level: somewhere between 0.5 and 1.0 mol% loading, there appears to be a crossover in competition between the cleavage and quenching mechanisms. The TREPR experiment provides a very sensitive measurement device for the encounter processes necessary to probe the long-range motions. We are now seeking a suitable model to help us simulate the polymer motion to correlate with the observed results. Future synthetic efforts are focused on studying block copolymers, trying to place the nitroxide at specific sites on the polymer chain, and trying to excite the ester side chains more at specific sites, in particular closer to the ends or the center of the polymer backbone.

4.6 Experimental

Materials. Methyl methacrylate (MMA), n-butyl methacrylate (*n*BMA) and *tert*-butyl methacrylate (*t*BMA), (Sigma Aldrich) were passed through activated aluminum oxide to remove inhibitors. 4-hydroxy-2,2,6,6-tetramethylpiperidine, methacrylic acid anhydride, 4-dimethylaminopyridine (DMAP) and pyridine from Sigma-Aldrich were used as received. Azobisisobutyronitrile (AIBN) and *meta*-Chloroperoxybenzoic acid (*m*-CPBA) as obtained from Sigma-Aldrich were recrystallized before use. Acetonitrile, methylene chloride and methanol (Fisher) were used without further purification. PMMA ($M_w = 50,000$) and (2,2,6,6-Tetramethylpiperidin-1-yl)oxyl (TEMPO) were purchased from Sigma-Aldrich and used as received.

Monomer Synthesis. 4-Methacryloyloxy-2,2,6,6-tetramethylpiperidine was synthesized according to a procedure described by Shea *et al.*[109]. Briefly, this compound is prepared by adding 4-hydroxy-2,2,6,6-tetramethylpiperidine, methacrylic acid anhydride, DMAP and pyridine to dry methylene chloride (30 mL). The solution is stirred at ambient temperature for 12 h, and the product shown in Scheme 3 is purified by flash chromatography (silica, 20:80 ethyl acetate:hexane). **Copolymer Synthesis.** The free radical copolymerization of 4-methacryloyloxy-2,2,6,6-tetramethylpiperidine with either MMA, *n*-BMA, or *t*-BMA was dissolved in acetonitrile, then transferred in a flamed-dried 3-neck round bottom flask. For nitroxide concentration studies, different mole ratios (0.1, 0.5, 1 and 2 mol %) of **5** were used during the polymerization. While stirring, the initiator AIBN was transferred into the solution with syringe. The solution was degassed with argon for 20 min before immersion in an oil bath at 65 °C. After 24 h, the copolymer was diluted with methylene chloride and precipitated into methanol. The crude copolymer was dried under vacuum at 80 °C for 24 h.

Spin-Labeling. To synthesize spin-labeled copolymers, side chains of 4-methacryloyloxy-2,2,6,6-tetramethylpiperidine on the copolymer is converted to 2,2,6,6-tetramethylpiperidine-oxyl stable free Radical via oxidation. The precursor copolymer was dissolved in CH_2Cl_2 and excess MCPBA was added. The suspension was stirred for 24 h and then filtered and washed with MeOH. After drying under high pressure, the nitroxide-containing polymer was a light pink powder.

4.6.1 Analysis of polymer samples

Gel Permeation Chromatography (GPC). Molecular weights, relative to narrow poly methyl methacrylate standards, were measured using a Waters GPC system consisting of a Waters 510 pump, a Waters 717 autosampler, a Wyatt Optilab DSP refractometer, and a Wyatt Dawn EOS light scattering detector. THF was used as the mobile phase at a flow rate of 1 mL/min with a sample injection volume of 100 μL . The concentration of sample 5mg/ml. The molecular weights and molecular weight distributions were determined by GPC.

SSEPR. Steady-state EPR spectroscopy was performed on a JEOL USA Inc. FA-100 X-band (9.5 GHz) spectrometer with a cylindrical TE_{011} resonator and quartz capillary sample tubes. Field modulation of 0.5 Gauss was applied for a scan time of 4 minutes and an output time constant of 0.3 s.

TREPR. Continuous wave TREPR experiments were performed as previously described [123]. All experiments were performed on a JEOL USA Inc. JES-RE1X X-band EPR spectrometer equipped with a wide bandwidth preamplifier and a low-noise GaAsFET microwave amplifier. Samples were typically prepared as solutions of nitroxide-containing polymer (0.5–1.2 g) in propylene carbonate or dimethyl ethyl ether (diglyme) (20–35 ml) and circulated through a quartz flat cell (0.4 mm path length) positioned in the center of a Varian TE_{103} optical transmission cavity.

The solutions were photolyzed using a Lambda Physik Compex 120 excimer laser (248 nm, KrF) running at 60 Hz with a pulse energy of 100 mJ (~20 mJ per pulse hitting the sample) and a pulse width of 17 ns. Spectra were collected in the absence of field modulation at a fixed delay time after the laser flash using a two-gate boxcar integrator (Stanford, 100 ns gates), while the external magnetic field was swept with a scan time of 4 min.

For high-temperature TREPR experiments, the deoxygenated sample solution was circulated using a micropump through Teflon PFA 1/8 in. tubing insulated with polyurethane foam tape. From the pump, the sample tubing passed through a copper coil wrapped with heating tape (Omega Inc.), which was controlled using a feedback circuit between a variable power temperature controller and thermocouples placed at the entrance and exit of the quartz flow cell. The sample was recirculated between the flat cell and the reservoir. Reported temperatures are the average of three measurements from the top and bottom of the flat cell and the reservoir. The maximum temperature gradient at the highest temperatures was 10 °C; therefore, all temperature are reported as ± 5 °C. Both propylene carbonate and diglyme were used as solvents due to their transparency at 248 nm and their high boiling points.

REFERENCES

1. Kremer, K.; Grest, G. S. *J. Chem. Phys.* **1990**, *92*, 5057.
2. Harmandaris, V. A.; Mavrantzas, V. G.; Theodorou, D. N.; Kröger, M.; Ramirez, J.; Öttinger, H. C.; Vlassopoulos, D. *Macromolecules* **2003**, *36*, 1376.
3. Zhang, M.; Müller-Plathe, F. *J. Chem. Phys.* **2006**, *125*, 124903.
4. Rapaport, D. C. *J. Chem. Phys.* **1979**, *71*, 3299.
5. a) Larson, R. G. *Macromolecules* **2004**, *37*, 5110, b) Bulacu, M.; Goga, N.; Zhao, W.; Rossi, G.; Monticelli, L.; Periole, X.; Tieleman, D. P.; Marrink, S. J. *J. Chem. Theory Comp.* **2013**, *9*, 3282, c) Latinwo, F.; Schroeder, C. M. *Macromolecules* **2013**, *46*, 8345.
6. Alan E. Tonelli, *Modern Magnetic Resonance*, 2006, pp 567-574.
7. Levy, G. C.; Wang, D. *Macromolecules* **1986**, *19*, 1031.
8. a) Kivelson, D. *J. Chem. Phys.* **1960**, *33*, 1094, b) Hudson, A.; Luckhurst, G. R. *Chem. Rev.* **1969**, *69*, 191.
9. Harbron E. J.; McCaffrey V. P.; Xu R.; Forbes M. D. E. *J Am Chem Soc.* **2000**, *122*, 9182.
10. McCaffrey, V. P.; Harbron, E. J.; Forbes, M. D. E. *Macromolecules* **2005**, *38*, 3342.
11. McCaffrey, V. P.; Harbron, E. J.; Forbes, M. D. E. *J. Phys. Chem. B* **2005**, *109*, 10686
12. Rabek, J. F. *Mechanisms of Photophysical Processes and Photochemical Reactions in Polymers*. New York: Wiley; **1987**.
13. Nagai, Y.; Nakamura, D.; Miyake, T. et al. *Polym. Degrad. Stab.* **2005**, *88*, 251.
14. McCaffrey, V.P.; Forbes, M. D. E. *Macromolecules* **2005**, *38*, 3334.
15. Lebedeva, N. V.; Forbes, M. D. E. *Macromolecules* **2008**, *41*, 1334.
16. Ranby, B.; Rabek, J. F. *ESR Spectroscopy in Polymer Research*. Berlin: Springer-Verlag; **1977**.
17. DeSimone, J. M.; Romack, T.; Betts, D. E.; McClain J.B. U.S. Patent 5, 783, 082, **1998**
18. Tsentalovich, Y.P.; Forbes, M. D. E. *Mol. Phys.* **2002**, *100*, 1209.
19. Weil, J. A.; Bolton, J. R. *Electron Paramagnetic Resonance: Elementary Theory and*

- Practical Applications. 2nd ed.; John Wiley & Sons, Inc.: Hoboken, NJ, **2007**.
20. Murai, H.; Sakaguchi, Y.; Hayashi, H.; I'Haya, Y.J. *J. Phys. Chem.* **1986**, *90*, 113.
 21. Atkins, P. W.; McLauchlan, K. A.; Lepley, A. R.; Closs, G. L. eds. *Chemically Induced Magnetic Polarization*. London: Wiley; 1978, 41–93.
 22. Scaiano, J.C. *Chem. Phys. Lett.* **1981**, *79*, 441.
 23. Watkins, A. R. *Chem. Phys. Lett.* **1974**, *29*, 526.
 24. Watkins, A. R. *Chem. Phys. Lett.* **1980**, *70*, 262.
 25. Kuzmin, V. A.; Tatikolov, A. S. *Chem. Phys. Lett.* **1978**, *53*, 606.
 26. Naqvi, K. R.; Wild, U. P. *Chem. Phys. Lett.* **1976**, *41*, 570.
 27. Naqvi, K. R.; Staerk, H.; Gillboro, T. *Chem. Phys. Lett.* **1970**, *49*, 160.
 28. Imamura, T.; Onitsuka, O.; Obi, K. *J. Phys. Chem.* **1986**, *90*, 6741.
 29. Kawai, A.; Okutsu, T.; Obi, K. *J. Phys. Chem.* **1991**, *95*, 9130.
 30. Blattler, C.; Paul, H. *Res Chem. Intermed.* **1991**, *16*, 201.
 31. Goudsmit, G. H.; Paul, H.; Shushin, A. I. *J. Phys. Chem.* **1993**, *97*, 13243.
 32. Kobori, Y.; Mitsui, M.; Kawai, A.; Obi, K. *Chem. Phys. Lett.* **1996**, *252*, 355.
 33. Kobori, Y.; Takeda, K.; Tsuji, K.; Kawai, A.; Obi, K. *J. Phys. Chem. A* **1998**, *102*, 5160.
 34. Evans, D. F. *Nature* **1956**, *173*, 534.
 35. Hoijtink, G. J. *Mol. Phys.* **1960**, *3*, 67.
 36. Murrell, J. N. *Mol. Phys.* **1960**, *3*, 319.
 37. Weiss, D. S. *J. Photochem.* **1996-7**, *6*, 301.
 38. Chattopadhyay, S. K.; Das, P. K.; Hug, G. L. *J Am Chem Soc.* **1983**, *105*, 6205.
 39. Kobori, Y.; Kawai, A.; Obi, K. *J. Phys. Chem.* **1994**, *98*, 6425.
 40. Kawai, A.; Obi, K. *J Phys Chem.* **1992**, *96*, 52.
 41. Wu, J.; Mather, P. T. *Polymer Reviews* **2009**, *49*, 25.

42. Bin Zhang a; Yu Chen a; Jun Wang b; Werner J Blau b; a, X. Z.; a, N. H. **2010**, *48*, 1738.
43. Lee, Y.-J.; Huang, J.-M.; Kuo, S.-W.; Lu, J.-S.; Chang, F.-C. *Polymer* **2005**, *46*, 173.
44. Fan, H.; Li, X.; Liu, Y.; Yang, R. *Polymer Degradation and Stability* **2013**, *98*, 281.
45. Phillips, S. H.; Haddad, T. S.; Tomczak, S. J. *Current Opinion in Solid State and Materials Science* **2004**, *8*, 21.
46. Baney, R. H.; Itoh, M.; Sakakibara, A.; Suzuki, T. *Chem. Rev.* **1995**, *95*, 1409.
47. Lichtenhan, J. D. *Comments on Inorganic Chemistry* **1995**, *17*, 115.
48. Haddad, T. S.; Lichtenhan, J. D. *Macromolecules* **1996**, *29*, 7302.
49. Scott, D. W. *J. Am. Chem. Soc.* **1946**, *68*, 356.
50. Lichtenhan, J. D.; Otonari, Y. A.; Carr, M. J. *Macromolecules* **1995**, *28*, 8435.
51. Lichtenhan, J. D.; Vu, N. Q.; Carter, J. A.; Gilman, J. W.; Feher, F. J. *Macromolecules* **1993**, *26*, 2141.
52. Mather, P. T.; Jeon, H. G.; Romo-Uribe, A.; Haddad, T. S.; Lichtenhan, J. D. *Macromolecules* **1999**, *32*, 1194.
53. Chiantore, O. *Polymer* **2000**, *41*, 1657.
54. Ali, A. H.; Srinivasan, K. *Journal of Macromolecular Science, Part A: Pure and Applied Chemistry* **1997**, *34*, 235.
55. Gilman, J. W.; Schlitzer, D. S.; Lichtenhan, J. D. *J. Appl. Polym. Sci.* **1996**, *60*, 591.
56. Brunsvold, A. L.; Minton, T. K.; Gouzman, I.; Grossman, E.; Gonzalez, R. *High Performance Polymers* **2004**, *16*, 303.
57. Bolln, C.; Tsuchida, A.; Frey, H.; Mülhaupt, R. *Chem. Mater.* **1997**, *9*, 1475.
58. Fina, A.; Tabuani, D.; Carniato, F.; Frache, A.; Boccaleri, E.; Camino, G. *Thermochimica Acta* **2006**, *440*, 36.
59. Blanco, I.; Bottino, F. A.; Cicala, G.; Cozzo, G.; Latteri, A.; Recca, A. *Polym Compos* **2014**.
60. Dintcheva, N. T.; Morici, E.; Arrigo, R.; La Mantia, F. P.; Malatesta, V.; Schwab, J. J.

61. Harbron, E. J.; McCaffrey, V. P.; Xu, R.; Forbes, M. D. *J. Am. Chem. Soc.* **2000**, 122, 9182.
62. McCaffrey, V. P.; Harbron, E. J.; Forbes, M. D. *Macromolecules* **2005**, 38, 3342.
63. Tsentalovich, Y. P.; Forbes, M. D. E.; Morozova, O. B.; Plotnikov, I. A.; McCaffrey, V. P.; Yurkovskaya, A. V. *J. Phys. Chem. A* **2002**, 106, 7121.
64. Griller, D.; Roberts, B. P. *J. Chem. Soc., Perkin Trans. 2* **1972**, 747.
65. Vogl O. *J Macromol Sci Pure Appl Chem A* **1996**, 33, 1571.
66. Archer, L. A.; Fuller, G. G. *Macromolecules* **1994**, 27, 4359.
67. Brochard, F.; de Gennes, P. G. *Macromolecules* **1977**, 10, 1157.
68. Srinivas, G.; Discher, D. E.; Klein, M. L. *Nat Mater* **2004**, 3, 638.
69. Shvartzman-Cohen, R.; Monje, I.; Florent, M.; Frydman, V.; Goldfarb, D.; Yerushalmi-Rozen, R. *Macromolecules* **2010**, 43, 606.
70. Li, S.; Clarke, C. J.; Lennox, R. B.; Eisenberg, A. *Colloids and Surfaces A: Physicochemical and Engineering Aspects* **1998**, 133, 191.
71. Fredrickson, G. H.; Bates, F. S. *Annual Review of Materials Science* **1996**, 26, 501.
72. Konak, C.; Podesva, J. *Macromolecules* **1991**, 24, 6502.
73. Tsunashima, Y.; Kawamata, Y. *Macromolecules* **1993**, 26, 4899.
74. McCaffrey, V. P.; Forbes, M. D. E. *Macromolecules* **2005**, 38, 3334.
75. Harbron, E. J.; McCaffrey, V. P.; Xu, R.; Forbes, M. D. *J. Am. Chem. Soc.* **2000**, 122, 9182.
76. McCaffrey, V. P.; Harbron, E. J.; Forbes, M. D. *Macromolecules* **2005**, 38, 3342.
77. McCaffrey, V. P.; Harbron, E. J.; Forbes, M. D. *J. Phys. Chem. B* **2005**, 109, 10686.
78. McNeill, I. C. *European Polymer Journal* **1968**, 4, 21.
79. Weber, M.; Khudyakov, I. V.; Turro, N. J. *J. Phys. Chem. A* **2002**, 106, 1938.
80. Gupta, A.; Liang, R.; Tsay, F. D.; Moacanin, J. *Macromolecules* **1980**, 13, 1696.

81. North, A. M. *Chemical Society Reviews* **1972**, *1*, 49.
82. Lebedeva, N. V.; Gorelik, E. V.; Prowatzke, A. M.; Forbes, M. D. E. *J. Phys. Chem. B* **2008**, *112*, 7574.
83. Fraenkel, G. K. *J. Phys. Chem.* **1967**, *71*, 139.
84. Papanagopoulos, D.; Dondos, A. *Polymer* **1995**, *36*, 369.
85. Yee, G. G.; Fulton, J. L.; Smith, R. D. *J. Phys. Chem.* **1992**, *96*, 6172.
86. Kajiwara, A.; Maeda, K.; Kubo, N.; Kamachi, M. *Macromolecules* **2003**, *36*, 526.
87. Bolton, J. R.; Carrington, A. *Molecular Physics* **1962**, *5*, 161.
88. Kamachi, M.; Kohno, M.; Jang Liaw, Der; Katsuki, S. *Polymer Journal* **1977**, *10*, 69.
89. Harbron, E. J. Thesis **1999**
90. Forbes, M. D. E.; Schulz, G. R.; Avdievich, N. I. *J. Amer. Chem. Soc.* **1996**, *118*, 10652
91. Levstein, P. R.; van Willigen, H. *Chem. Phys. Lett.* **1991**, *187*, 415
92. Turro, N. J.; Wu, C.-H. *J. Amer. chem, Soc.* **1995**, *117*, 11031.
93. Hautekeer, J.-P.; Varshney, S. K.; Fayt, R.; Jacobs, C.; Jérôme, R.; Teyssie, P. *Macromolecules* **1990**, *23*, 3893–3898.
94. Zhang, M.; Müller-Plathe, F. *J. Chem. Phys.* **2006**, *125*, 124903.
95. Rapaport, D. C. *J. Chem. Phys.* **1979**, *71*, 3299.
96. Ahlrichs, P.; Dünweg, B. *J. Chem. Phys.* **1999**, *111*, 8225.
97. a) Larson, R. G. *Macromolecules* **2004**, *37*, 5110, b) Bulacu, M.; Goga, N.; Zhao, W.; Rossi, G.; Monticelli, L.; Periole, X.; Tieleman, D. P.; Marrink, S. J. *J. Chem. Theory Comp.* **2013**, *9*, 3282, c) Latinwo, F.; Schroeder, C. M. *Macromolecules* **2013**, ASAP.
98. Kremer, K.; Grest, G. S. *J. Chem. Phys.* **1990**, *92*, 5057.
99. Harmandaris, V. A.; Mavrantzas, V. G.; Theodorou, D. N.; Kröger, M.; Ramirez, J.; Öttinger, H. C.; Vlassopoulos, D. *Macromolecules* **2003**, *36*, 1376.

100. Pilar, J.; Labsky, A.; Marek, A.; Budil, D. E.; Earle, K.A.; Freed, J. H. *Macromolecules* **2000**, *33*, 4438
101. Harbron, E. J.; McCaffrey, V. P.; Xu, R.; Forbes, M. D. E. *J. Am. Chem. Soc.* **2000**, *122*, 9182.
102. McCaffrey, V. P.; Forbes, M. D. E. *Macromolecules* **2005**, *38*, 3334.
103. Moore, J. A.; Choi, J. O. in *Radiation Effects on Polymers*, Clough, R. L. and Shalaby, S. W., Ed.; American Chemical Society: Washington, D.C., **1991**, p. 156.
104. Budil, D. E.; Lee, S.; Saxena, S.; Freed, J. H. *J. Magn. Reson., Ser A* **1996**, *120*, 155.
105. Shiotani, M.; Sohma, J.; Freed, J. H. *Macromolecules*, **1983**, *16*, 1495
106. Ge, M. T.; Freed, J. H., *Biophys. J.* **1993**, *65*, 2106.
107. Pilar, J.; Labsky, J.; Marek, A.; Budil, D. E.; Earle, K. A.; Freed, J. H. *Macromolecules* **2000**, *33*, 4438.
108. Atherton, N. M. "Advanced EPR: Applications in biology and biochemistry"; Elsevier, Amsterdam. **1989**.
109. Anderson, C. D.; Shea, K. J.; Rychnovsky, S. D. *Org. Lett.* **2005**, *7*, 4879.
110. Shiotani, M.; Sohma, J.; Freed, J. H. *Macromolecules* **1983**, *16*, 1495.
111. Teraoka, I. "Polymer Solutions: An Introduction to Physical Properties"; Wiley: NY, **2002**.
112. Wong, S. K.; Hutchinson, D. A.; Wan, J. *J. Chem. Phys.* **1973**, *58*, 985.
113. Atkins, P. W.; Evans, G. T. *Chem. Phys. Lett.* **1974**, *25*, 108.
114. McCaffrey, V. P.; Harbron, E. J.; Forbes, M. D. E. *Macromolecules* **2005**, *38*, 3342.
115. McCaffrey, V. P.; Harbron, E. J.; Forbes, M. D. E. *J. Phys. Chem. B* **2005**, *109*, 10686.
116. Kawai A.; Okutsu T.; Obi K. *J. Phys. Chem.* **1991**, *95*, 9130.
117. Goudsmit, G. H.; Paul H.; Shushin A. I. *J. Phys. Chem.* **1993**, *97*, 13243.
118. Winnik, F. M.; Ottaviani, M. F.; Bossman, S. H.; Pan, W.; Carcia-Caribay, M.; Turro,

- N. J. *J. Phys. Chem.* **1993**, 97, 12998.
119. a) Scaiano, J. C.; Lissi, E. A.; Stewart, L. C. *J. Am. Chem. Soc.* **1984**, 106, 1539, b) Williams, R. M.; Verhoeven, J. W. *Chemical Physics Letters* **1992**, 194, 446, c) Jockusch, S.; Dedola, G.; Lem, G.; Turro, N. J. *J. Phys. Chem. B* **1999**, 103, 9126.
120. Wymann, L; Kaiser, T.; Paul, H.; Fischer, H. *Helv. Chim. Acta* **1981**, 64, 1739.
121. a) Kaiser, T.; Grossi, L; Fischer, H. *Helv. Chim. Acta* **1978**, 61, 223, b) Kaiser, T.; Fischer, H. *Helv. Chim. Acta* **1979**, 62, 1475.
122. Wagner P.J.; Hammond G.S.; in *Advances in Photochemistry*, Noyes A.W., Hammond G.S., Pitts, J.N., eds., Hoboken, New Jersey: Wiley, **2007**, p. 5.
123. a) Forbes, M. D. E. "Carbon-Centered Free Radicals and Radical Cations"; Wiley: NY, **2010**, b) Forbes, M. D. E.; Jarocho, L. E.; Sim, S.; Tarasov, V. F. *Adv. Phys. Org. Chem.* **2013**, 47, 1.